Cape Peninsula University of Technology

EXPLORING HIGH-LEVEL TOPOLOGY FRAMEWORKS FOR NANO-SATELLITES

by

STUART BARTER

Thesis submitted in fulfilment of the requirements for the degree

Master of Engineering in Electrical Engineering

In the Faculty of Engineering & the Built Environment

At the Cape Peninsula University of Technology

Supervisor: Dr. Laban Mwansa
Co-supervisor: Prof. Francois Rocaries

Bellville Campus

JANUARY, 2021

DECLARATION

I, Stuart Barter, declare that the contents of this thesis represent my own unaided work, and that the thesis has not previously been submitted for academic examination towards any qualification. Furthermore, it represents my own opinions and not necessarily those of the Cape Peninsula University of Technology.

Signed

19/01/2021

Date

ABSTRACT

Nanosatellite networks have become a major research topic over the last few years. With their small size and relatively cheap cost, launching many of these nanosatellites at once is becoming more and more common. With the advent of P2P capabilities in nanosatellites, the question of node positions becomes a major topic. This thesis focuses on a proposed swarm of nanosatellites with P2P capabilities forming a partially connected mesh topology. Attention was given to the physical laws of orbital mechanics, making it possible to obtain numerical solutions to node location. Advantage was taken of orbital data to predict the positions of nanosatellites relative to one another in order to determine future dates of intersection. The virtual nodes were equipped with proven P2P technology. The reach capabilities were then hypothetically extended for future consideration in technological development. Analysis was performed on the frequency of intersection times based on various link budget specifications. Simulation results are used to draw conclusions on the parameters affecting connectivity within different swarm sizes and antenna ranges. The work presented here contributes toward P2P nanosatellite swarm research and can help to determine the feasibility and planning of running future space networks using nanosatellite swarms.

ACKNOWLEDGEMENTS

The author would like to thank the following people for their contribution which led to the success of this thesis, and without whose support its completion would not have been possible:

- **Dr. Laban Mwansa** as supervisor and **Prof. Francois Rocaries** as co-supervisor, for their guidance and support.
- My parents, for their love and support: My mother, **Karin Barter,** who would gladly take on my stress if she could. And my father, **John Barter**, who's always reminding me to stay focused.
- **Susan "Ouma" Botha** for her love, endless prayers and only wanting the best for me.
- **Matthew Coetzee** for his patience and support.
- **God**, without His will and guidance none of this would be possible.
- My **friends** who are always wishing me the best.
- **Justin Unwin**, for our discussions about the marvels of space and coding.
- The partial financial assistance of the **National Research Foundation** towards this research is acknowledged. Opinions expressed in this thesis and the conclusions arrived at, are those of the author, and are not necessarily to be attributed to the National Research Foundation.

TABLE OF CONTENTS

LIST OF FIGURES

LIST OF TABLES

NOMENCLATURE

18 SPCS	18 Space Control Squadron
AIS	Automatic Identification System
API	Application Programming Interface (API)
Cubesat	Cube satellite form factor
DoD	United States Department of Defence
DSCN	Distributed Satellite Cluster Network
ECI	Earth-Centered Inertial
F'SATI	French South African Institute of Technology
GDP	Gross Domestic Product
ISL	Inter-satellite link
ITU	International Telecommunication Union
JD	Julian date
JDN	Julian day number
JF	Julian date fraction
M2M	Machine to machine
MDA	Maritime Domain Awareness
MJD	Modified Julian Date
NDP	National Development Plan (for 2030)
NORAD	North American Aerospace Defense Command
OBC	On-board computer
P2P	Peer-to-peer
Peer	Nanosatellite connected to the network
PFF	Precise Formation Flying
PyPI	Python Package Index
PHAKISA	A Government operation to help implement the NDP
SDR	Software Defined Radio
S-NET	S-band network of distributed nanosatellites
SNN	United States Space Surveillance Network
STK	Systems Tool Kit (Software by Analytical Graphics, Inc)
TEME	True Equator Mean Equinox
TLE	Two-Line Element set
VDES	Very High Frequency Data Exchange Service
UID	Unique identifier

CHAPTER 1: INTRODUCTION

1.1 BACKGROUND

The National Development Plan 2030 (NDP) of South Africa seeks to eliminate poverty and reduce inequality by 2030. It was first announced on 19 February 2013. The plan aims to achieve its goals by drawing on the energies of its people, growing an inclusive economy, building capabilities, enhancing the capacity of the state, and promoting leadership and partnerships throughout society (South African Government, 2013).

In July 2014, Operation Phakisa was launched to help in the implementation of the NDP. Operation Phakisa provides a framework for government, businesses and organised labour in the public and private sectors to set out various initiatives. The ultimate goal of Operation Phakisa is to boost economic growth and create new jobs. Phakisa means “hurry up” in Sesotho and it thus emphasises the operation’s goal to be a fast-results programme. Operation Phakisa has three major collaboration sessions called “labs”: the oceans economy lab, e-health lab and education lab. The Oceans Economy Phakisa will focus on aquaculture, offshore oil and gas, marine protection and governance, marine transport and manufacturing, small harbours’ development and coastal and marine tourism (Operationphakisa.gov.za, n.d.). The Cape Peninsula University of Technology (CPUT) has adopted Operation Phakisa as a key research focus area. The main focus of research and technology is centred around marine protection and governance. There exists massive growth potential with the broadening of Maritime Domain Awareness (MDA). South Africa has a coastline of 3900 kilometres and an ocean territory of 1.5 million square kilometres, with most of the area having largely untapped resources and monitoring all passing ships within the territory is very difficult. The oceans’ economy has the potential to contribute up to 177 billion Rand to the gross domestic product (GDP) and create just over one million jobs by 2033 (Zuma, 2014). The aim is to improve and grow South Africa’s ocean economy to increase GDP and promote job creation, while having control and monitoring of its coastline and ocean territory.

Agreements have been set out between CPUT and the Department of Environmental Affairs and the Department of Science for the development of nanosatellite-based solutions for Operation Phakisa. The potential to launch several nanosatellites into space and create a communications framework that could be used for MDA, will enable South Africa to monitor data of the current Automatic Identification System (AIS) standard to the future Very High Frequency Data Exchange Service (VDES) of ships in its coastal waters for security and control purposes.

1.2 PROBLEM STATEMENT

Since AIS transmissions are limited to a range of 50 to 100 km, tracking ships along the coast with traditional coast-based receivers are only viable within that range (Pranajaya et al., 2010). This leads to the conclusion that there is a need for a nanosatellite solution that would enable the tracking of ships outside the current limit and would benefit the country in terms of national security, sea rescue, environmental studies and the marine economy. But because one nanosatellite is not enough to cover the entire coast for most of its orbit, a swarm or constellation of these nanosatellites would need to be implemented to constantly have full access to tracking information.

Taking this into account, the question arises on whether a swarm or a constellation would best benefit MDA. In theory, each satellite could respond to a base station individually, but having them interconnected as a peer-to-peer network opens up more possibilities for communication and access to other areas around the world. There is currently no fixed answer as to which type of topology would best suit such a network. Thus, to incorporate both of these ideas, this thesis chose to showcase a swarm topology with peer-to-peer capabilities in order to contribute to nanosatellite topology research for MDA.

1.3 RESEARCH SIGNIFICANCE

A CPUT nanosatellite, called ZACUBE-2, was launched in December 2018 into space to demonstrate the technology that could be used for nanosatellite ship tracking. A key technology on-board the satellite includes Software Defined Radio (SDR), which can be configured after launch for a wide range of communication purposes. If SDR capable nanosatellites could be interconnected in a swarm, then in addition to its primary function to facilitate MDA, the nanosatellites' communication payload can be reconfigured in order to address a wide range of communication needs in other industries (Cput.ac.za, n.d.). Such industries could include healthcare, where communication to hospitals in rural Africa is not always possible due to the lack of mobile infrastructure.

The network of nanosatellites with peer-to-peer capabilities is also a flexible system that can relay information to one another, which allows them to be used for purposes like rapid responses, asset tracking, disaster management, telemedicine and environmental management such as illegal mining, water use and deforestation. The African continent is also prone to get stricken by natural disasters such as drought and locusts. In May 2017, Ghana declared a state of emergency with the appearance of a fall armyworm plague sweeping across the country and other parts of the African continent, threatening food security and leaving ~2.7

million people in need of food aid (Africanews, 2017). These locusts could potentially be monitored by cubesats to track the swarm's movement and provide an early warning signal, creating a window of opportunity for crop protection. Cubesats may also provide useful information to farmers by monitoring crops over time and over large areas. Such solutions include, but are not limited to, smart farming, crop-water usage for precision agriculture (Aragon et al., 2018) and fruit development (Khabbazan et al., 2019). The use cases are believed to be enormous.

1.4 RESEARCH GOAL AND OBJECTIVES

The main goal of this thesis is to analyse, design and implement a peer-to-peer nanosatellite swarm. This is achieved by giving a chance for physical interaction based on antenna reach. The reach capabilities are further extended hypothetically, to measure the connectivity performance of different swarms. The research objectives are listed as follow:

1. To produce a method by which a calculated chance for intersection can be achieved.
2. To find the minimum number of calculations needed to be performed by each nanosatellite node in order not to miss a passing node.
3. To find the number of unique nanosatellite nodes intersecting the main node within 24 hours, in different swarm sizes.
4. To find the number of intersections that the main node will experience within 24 hours, in different swarm sizes.
5. To find the average time between intersecting nodes within different swarm sizes.

1.5 RESEARCH QUESTIONS

1. What data, algorithm, and coordinate system would nodes in a swarm need to predict the movement of themselves and their peers?
2. What is the frequency of calculations needed to be performed by nodes in the swarm before data becomes redundant?
3. How well does node utilisation scale in different swarm sizes?
4. How many opportunities for communication are available to a node, in different swarm sizes?
5. What is the deviation in time of intersection of a swarm vs a theoretically perfect constellation that has equally spaced intersection intervals?

1.6 DELINEATION

In this section, the researcher will address the limitations of the scope and state the boundaries of the research study.

- Whether or not the interaction is successful in real life, will be dependent on mission specifications and many other factors. Some of these factors include the frequency, symbol rate, protocol, speed of the onboard computer, the accuracy of the attitude control etc. The simulations that follow, will assume that the mission requirements have been taken into account by the team designing their swarm.
- The simulations are not application-specific. However, real cubesat orbital data is used to produce the simulations to make the results more realistic.
- The effects of space weather are ignored.
- It is assumed all nanosatellite nodes within the network are fully operational and their antennae systems and attitude control system etc, are working at all times.
- It is assumed that the energy of the signals is enough to sustain communication via the hypothetically extended distances.

CHAPTER 2: LITERATURE REVIEW

2.1 TOPOLOGY

2.1.1 Physical vs Logical

Topology, in the context of networks, has a physical and logical interpretation. Physical topology refers to how the real-world mediums connect nodes to a network. These include (but are not limited to) copper cables, fibre optical cables and electromagnetic waves. Once nodes have a medium to communicate through, they need a system to be able to uniquely represent themselves and identify others. These means are usually achieved through software, firmware and protocols, which all form part of the logical topology. It is important to note that the physical and logical topologies are distinct from one another: nodes in a network can be geographically separated over large distances, but be logically close in the network or vice versa.

2.1.2 Earth vs Space

There is a vast range of physical medium used to establish networks on Earth. In space, nodes are forced to move around constantly as they orbit the Earth. Because of this limitation, certain topological structures cannot be used in space, like bus topology (discussed below). Since the luxury of copper cables is not available, the most widely used physical medium is electromagnetic waves, which include UHF radio (de Villiers and van Zyl, 2015) and laser (Spacetrack.org, 2020).

2.1.3 Common topologies

2.1.3.1 Line topology

In a line topology (figure 2.1), a node is connected by a single line of connection between itself and another node in the graph. The graph is not interconnected, i.e., node 1 (N1) cannot reach node 5 (N5) directly. However, if the nodes in the graph have P2P capabilities, then N1 would be able to reach N5 via the other nodes in the graph. N1 would thus have means of contacting other nodes as long it stays connected. Dong et al. (2015) note that because nodes only share one link with their neighbour, information will be relayed throughout the entire network, which will result in low information transmission efficiency and poor robustness. If the connection between N1 and N2 is severed, then the other nodes would have no way to connect to N1. If the line topology suffers a break in the graph half-way (N3/N4), then you would have two independent graphs N1-N2-N3 and N4-N5 that could still operate independently from each other if they are fitted with P2P capabilities. In space, a break in the network could occur if the

nanosatellites drift out of communication range, but should they be fitted with manoeuvring mechanisms, the network connectivity can be maintained. Line topology can be used together with a fractioned spacecraft architecture for Earth observation missions (Yaglioglu, 2011).

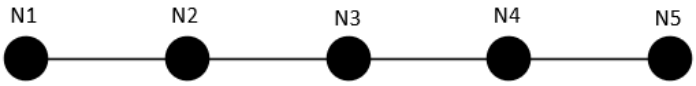

Figure 2.1: Line topology

2.1.3.2 Ring topology

The ring topology (figure 2.2) is an extension of the line topology. The last node in the line connects to the first node in the line to form a ring. The ring topology has the same properties as the line topology but is more robust as there is an alternative route for the network to take in case a connection is severed between two nodes. If the graph breaks between N1/N6, then N1 can still reach N6 via nodes N2-N3-N4-N5. It will then reduce to a line topology. Connecting the graph in a ring thus makes routing to a specific node more efficient, N5 is only one hop away from N1, instead of four hops if N6 was not connected.

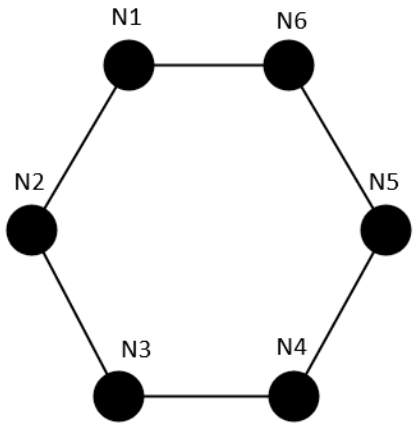

Figure 2.2: Ring topology

2.1.3.3 Bus topology

The bus topology (figure 2.3) is commonly used in businesses and internet companies on Earth. All nodes in the network connect to a fixed-line called a “backbone”, which essentially can handle high data rates and is responsible for the majority of traffic in the network. There is, unfortunately, limited use for this topology in space, because there are no fixed physical

lines and therefore not feasible to implement. Perhaps in future, the topology might see some use with tethering technology.

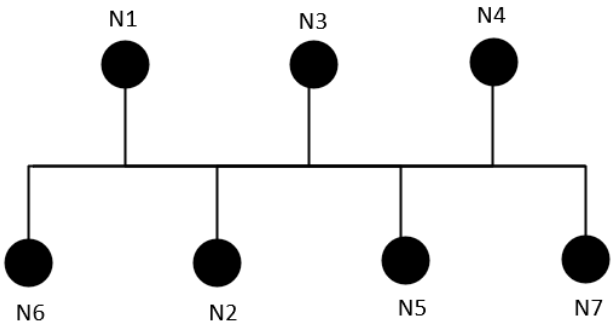

Figure 2.3: Bus topology

2.1.3.4 Star topology

A network is said to have a star topology when there exists a central node to which all other nodes in the network are connected (figure 2.4). Star topologies are used frequently with the client-server model as the central node could be represented as a server to which the clients connect. If one node fails, then it does not impact the network to a large extent, as all other nodes would still be able to connect to one another through the central node. The main drawback is that if the central node fails, the whole network fails. This model has seen some use in space where it is achieved with precise formation flying. The central node could be a satellite acting as a hub that handles data from one node to another. Another advantage of this topology is that the network can be scaled and maintain a linear time complexity of O(2), since there are only two connections between any two nodes.

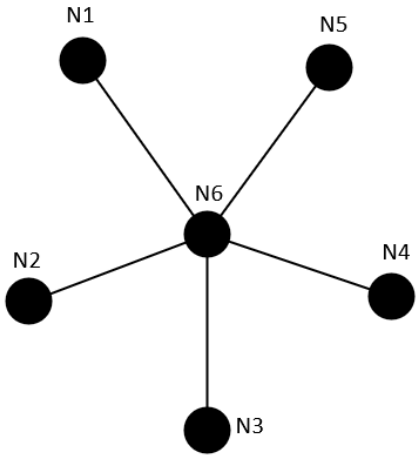

Figure 2.4: Star topology

2.1.3.5 Fully connected mesh topology

The fully connected mesh topology (figure 2.5) forms a network in which every node in the graph is connected to every other node in the graph. Unlike the star topology, there exists no central node, thus no central point of failure. Because the nodes are fully connected, there exists a one-way path for communication between nodes so no hopping is required. This property makes the network is extremely robust because the failure of one node will hardly have any effect on the data transmission between the other nodes. Unfortunately, the property of being fully connected also impacts the scalability of the network. The graph has quadratic time complexity $O(n^2)$, making routing exponentially difficult in large-scale networks.

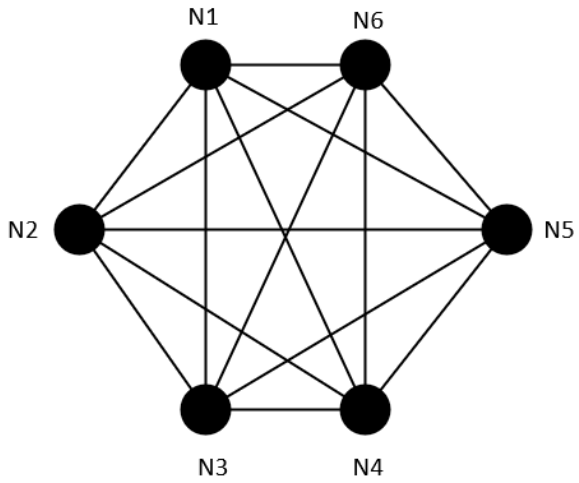

Figure 2.5: Fully connected mesh topology

2.1.3.6 Partially connected mesh topology

A partially connected mesh topology (figure 2.6) is a graph consisting of nodes that are only partially connected to each other, instead of fully connected. The lack of full connection implies that network performance will vary across different parts of the network, i.e., certain nodes might be more connected than others and thus require fewer hops to reach their destination node. A Partially connected mesh topology is associated with a swarm, where the structure and order are ever-changing. The partially connected mesh can also be a result of drift between nodes that are supposed to fly in formation like the fully connected mesh. This change in the structure of the topology creates difficulty in selecting a suitable routing algorithm. Although it might not be optimised, the solution to controlling a partially connected mesh would have the benefit of being able to work in all of the above-mentioned topologies (assuming P2P capabilities on all nodes). This is because the algorithm needs to be robust so that no single change can affect its operation. Section 2.5 will focus, in more detail, on a control solution for this kind of topology.

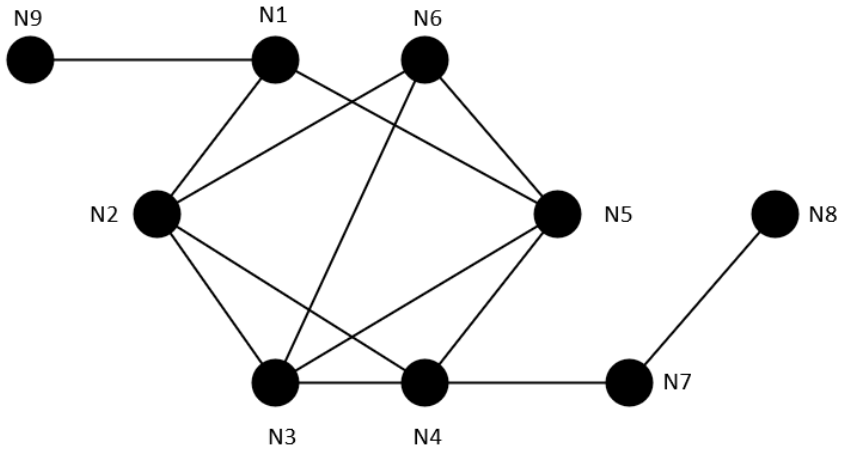

Figure 2.6: Partially connected mesh topology

2.1.3.7 Hybrid topology

A hybrid topology (figure 2.7) is the combination of two or more topologies. For example, two fully connected mesh networks connected to each other and combined with a ring network (figure 2.7). Such topologies can be seen in Dong et al. (2015) where they propose a distributed satellite cluster network (DSCN) in order to create an M2M backbone network architecture.

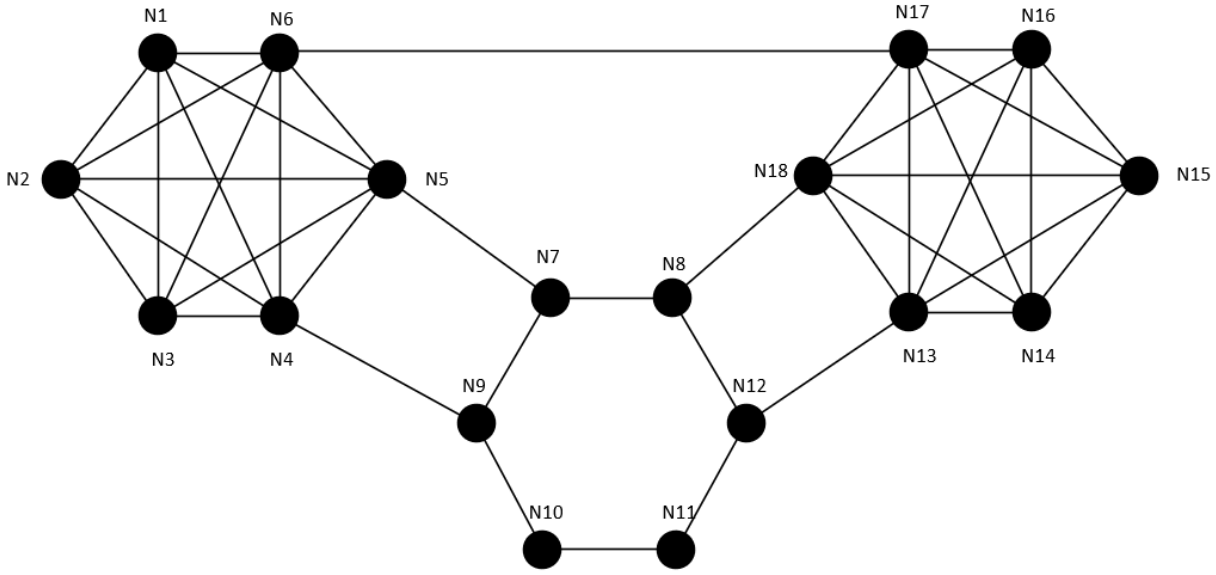

Figure 2.7: Hybrid topology

2.1.4 Swarm vs constellation

Some of the topologies discussed in the previous section can only be achieved through precise formation flying (PFF). In PFF, the nodes stay in the formation in which they were initially placed during ejection when the rocket reaches its mission orbit. This kind of setup is commonly referred to as a “constellation”. In time, they may drift away from one another due to drag forces in LEO or gravitational perturbations. With propulsion systems attached, the perturbations can be corrected and altitudes can be raised and kept. In order to self-correct, the nodes must have some kind of mechanism to detect when there are deviations in the formation. Line-, Ring-, Star and occasionally Fully connected mesh and partially connected mesh topologies can be achieved through PFF. If the connections of the network do not change, the formation is considered a constellation.

In contrast, a swarm indicates the absence of nodal formation. In a swarm, the nodes could be randomly distributed, in different orbit inclinations, altitude and velocities. Partially connected mesh topologies can be associated with swarms since the nodes will break away and connect to other nodes in the network regularly. These regular changes create a changing network topology. When coupled with the difficulty of controlling the movements of nanosatellites in space, a swarm becomes in many cases undesirable and missions tend to use constellations instead. If large scale nodes are deployed to form a swarm, the robustness of the network will increase and might become desirable for some applications, especially when coupled with efficient node finding techniques.

2.2 NETWORK MODELS

2.2.1 Client-server model

This type of model is well known throughout industry and have produced many successful models, such as the World Wide Web (HTTP), File Transfer Protocol (FTP), web services, emailing, online banking etc.

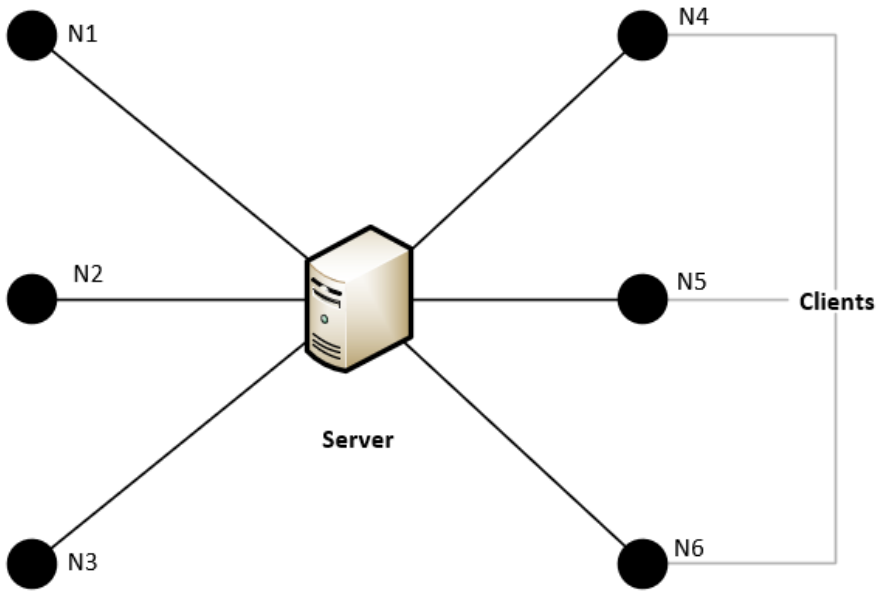

Figure 2.8: Client-server model

In the model, as seen in figure 2.8, a central server hosts and provides services and resources to clients that request them, either through a local area network or a wide area network. The server serves as the main point through which all information is passed and controlled. The whole system is said to be centralised. Such a model requires administration. Scalability is hard to achieve because of the resources involved as the number of clients increase. The servers provide a single point of failure. Thus, any loss on the server-side will provide a loss of communication to all the clients at once, which will only be restored once the server is back online.

2.2.2 Peer-to-peer (P2P)

The peer-to-peer model (figure 2.9) tries to address the limitations of the client-server model by having peers act as both clients and servers. Systems using P2P include BitTorrent, Bitcoin and Gnutella.

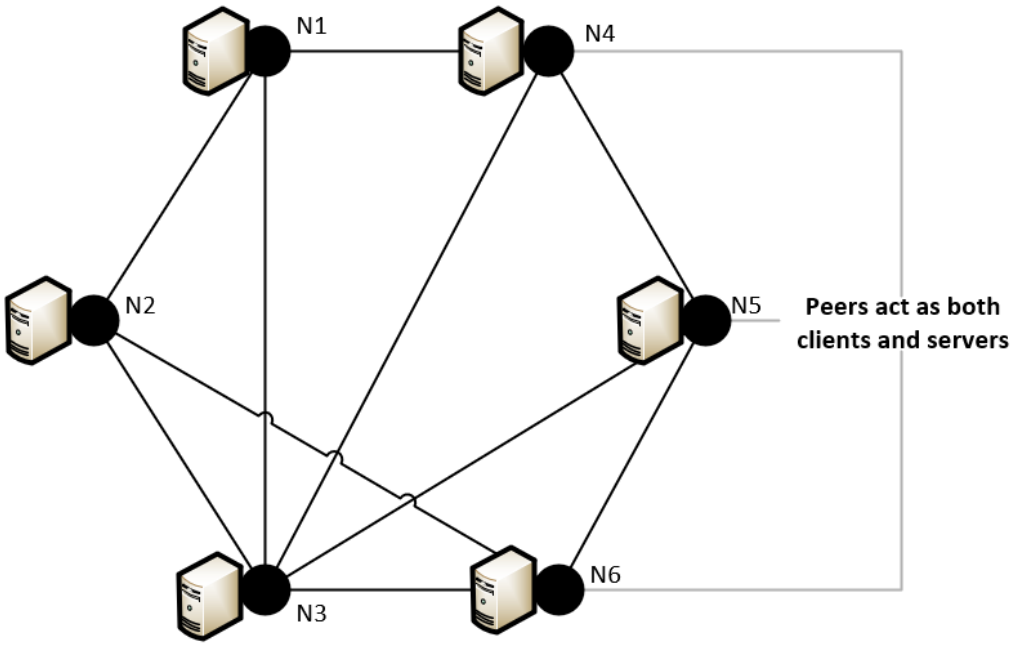

Figure 2.9: Peer-to-peer model

In this model, resources and services are shared among peers. This gives a computing advantage to the system as a whole when one peer on its own is not enough to provide a service or resource. All peers can initiate communication to any other peer in the network, thus no one peer controls access. The whole system is said to be decentralised. The points in the network through which one peer can communicate to another are called nodes. Nodes are just other peers that relay information. The information can be exchanged in cache storage, disk storage or processing cycles (Muthusamy, 2003).

Such a network model would be ideal for nanosatellites, since they do not possess large amounts of processing power, ruling out the possibility of having a server. The main benefit would thus be the efficient use of resources, coupled with scalability as more nanosatellites are added. The interconnectivity of nodes would make the system reliable since there is no single point of failure. They can be distributed in different orbits, self-organising themselves as they move toward and away from each other to relay information to ground stations. This would ease the administration process of controlling processes and services by the nanosatellites.

2.3 ROUTING

Since nodes stay connected during PFF, the issue of “finding” a node, comes down to using a suitable search algorithm. Dijkstra’s algorithm is a possible solution as it can find the shortest path between one node and another (Dijkstra, 1959). Nodes within the network might change over time as some nodes may fail and others may join in subsequent launches. Using a min-priority queue, Dijkstra’s algorithm has a time complexity of

$$O\left((|E| + |V|) \cdot \log |V|\right)$$

Where E = total number of edges (connections)

V = total number of vertices (nodes)

It will become increasingly slow to compute with large scale constellations. It also requires each node in the network to know the relative distance information of all nodes in the network to calculate the path.

In contrast, a Swarm is prone to churning, i.e., the joining and leaving of nodes in the network at random (Earth networks). Thus, the network might not be stable enough to run search algorithms on, because the chance that all the nodes will be connected at any given time is rather low. However, nodes in space are in orbit and have to adhere to Kepler’s laws. Churning events can be predicted if enough information is known about the nodes’ positions relative to one another in space. Once the orbital information is obtained, predictions can then be realised using an orbital prediction algorithm.

2.4 FREQUENCY USAGE

The International Telecommunication Union (ITU) oversees the global use of the radio spectrum and produces regulations for its use on Earth and in space. Table 2.1 forms a summary of the prominently available frequency ranges for space-to-space communication links (ITU, 2016).

Table 2.1: ITU space-to-space frequency allocations

Band	Frequency allocation	Description
UHF	410 – 420 MHz	Space research (link to an orbiting manned space vehicle)
L	1164 – 1215 MHz 1215 – 1240 MHz 1240 – 1300 MHz 1559 – 1610 MHz	Radionavigation-satellite
S	2025 – 2110 MHz 2200 – 2290 MHz	Space operation, Earth exploration-satellite, space research
C	5010 – 5030 MHz	Radionavigation-satellite
Ku	13.4 – 13.65 GHz	Space research
K	22.55 – 23.55 GHz 24.45 – 24.65 GHz 25.25–27.5 GHz	Inter-satellite
Ka	32.3 – 33 GHz	Inter-satellite
V	54.25 – 55.78 GHz +	Higher frequency allocations are available to high-Earth orbit and geostationary satellites.

2.5 TOPOLOGY CHOSEN

The topology chosen to simulate was that of a swarm of nanosatellites (cubesats) with P2P capabilities (see figure 2.10). The swarm is chaotic because the cubesats move in different orbits and deviate in altitude, thus do not adhere to formation flying.

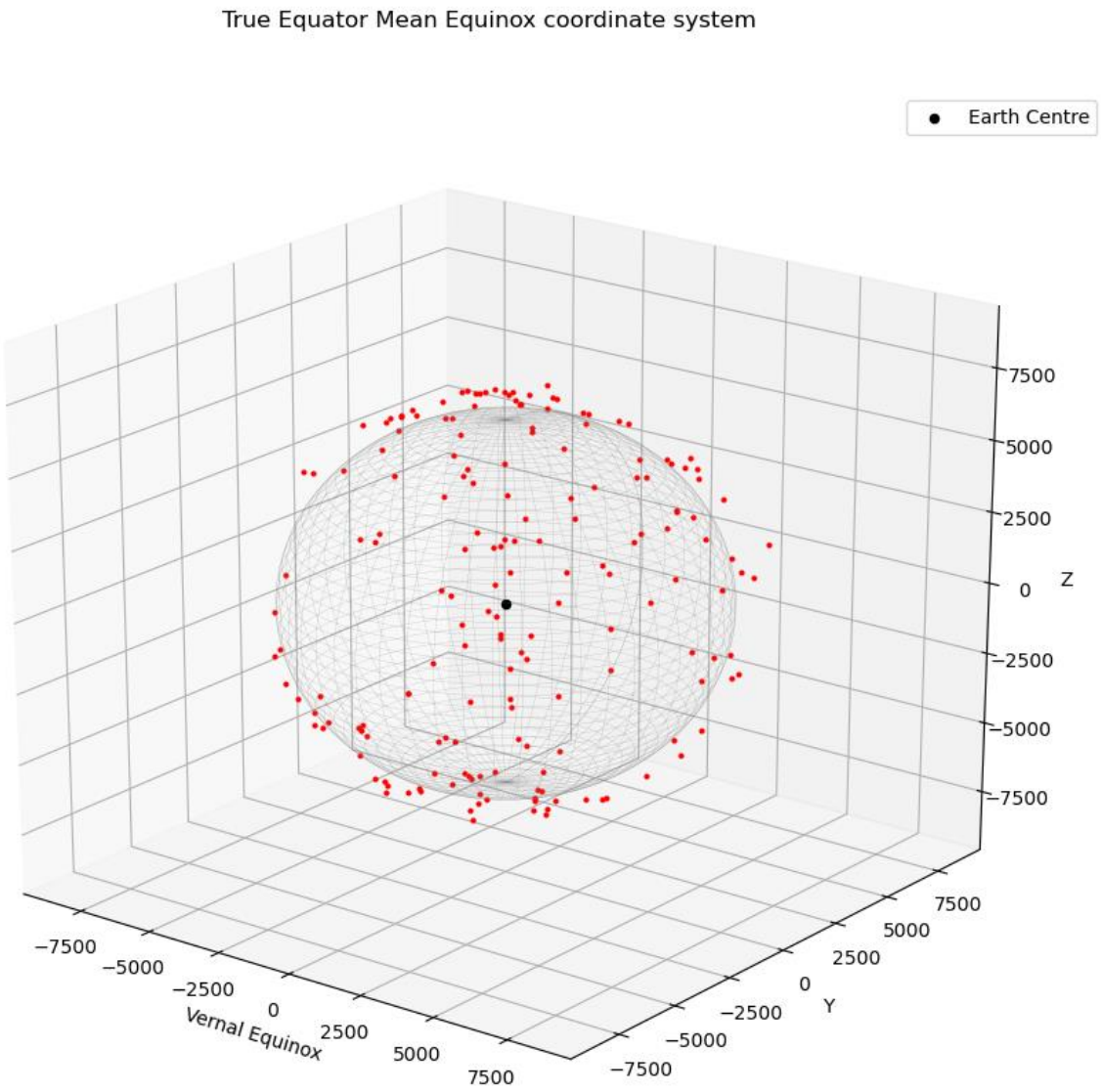

Figure 2.10: Swarm topology nodes

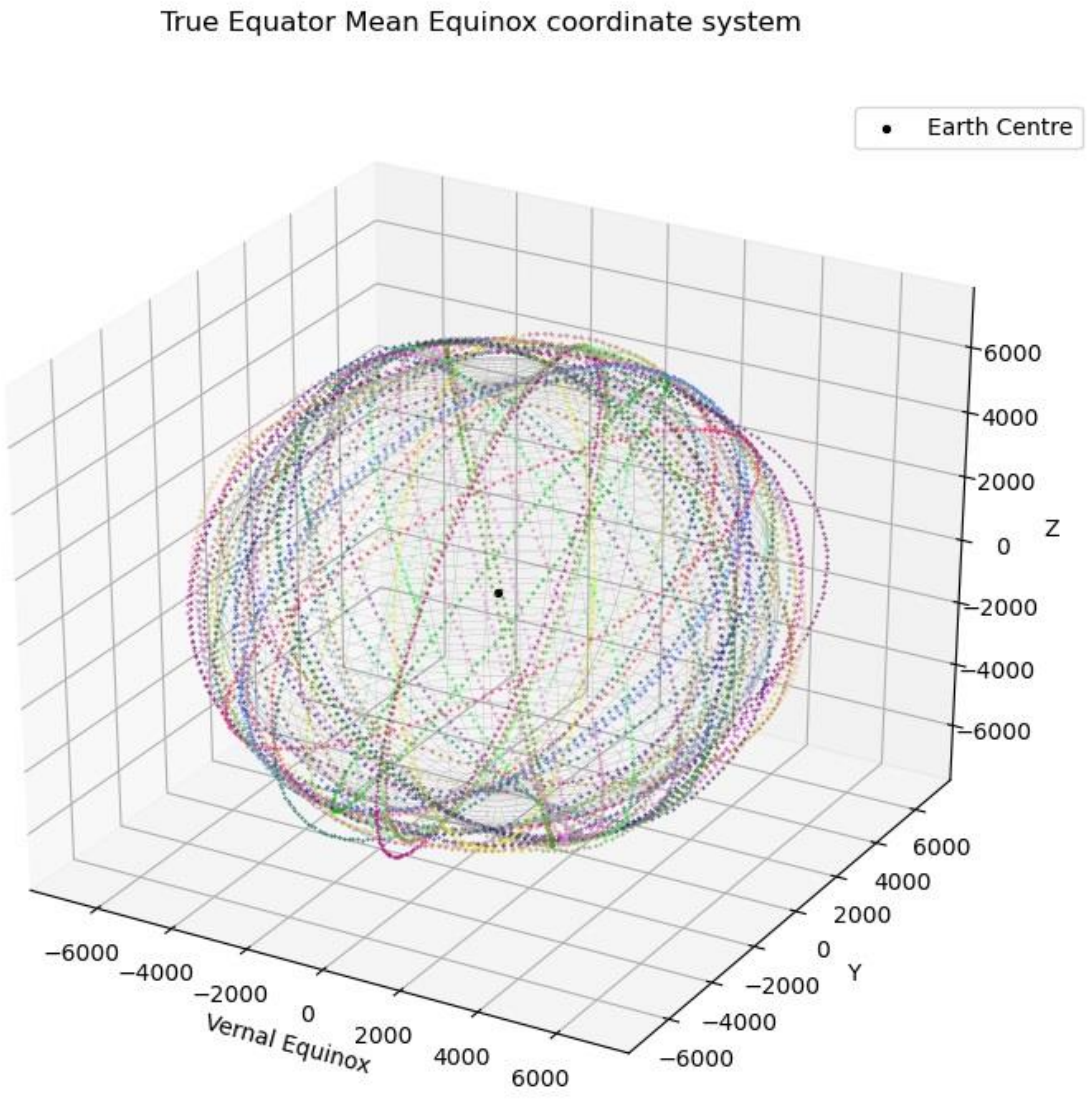

Figure 2.11: Swarm topology node orbits

P2P capabilities allow the different cubesats to act as nodes in a network. P2P is only possible if the nodes are aware of one another. The unpredictable nature of a swarm makes it hard to predict the joining and leaving of nodes so connectivity could be unstable. Advantage was taken of the fact that the positions of orbiting objects in space around the Earth can be predicted to a relative degree of accuracy, thus minimising the uncertainty of when a node will be connected. The chosen orbit prediction algorithm was SGP4. To create the swarm, real orbital data of cubesats were obtained in TLE format to represent the nodes. Real data allowed for more accurate representation when incorporating the SGP4 algorithm. Section 2.5.3 will elaborate on the details of SGP4. A visualisation of the swarm orbits can be seen in figure 2.11. The subsequent illustrations are not drawn to scale and the size of the cubesats are neglected - that is, the cubesats are treated as point nodes, with a single set of coordinates representing their positions at a specific epoch.

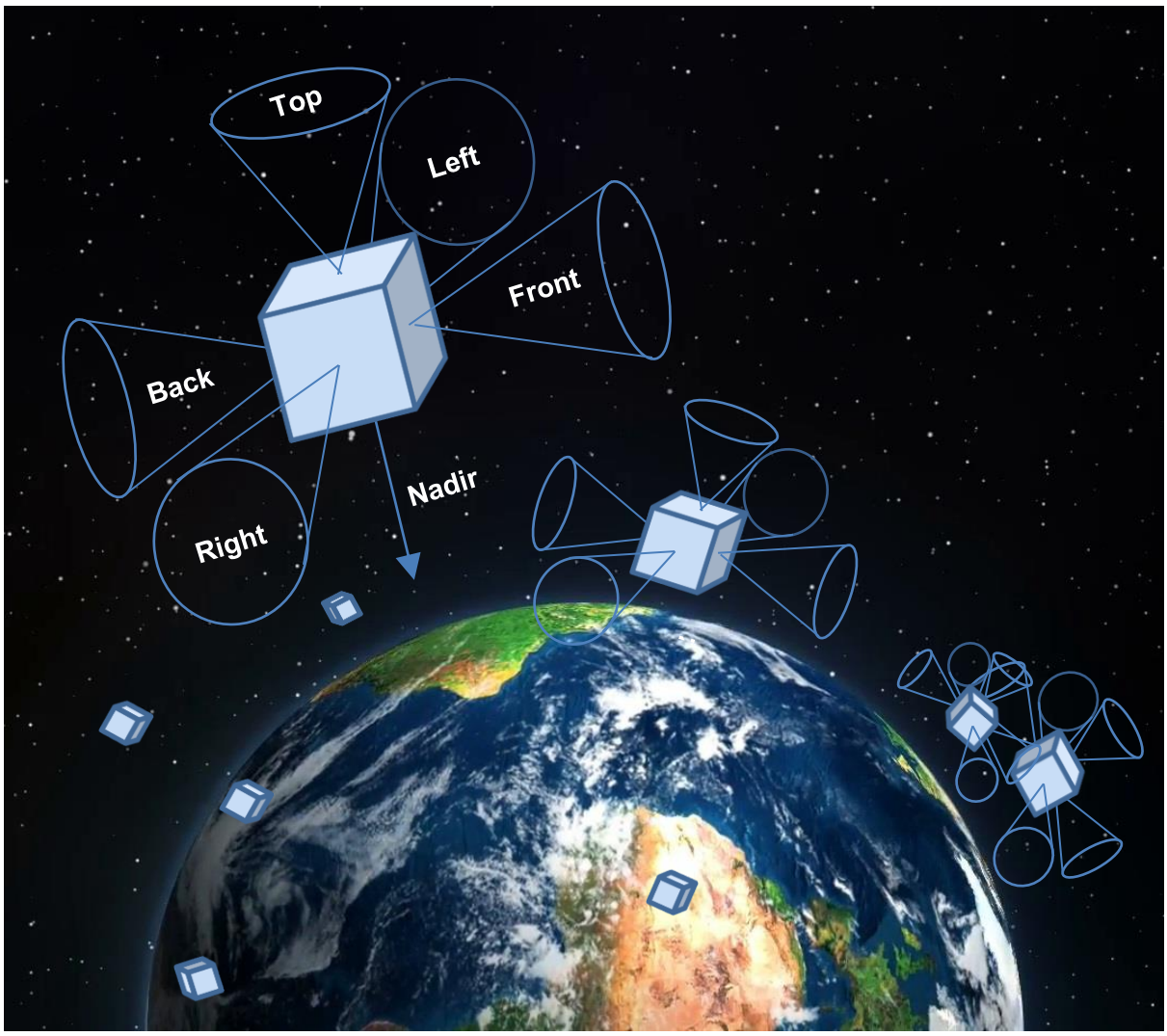

Figure 2.12: Swarm simulation outlay (Earth background from Jooinn, 2021)

The nodes in the swarm were able to predict the time of intersection and switch on when another node is in range so that connectivity could be achieved. Figure 2.12 illustrates the node antenna directions and figure 2.13 illustrates connectivity in range (green) and out of range (red), based on the reach capabilities of the nodes.

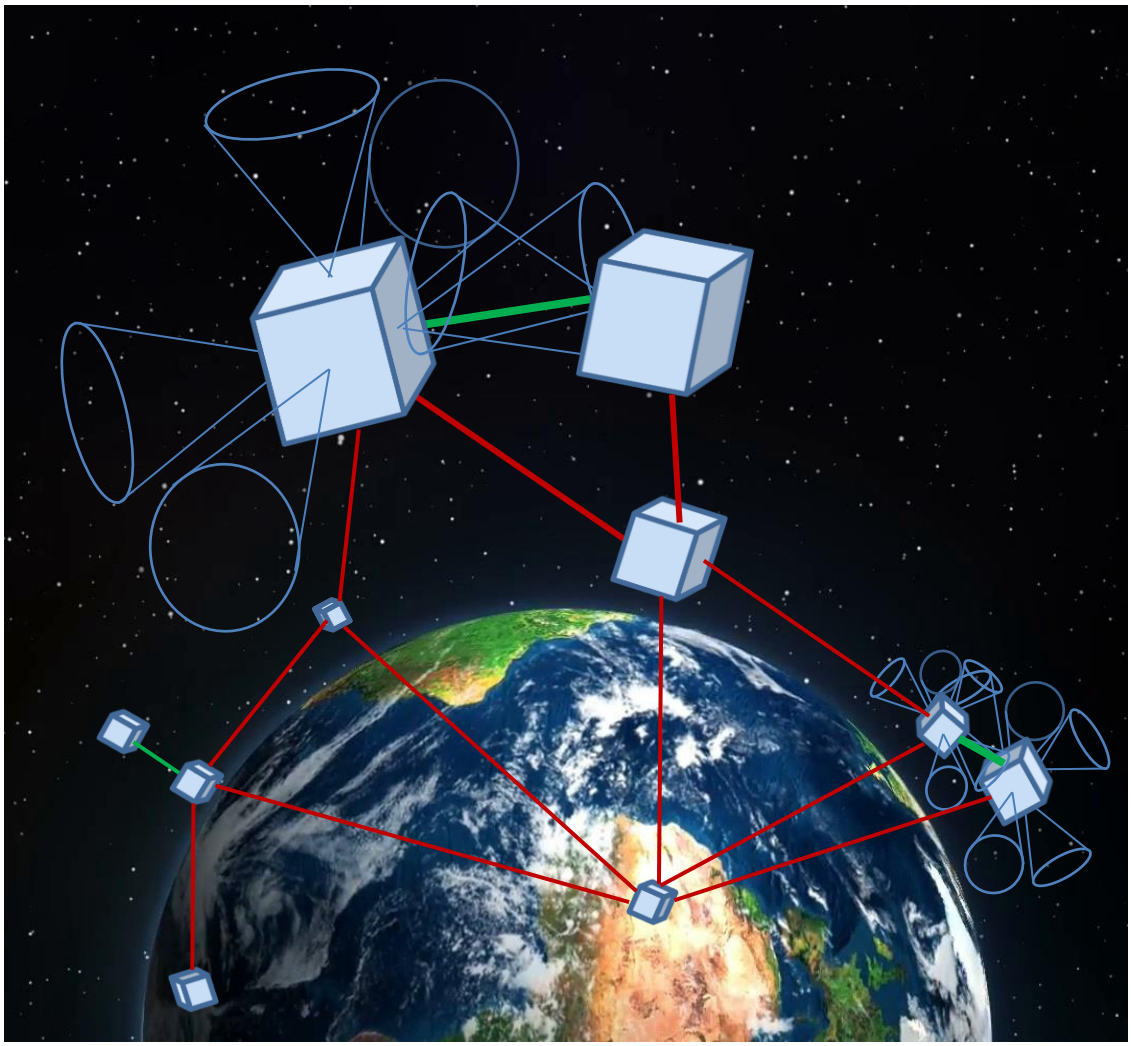

Figure 2.13: Swarm simulation connection (Earth background from Jooinn, 2021)

2.5.1 Peer-to-peer capabilities

P2P (peer-to-peer) capabilities are only realisable if the cubesat hardware supports it.
The S-band network of distributed nanosatellites (S-NET) mission (Yoon et al., 2019) has demonstrated that P2P functionality is possible with cubesats. The S-NET link budget specifications were incorporated into the simulations to represent a more realistic simulation. To achieve an inter-satellite link (ISL), S-NET made use of five planar antennas mounted on each of the non-nadir sides of the cubesats with a beam pattern of approximately $\pm 30°$. In the simulation, it was assumed that all nodes in the swarm were equipped with this technology. Figure 2.14 illustrates the antenna pattern (horisontal, phi = 0 and vertical, phi = 90).

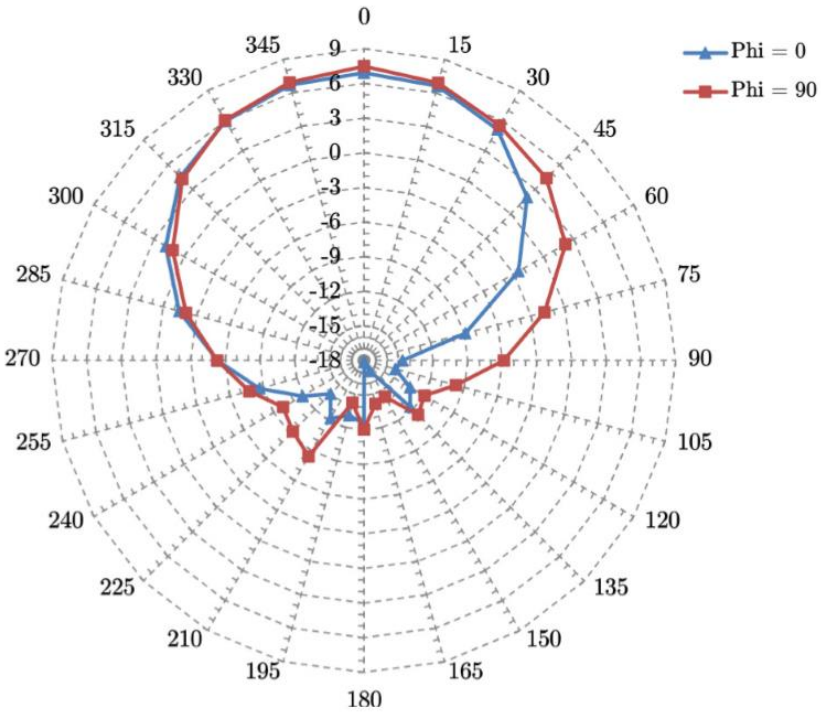

Figure 2.14: Beam pattern (Yoon et al., 2019, p.19)

Yoon et al. further elaborates that due to limited onboard resources, it is not possible to activate all antennas simultaneously. Instead, they make use of a scan algorithm and an antenna switch unit, where caller and responder antennas are switched consecutively until a match is detected. They also suggest the possibility of optimising link establishment, by making use of analytical tools like orbit propagation to shorten time delays. The latter is precisely what the upcoming simulations try to implement.

S-NET link budget specifications are summarised in table 2.2 below

Table 2.2: Link budget specifications (Yoon et al., 2019, p.20)

	Scenario				Unit	Remark
ISL Distance **Pointing Offset**	**10 km** **45 °**	**65 km** **45 °**	**148 km** **30 °**	**400 km** **0 °**		
Frequency	2266	2266	2266	2266	MHz	
TX power output	27	27	27	27	dBm	
TX losses	1.5	1.5	1.5	1.5	dB	cable and connector
TX antenna gain	0	0	5	7.5	dBi	pointing offset
RX antenna gain	0	0	5	7.5	dBi	pointing offset
RX losses	1.5	1.5	1.5	1.5	dB	
RX sensitivity	−116.50	−116.50	−116.50	−116.50	dBm	
Roll-off factor	0.25	0.25	0.25	0.25	-	
Symbol rate	80	80	80	80	kbps	
RX noise factor	3.5	3.5	3.5	3.5	dB	
Link budget	140.50	140.50	150.50	155.50	dB	
Free space path loss	119.55	135.81	142.95	151.58	dB	
Margin SNR	**20.96**	**4.69**	**7.56**	**3.93**	dB	DBPSK+ CC r=0.5
SNR required		4.00			dB	DBPSK+ CC r = 0.5
SNR required		6.00			dB	DBPSK+ CC r = 0.75
SNR required		9.00			dB	DQPSK+ CC r = 0.75
SNRrequired		13.00			dB	8ADPSK+ CC r = 0.75
SNR required		17.00			dB	16ADPSK+ CC r = 0.75

2.5.2 TLE data

Two-Line Elements (TLE) lies at the heart of the simulations that follow. The TLE set is a data format used and given by the North American Aerospace Defense Command (NORAD) to represent the positional state of near-Earth orbiting objects (Kelso, 2019c). It is used in conjunction with an orbital determination algorithm (discussed in the next section) to compute the position and velocity of Earth-orbiting objects in space. Since TLE data is specific to NORAD's SGP4/SDP4 algorithms, it should be used with one of the SGP models to implement it correctly, otherwise, errors might occur. The TLE set can be used to generate the state of an object at any future or past time from the specific epoch at which the data set was generated, to a certain degree of accuracy.

The data is created by the United States Space Surveillance Network (SNN), which is a network operated by the U.S. Army, Navy and Airforce, consisting of 30+ ground-based radars and optical telescopes all over the world, plus 6 satellites in orbit. The network maintains a tracking database of 23000+ space objects bigger than 10cm (Weeden, 2019). Full details of military or classified objects are not given to the public. An overview of the network can be seen in figure 2.15 below, provided by the 18 Space Control Squadron (18 SPCS).

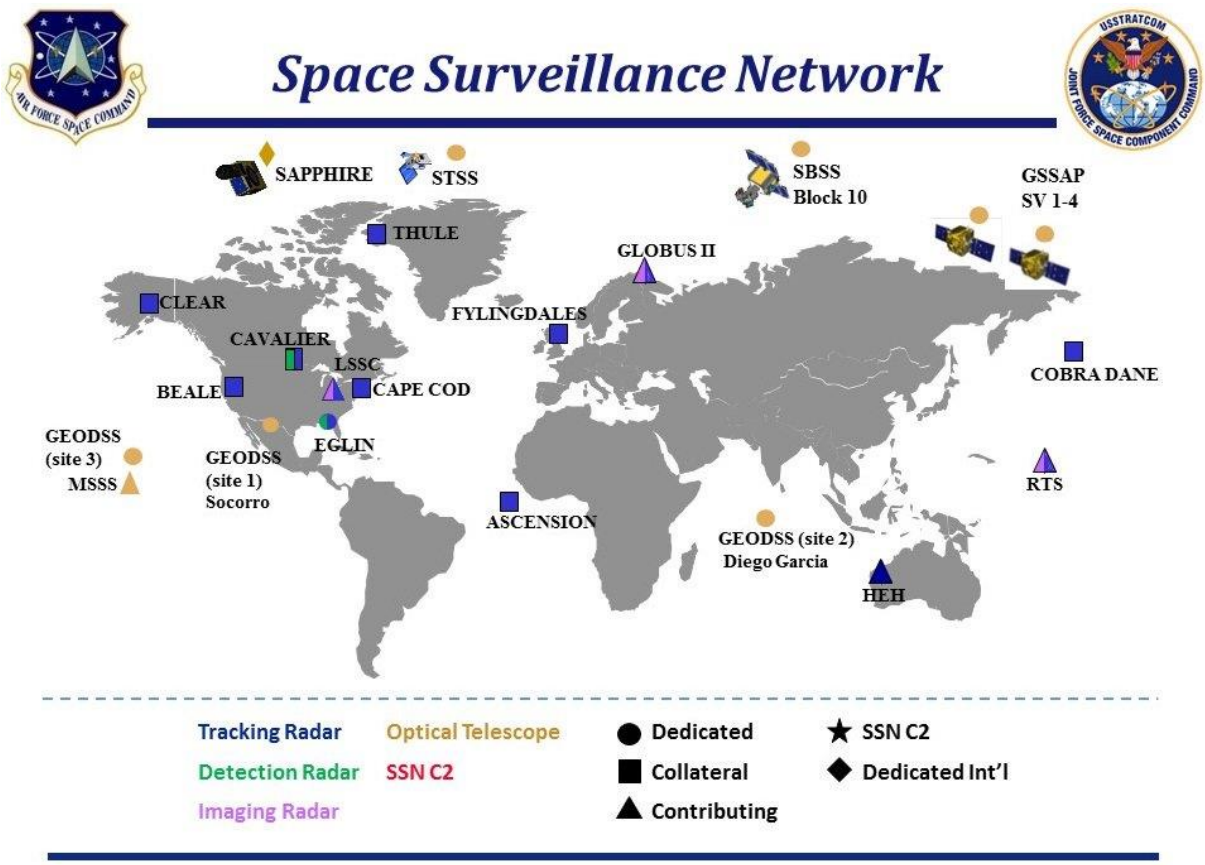

Figure 2.15: US SSN (18 SPCS, 2018)

Historically, TLE sets were designed to be used in punch cards. The data was published in Part I of the NASA Prediction Bulletins, but after failed attempts to convince NASA/GSFC to convert these to electronic format, Dr. T.S.Kelso converted them by hand from the paper copies. In 1986, he published the first electronic copies (Kelso, 2019d). The data is now freely available from *celestrak.com* and updated on a daily basis through Dr. T.S.Kelso at the Center for Space Standards & Innovation (CSSI), which also provides other tools for space applications (CSSI, 2020). TLE data is also freely available on *space-track.org*, which also allows the use of an application programming interface (API) to retrieve TLE data once every hour (Space-track.org, n.d.)

Here is an example of the orbital element set in TLE format for ZACube-2:

```
ZACube-2
1 43907U 18111AH  20242.17299443  .00000496  00000-0  22826-4 0  9997
2 43907  97.2573 139.7194 0019833 245.0879 114.8298 15.24652637 93096
```

Descriptions for the designations of the columns in the TLE format is detailed in Table 2.3 and Table 2.4 below.

Table 2.3: TLE line 1

LINE 1	
Column	**Description**
01	Line number
03-07	Satellite catalogue number
08	Classification ('U' for unclassified, 'C' for classified, 'S' for secret)
10-11	International designator (Last two digits of launch year)
12-14	International designator (Launch number of the year)
15-17	International designator (Piece of launch)
19-20	Epoch year (Last two digits of year)
21-32	Epoch (Day of the year and fractional portion of the day)
34-43	First Time Derivative of the Mean Motion
45-52	Second Time Derivative of the Mean Motion (leading decimal point assumed)
54-61	BSTAR drag term (leading decimal point assumed)
63	Ephemeris type
65-68	Element number
69	Checksum (modulo 10) (Letters, blanks, periods, plus signs = 0; minus signs = 1)

Table 2.4: TLE line 2

LINE 2	
Column	**Description**
01	Line number
03-07	Satellite catalogue number
09-16	Inclination [degrees]
18-25	Right Ascension of the Ascending Node [degrees]
27-33	Eccentricity (decimal point assumed)
35-42	Argument of Perigee [degrees]
44-51	Mean Anomaly [degrees]
53-63	Mean Motion [revolutions per day]
64-68	Revolution number at epoch [revolutions]
69	Checksum (modulo 10)

Sometimes the TLE set includes a title preceding the two lines containing the element data. This title is not part of the format. The satellite can already be identified through its catalogue number but might have a common name that can help with identification when searching through public TLE data sets, thus each listing might consist of three lines.

2.5.3 Simplified General Perturbations Models

The orbit determination algorithm used during simulation is Simplified General Perturbations 4 (SGP4). The propagation models are a set of mathematical models: SGP, SGP4, SDP4 and SGP8.

2.5.3.1 SGP

SGP was developed in 1966 by Hilton and Kuhlman and is only applicable to near-Earth orbiting satellites. This model simplifies work done by Kozai in 1959 for its gravitational model and takes the drag effect on mean motion as linear in time. “This assumption dictates a quadratic variation of mean anomaly with time. The drag effect on eccentricity is modelled in such a way that perigee height remains constant.” (Hoots, 1980).

2.5.3.2 SGP4

SGP4 comes from a lineage of previous theories including AFGP4 and IGP4. Eventually, SGP4 was developed by Kenneth H. Cranford (Lane, 1979). Lane and Hoots expanded the

theory in "*General Perturbations theories derived from the 1965 Lane drag theory*" in 1979. In "*Revisiting Spacetrack Report #3"* from 2006, Vallado et al. (2006) made a non-proprietary version in C++, which they believe is up to date and compatible with the United States Department of Defence (DoD)'s version of the code which is used to produce the TLE sets to the public. This model gives sub-kilometre accuracy. SGP4 is thus the most compatible algorithm with the TLE sets and that is the reason why it is used in the upcoming simulations.

SGP4 was ported to Python in 2010 by Brandon Rhodes. The upcoming simulations make use of the Python implementation version 2.12 (released 25 May 2020) and found at Python Package Index (PyPI) (Rhodes, 2020a). The full history and source code are maintained on Github (Rhodes, 2020b). Rhodes claims that this implementation agrees "to within 0.1 mm with the predictions of the standard distribution of the algorithm". The Python SGP4 implementation makes use of TLE data as input in order to compute the state output of Earth-orbiting objects. The gravity model WGS-72 is used.

2.5.3.3 SDP4

SDP4 is used for deep-space satellite tracking and is an extension of SGP4. The gravitational effects of the sun and moon and other sectoral and tesseral Earth harmonics, which are important for half-day and one-day orbital periods, were modelled. The deep-space equations were developed by Hujsak in 1979 (Hoots, 1980).

2.5.3.4 SGP8

SGP8 is also used to track near-Earth objects. The model encompasses a simplification of analytical theory by Hoots, but uses the same models for atmospheric drag and gravitation as modelled by Lane and Cranford. However, the integrations of the differential equations are performed in a different manner (Hoots, 1980).

2.5.4 Julian dates

Julian date is a commonly used time format in astronomy and was used extensively throughout the design and simulation of the swarm network. Herschel (1870) describes the start of the Julian date epoch as the 1st of January 4713 BC at noon. Herschel further states that the date was deduced by backtracing the start date of three cycles: solar cycle, lunar cycle and indiction cycle (used in the courts of law in the fiscal organisation of the Roman empire). The multiplication of these three cycles results in a Julian period of 7980 years. Table 2.5 shows an

example of how to calculate the Julian date (New Style). Dershowitz (2008) suggests it makes sense to start switching dates at noon because astronomers work through the night.

Table 2.5: Calculation of Julian Date, New Style (Herschel, 1870, p.535)

TABLE I. Multiples of 1461, the days in a Julian *Quadriennium*.

1	1461	4	5844	7	10227
2	2922	5	7305	8	11688
3	4383	6	8766	9	13149

TABLE 2. Days in Residual years.

0	0
1	366
2	731
3	1096

TABLE 3. Days elapsed from Jan. 1 to the 1st of each Month.

	In a common year.	In a leap year.		In a common year.	In a leap year.
Jan. 1.....	0	0	July 1.....	181	182
Feb. 1.....	31	31	Aug. 1.....	212	213
March 1.....	59	60	Sept. 1.....	243	244
April 1.....	90	91	Oct. 1.....	273	274
May 1.....	120	121	Nov. 1.....	304	305
June 1.....	151	152	Dec. 1.....	334	335

EXAMPLE.—What is the current day of the Julian period corresponding to the last day of Old Style in England, on Sept. 2, A. D. 1752?

1752	1000	1,461,000
4713	600	876,600
6465 year current.	10	14,610
1	6	8,766
4)6464 years elapsed.	R = 0	0
Q = 1616	Jan. 1 to Sept. 1,	244
R = 0	Sept. 1 to Sept. 2,	1
		2,361,221 days elapsed.
	Current day the	2,361,222d.

(930.) To find the same for any given date, New Style. Proceed as above, considering the date as a Julian date, and disregarding the change of style. Then, from the resulting days, subtract as follows:—

For any date of New Style, antecedent to March 1, A. D. 1700..... 10 days.
After Feb. 28, 1700, and before March 1, A. D. 1800..... 11 days.
" 1800 " " 1900..... 12 days.
" 1900 " " 2100..... 13 days, &c.

If the integer part, Julian Date Number (JDN), of a particular epoch is known, then the Julian date and remaining Julian Date Fraction (JF) can be calculated as shown below (12:00 UT). The JF is the remainder of the day and can be specified to any degree of accuracy with trailing decimals:

$$Julian\ Date = Julian\ Date\ Number + Julian\ Date\ Fraction$$

$$JD = JDN + \frac{Hour - 12}{24} + \frac{Minute}{1440} + \frac{second}{86400}$$

The results produced from the simulations in this thesis splits the whole number into two parts. The Julian date and Julian date fraction.

$$1\,JD = 0.5\,JD + 0.5\,JDF$$

Note that this is equivalent to the above definition of a Julian date. It should not be confused with the *Modified Julian Date* (MJD) standard. In this standard, a correction of 0.5 was made to have the date coincide with the start of day on the civil calendar and to drop the first two digits, "24". (McCarthy, 1998).

$$Modified\ Julian\ Date = JD - 2400000.5$$

The MJD standard was adopted by the International Astronomical Union (IAU) in 1997 (Chapter IV: Resolutions of the General Assembly,1999). The organisation mentions that both are in use, but it should be clearly stated which one is in use where applied.

2.5.5 TEME coordinates system

The SGP4 algorithm outputs satellite positions in the True Equator Mean Equinox (TEME) coordinate system (Vallado et al., 2006). TEME is a type of Earth-Centered Inertial (ECI) coordinate system, i.e., it does not rotate with respect to the stars. The X-axis points toward the vernal equinox. The Z-axis runs along the Earth's rotational axis, pointing towards the North pole. The Y-axis completes the right-handed orthogonal system (Kelso, 2019a). See figure 2.16 for an illustration. Because of Earth's axial precession, "True Equator" means that the Z-axis is aligned with the instantaneous North Pole. The Earth's axial tilt changes slightly with respect to the ecliptic due to nutation, so "Mean Equinox" refers to the mean direction of the vernal equinox (Kelso, 2019b). Kelso also mentions since observations of satellites are made by stations fixed to the Earth's surface, the elements generated will be referenced relative to the true equator, but this is not true for the vernal equinox, as it is not tied to the Earth's surface, but rather to the Earth's orientation in space. TEME is therefore only accurate for the epoch of the element set.

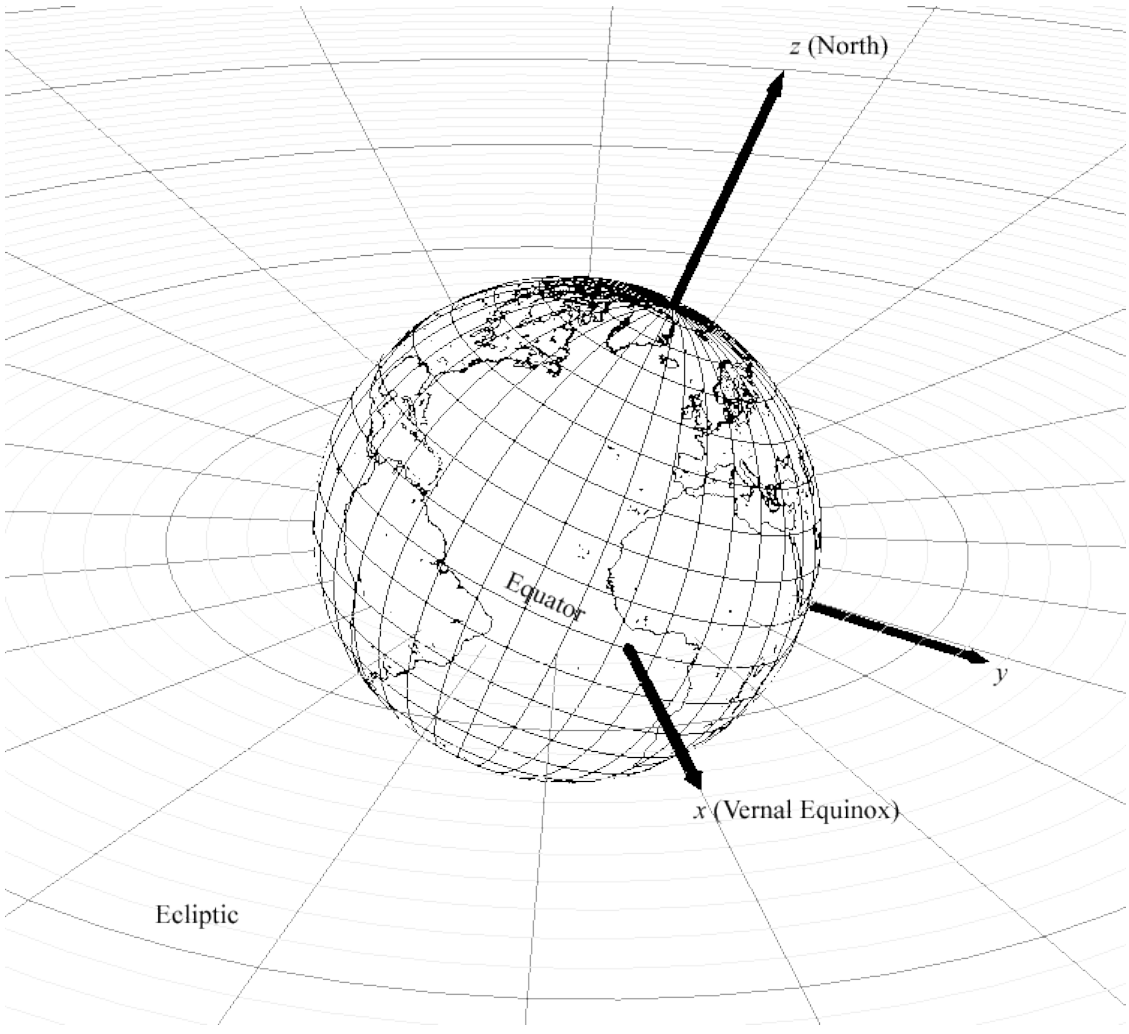

Figure 2.16: TEME reference frame (Kelso, 2019a)

CHAPTER 3: SIMULATION DESIGN AND IMPLEMENTATION

3.1 SIMULATION DESIGN

3.1.1 Design methodology

Cubesat data was downloaded from celestrak.com in the form of a text file. The text file was looped in the program to get an array of node objects (node-array). Each object contained the name and TLE data of the cubesats, every three lines. A future date array (date-array) was created using equal intervals in the form of Julian dates and Julian date fractions, which could be specified by the user.

The node-array and date-array were then fed into the SGP4 algorithm. SGP4 produced future data for each node object contained in three arrays: a position-array, velocity-array and error-array. The position-array contained the 3-axis coordinates of each node inside the TEME reference frame at the specified future Julian dates. The corresponding velocities at those positions are contained in the velocity-array. The auto-generated error-array contained errors (if any) of each data set produced.

In every set, the position array only contains single point values of the positions of the nodes in space. To achieve calculations of node intersection, the link budget specifications had to be applied. This was achieved by extending the coordinate system of the main node to represent the reach capabilities of the node. Since the assumption was made that the swarm of nodes have equal reach capabilities, the coordinate extension calculations need only be run on each node in the swarm for its own position to guarantee reach. For demonstration purposes, ZACube-2 was chosen to run the calculations on. Figure 3.1 demonstrates the outlay of the simulations.

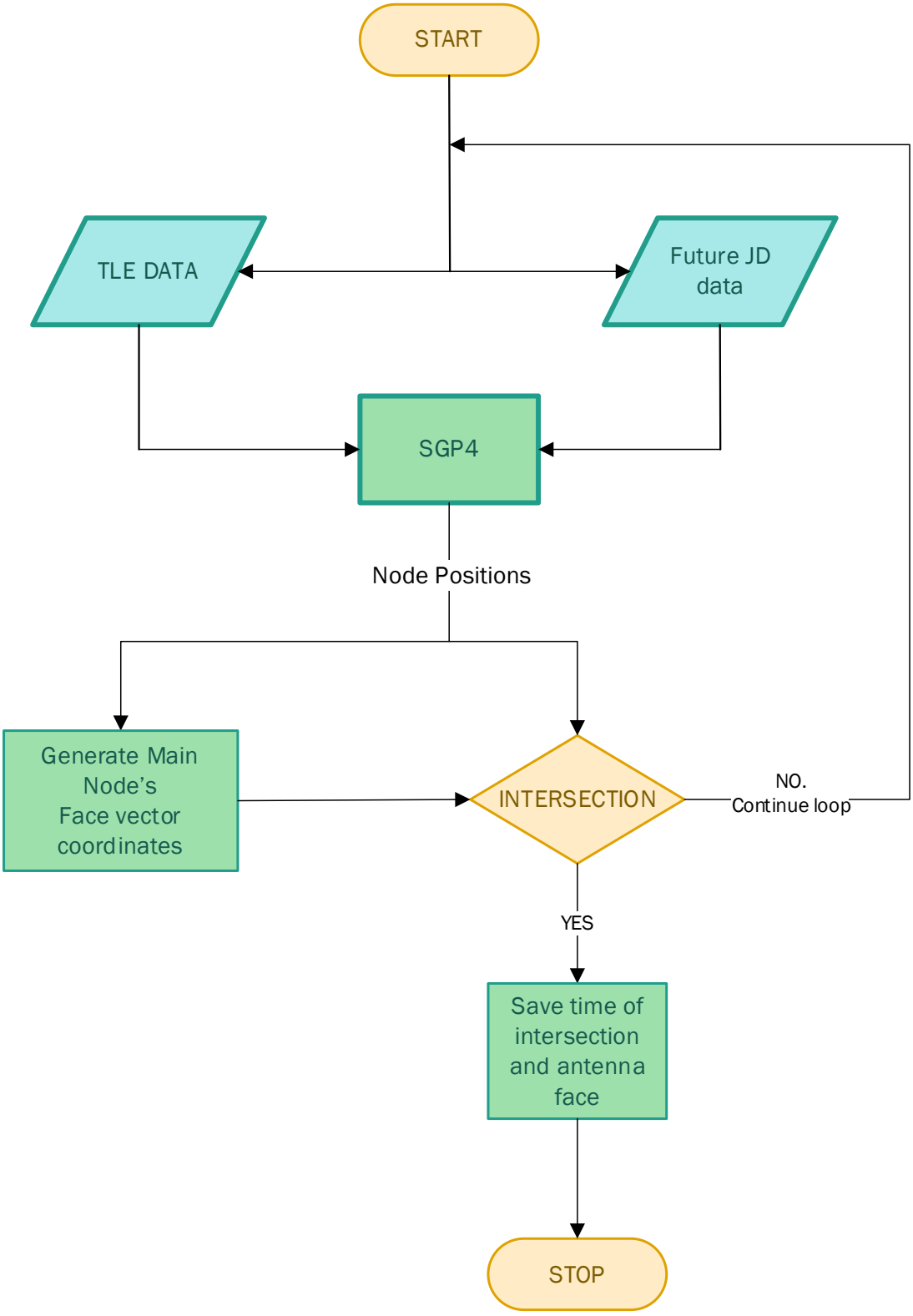

Figure 3.1: Simulation logic

3.1.2 Link establishment logic

With a set of stored data containing the time of intersection and matching antennae (from running the SGP4 algorithm in figure 3.1), the nodes can use their internal synchronised clocks to keep track of dates and activate the matching antenna at the time of intersection to establish a communication session. The link logic is showcased in figure 3.2.

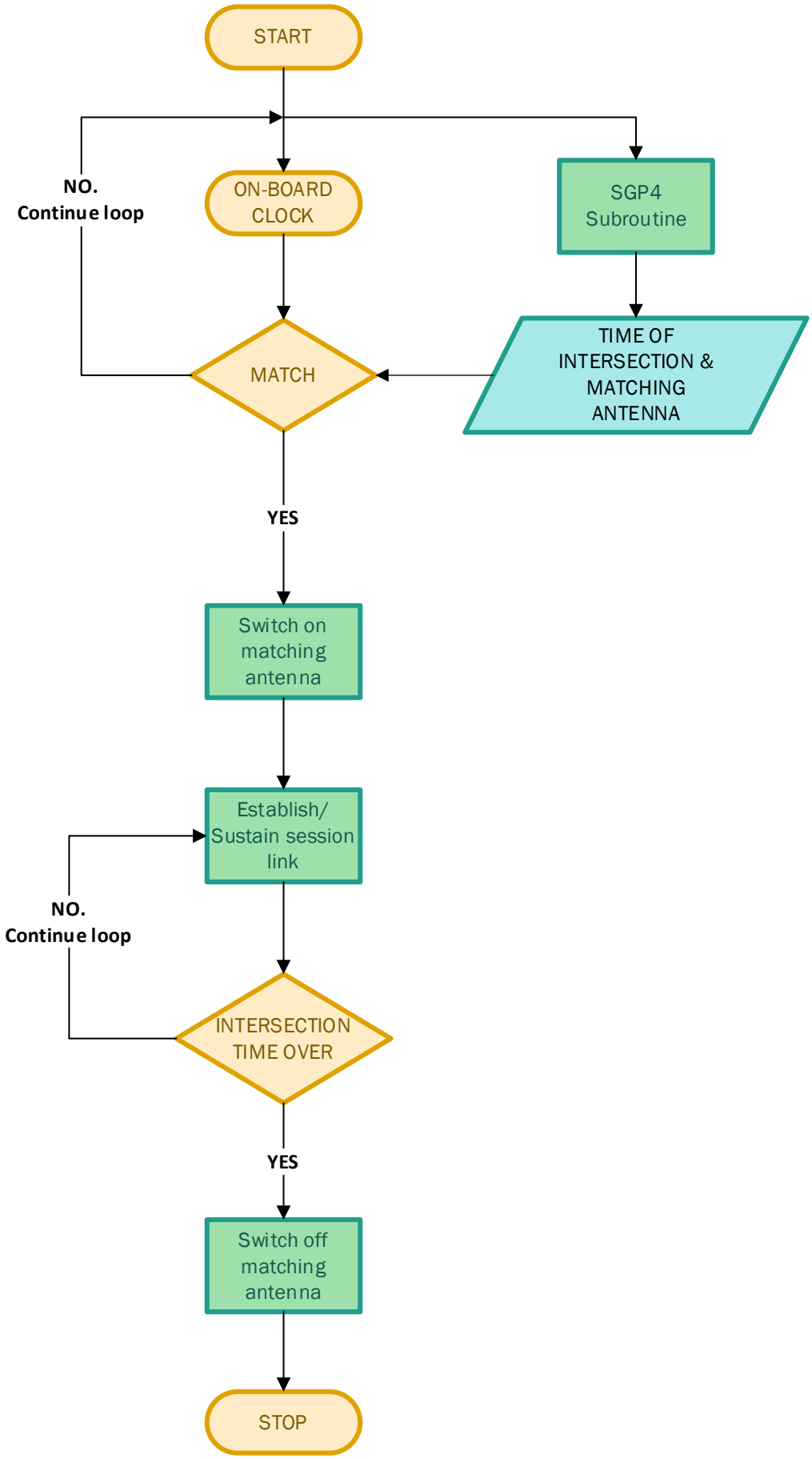

Figure 3.2: Link establishment logic

3.1.3 Face vector coordinates

This section discusses the creation of face vector coordinates, which are established in accordance with link budget specifications and are needed for intersection calculation checks. As indicated in figure 3.3, orbiting cubesats always have their nadir pointing towards the Earth using attitude control, therefore constantly changing their internal reference frame with respect to the Earth's reference frame (ECI). Taking this into account, the coordinates were calculated for the main node, producing a unique set of reference frames on every future date.

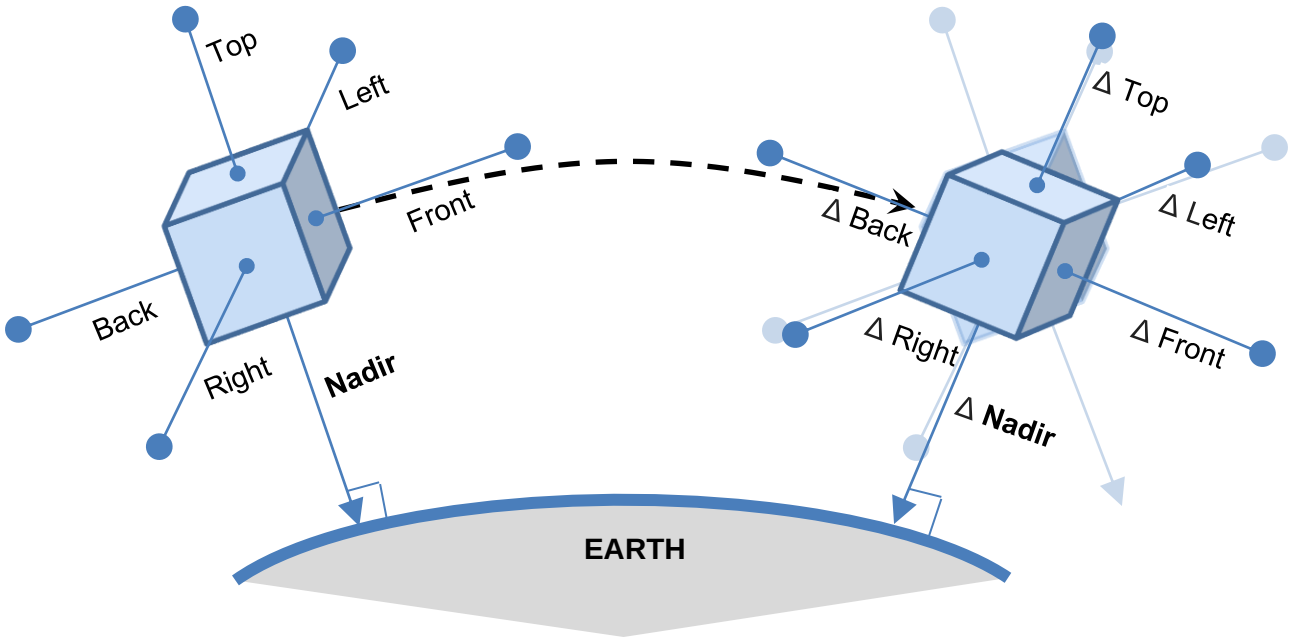

Figure 3.3: Changing reference frames

Following, is a demonstration of how this was achieved using ZACube-2's coordinates:

Table 3.1: ZACube-2 TLE data

```
                                INFORMATION
-------------------------------------------------------------------------------
Epoch:  2020-08-29 04:09:06.718752+00:00     Julian Date: 2459090.5  Fr:  0.17299443
-------------------------------------------------------------------------------
TLE Line 1:  1 45727U 20037E   20241.53941820  .00000438  00000-0  49559-4 0  9999

TLE Line 2:  2 45727  97.7048  59.9823 0014060  61.1123 299.1474 14.91221757  8769
```

TLE data at Epoch in table 3.1, corresponding to:

Julian date: 2459090.5

Fraction: 0.17299443

Coordinates: (-5247.75784913 , 4447.36848974 , 0.00061897)

Satellite reach capabilities were specified as follow:

$Pointing\ offset\ distance$: $148km$

$Antenna\ beam\ width$: 30°

The satellite's antenna beam was modelled as a cone as seen in figure 3.4.

The height of the cone:

$$Cone\ height = \cos\left({}^{beam\ width}/_{2}\right) \times pointing\ offset$$

$$Cone\ height = \cos(15°) \times 148\ km$$

$$Face\ vector = \ Cone\ height = \ 142.957km$$

$$Max\ beam\ radius = \tan\ ({}^{beam\ width}/_{2}) \times pointing\ offset$$

$$Max\ beam\ radius = \tan(15°) \times 148km$$

$$Max\ beam\ radius = \ 38.305\ km$$

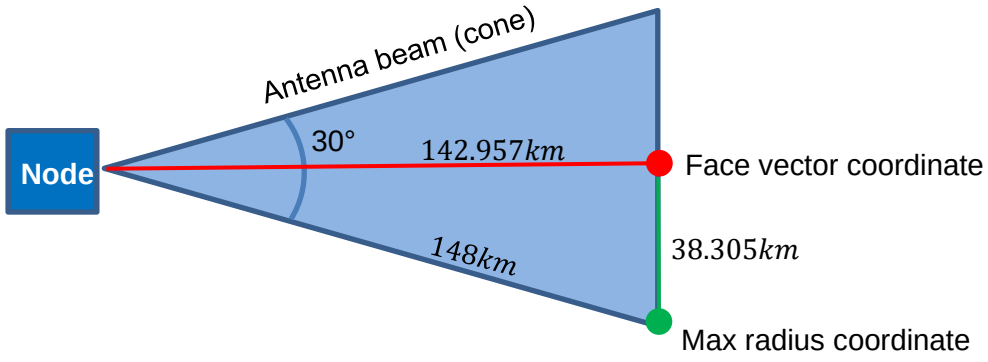

Figure 3.4: Antenna Beam stretch

In all simulations, the starting point of each cone is located at the node's centre (position coordinate).

3.1.3.1 Top coordinates

The Top coordinate was found by extending the altitude vector.

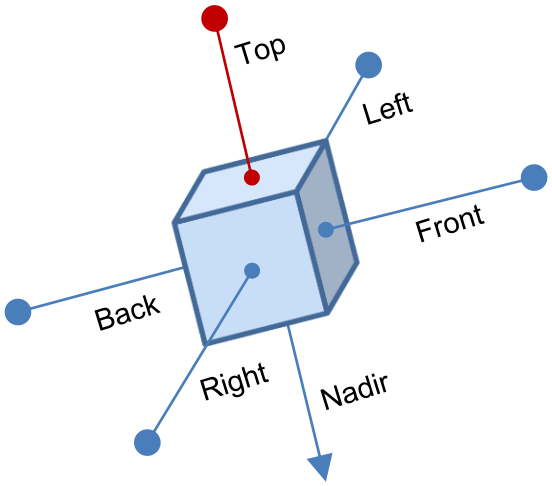

Figure 3.5: Top coordinate

$$\boldsymbol{MainNode}_{\boldsymbol{current\ position}} \approx (-5247.7578, 4447.3685, 0.0006)$$

$$Distance\ to\ centre\ of\ Earth = \sqrt{\sum \boldsymbol{MainNode}_{\boldsymbol{current\ position}}^{\boldsymbol{2}}}$$

$$Distance\ to\ centre\ of\ Earth = \sqrt{(-5247.7578)^2 + 4447.3685^2 + 0.00062^2}$$

$$Distance\ to\ centre\ of\ Earth \approx 6878.8116\ km$$

$$Top\ Distance = Distance\ to\ centre + Cone\ height$$

$$Top\ Distance \approx 6878.8116\ km + 142.957\ km$$

$$Top\ Distance \approx 7021.7686\ km$$

$$Extend\ ratio = \frac{Top\ Distance}{Distance\ to\ centre\ of\ Earth}$$

$$Extend\ ratio \approx \frac{7021.7686}{6878.8116}$$

$$Extend\ ratio \approx 1.0207822267503797$$

$$\boldsymbol{Top}_{\boldsymbol{Coordinates}} = Extend\ Ratio \times (\boldsymbol{MainNode}_{\boldsymbol{current\ position}})$$

$$\boldsymbol{Top}_{\boldsymbol{Coordinates}} \approx 1.0207822267503797 \times (-5247.7578, 4447.3685, 0.00062)$$

$$\boldsymbol{Top}_{\boldsymbol{Coordinates}} \approx (-5356.8179, 4539.7947, 0.0006)$$

3.1.3.2 Right and Left coordinates

The Right and Left coordinates were obtained using vectors perpendicular to the orbital plane. The forward direction of the satellite was deduced by taking the next future date position into account. The straight-line vector pointing from the current position to the future position contains the direction of orbit, hence the direction of the front part of the satellite. The current position, future position and earth centre position form an osculating plane containing the current orbital plane. The normal vector to this plane was obtained using the cross product between the Top Coordinate vector and future date vector.

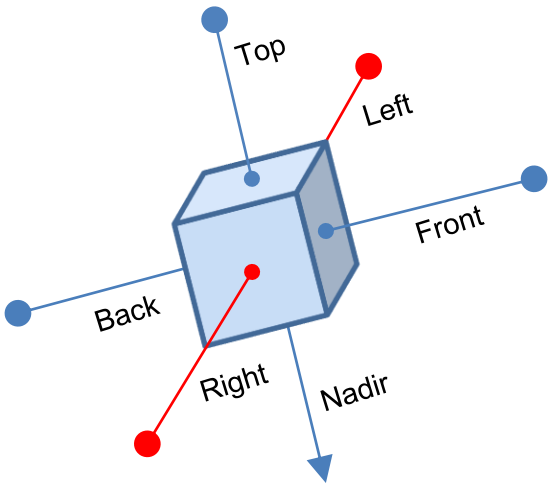

Figure 3.6: Right and Left coordinates

$$\boldsymbol{MainNode_{future\ position}} = (-5247.1376\ ,4448.1023\ ,7.5506)$$

$$\boldsymbol{Forward_{vector}} = \boldsymbol{MainNode_{future\ position}} - \boldsymbol{MainNode_{current\ position}}$$

$$\boldsymbol{Forward_{vector}} \approx (-5247.1376\ ,4448.1023\ ,7.5506) - (-5247.7578\ ,4447.3685\ ,0.0006)$$

$$\boldsymbol{Forward_{vector}} \approx (0.62021656\ ,0.73378567\ ,7.54999682)$$

$$\boldsymbol{Top_{vector}} = \boldsymbol{Top_{Coordinates}} - \boldsymbol{MainNode_{current\ position}}$$

$$\boldsymbol{Top_{vector}} \approx (-5356.8179\ ,4539.7947\ ,0.0006) - (-5247.7578\ ,4447.3685\ ,0.0006)$$

$$\boldsymbol{Top_{vector}} = (-109.06009355\ ,92.4262204\ ,0.00001286)$$

$$\boldsymbol{Crossproduct_{orbital\ plane}} = \boldsymbol{Top_{vector}} \times \boldsymbol{Forward_{vector}}$$

$$\boldsymbol{Crossproduct_{orbital\ plane}} = (-109.06009355\ ,92.4262204\ ,0.00001286) \times (0.62021656\ ,0.73378567\ ,7.54999682)$$

$$\boldsymbol{Crossproduct_{orbital\ plane}} = (-697.81766065\ ,-823.4033675\ ,137.35100599)$$

$$Crossproduct_{Length} = \sqrt{\sum \boldsymbol{Crossproduct_{orbital\ plane}}^{2}}$$

$$Crossproduct_{Length} = \sqrt{(-697.81766065\ )^2 + (-823.4033675)^2\ +\ 137.35100599^2}$$

$$Crossproduct_{Length} \approx\ 1088.0294 \text{ km}$$

$$\boldsymbol{Crossproduct_{Normalised}} = \frac{\boldsymbol{Crossproduct_{orbital\ plane}}}{Crossproduct_{Length}}$$

$$\boldsymbol{Crossproduct_{Normalised}} = (-0.64135922\ , -0.75678414\ , 0.12623833)$$

$$\boldsymbol{Right_{Coordinates}} = \boldsymbol{Crossproduct_{Normalised}} \times\ Cone\ height + \boldsymbol{MainNode_{current\ position}}$$

$$\boldsymbol{Right_{Coordinates}}$$
$$= (-0.64135922\ , -0.75678414\ , 0.12623833) \times 142.957$$
$$+\ (-5247.7578\ , 4447.3685\ , 0.0006)$$

$$\boldsymbol{Right_{Coordinates}} = (-5339.4447\ , 4339.1809\ , 18.0473)$$

The Left coordinates were calculated in the same manner as the Right coordinates, but in the opposite direction by making the norm negative.

$$\boldsymbol{Left_{Coordinates}} = -\boldsymbol{Crossproduct_{Normalised}} \times\ Cone\ height + \boldsymbol{MainNode_{current\ position}}$$

$$\boldsymbol{Left_{Coordinates}}$$
$$= -(-0.64135922\ , -0.75678414\ , 0.12623833) \times 142.957$$
$$+\ (-5247.7578\ , 4447.3685\ , 0.0006)$$

$$\boldsymbol{Left_{Coordinates}} = (-5156.0710\ , 4555.5561\ , -18.0460)$$

3.1.3.3 Front and Back coordinates

The Front and Back coordinates, as indicated in figure 3.7, could be obtained by utilising a future position. A future position vector would point in the forward direction, but it is not completely 90° to the Top coordinate since the orbital path is radial and not straight. It must be mentioned that it would suffice with increasing accuracy if shorter future date intervals are taken, but if the user specifies a longer interval, the coordinates would be off. It was therefore not used as a method of calculation. Instead, the Front and Back coordinates were obtained by calculating the normal vector of the plane which is perpendicular to the orbital plane.

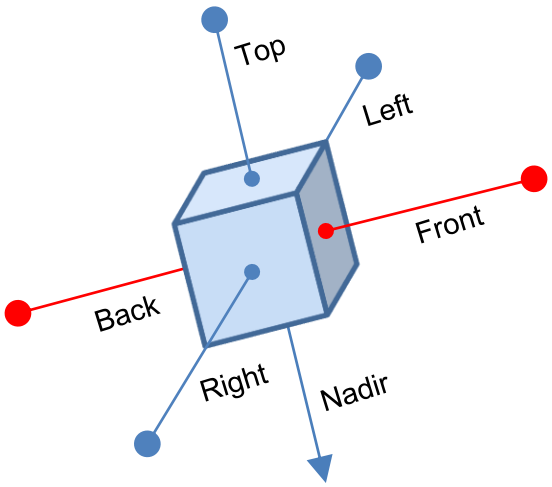

Figure 3.7: Front and Back coordinates

$$\boldsymbol{Right}_{\boldsymbol{vector}} = \boldsymbol{Right}_{\boldsymbol{Coordinates}} - \boldsymbol{MainNode}_{\boldsymbol{current\ position}}$$

$$\boldsymbol{Right}_{\boldsymbol{vector}} = (-5339.4447\,, 4339.1809\,, 18.0473) - (-5247.7578\,, 4447.3685\,, 0.0006)$$

$$\boldsymbol{Right}_{\boldsymbol{vector}} = (-91.68680396, -108.1876\,, 18.0467)$$

$$\boldsymbol{Crossproduct}_{\boldsymbol{plane}\ \perp \boldsymbol{to\ orbital\ plane}} = \boldsymbol{Right}_{\boldsymbol{vector}} \times \boldsymbol{Top}_{\boldsymbol{vector}}$$

$$\boldsymbol{Crossproduct}_{\boldsymbol{plane}\ \perp \boldsymbol{to\ orbital\ plane}} = (-91.68680396, -108.1876\,, 18.0467) \times (-109.06009355\,, 92.4262204\,, 0.00001286)$$

$$\boldsymbol{Crossproduct}_{\boldsymbol{plane}\ \perp \boldsymbol{to\ orbital\ plane}} = (-1667.9856, -1968.1688, -20273.2153)$$

$$Crossproduct_{Length} = \sqrt{\sum \boldsymbol{Crossproduct}_{\boldsymbol{plane}\ \perp \boldsymbol{to\ orbital\ plane}}^{\boldsymbol{2}}}$$

$$Crossproduct_{Length} = \sqrt{(-1667.9856\,)^2 + (-1968.1688)^2 + (-20273.2153)^{\boldsymbol{2}}}$$

$$Crossproduct_{Length} \approx 20436.7102\ km$$

$$\boldsymbol{Crossproduct_{Normalised}} = \frac{\boldsymbol{Crossproduct_{plane\ \perp to\ orbital\ plane}}}{Crossproduct_{Length}}$$

$$\boldsymbol{Crossproduct_{Normalised}} = (-0.08161712\,, -0.09630556\,,\ -0.99199994)$$

$$\boldsymbol{Back_{Coordinates}} = \boldsymbol{Crossproduct_{Normalised}} \times Cone\ height + \boldsymbol{MainNode_{current\ position}}$$

$$\boldsymbol{Back_{Coordinates}} = (-0.08161712\,, -0.09630556\,, -0.99199994) \times 142.957 + (-5247.7578\,, 4447.3685\,, 0.0006)$$

$$\boldsymbol{Back_{Coordinates}} = (-5259.4256\,, 4433.6009\,, -141.8127)$$

The Front coordinates were calculated in the same manner as the Right coordinates, but in the opposite direction by making the norm negative.

$$\boldsymbol{Front_{Coordinates}} = -\boldsymbol{Crossproduct_{Normalised}} \times Cone\ height + \boldsymbol{MainNode_{current\ position}}$$

$$\boldsymbol{Front_{Coordinates}} = -(-0.08161712\,, -0.09630556\,, -0.99199994) \times 142.957 + (-5247.7578\,, 4447.3685\,, 0.0006)$$

$$\boldsymbol{Front_{Coordinates}} = (-5236.0901\,, 4461.1360\,, 141.8140)$$

The Main node's cone centre coordinates on all faces are visualised in figure 3.8:

$$\boldsymbol{Top_{Coordinates}} = (-5356.8179\,, 4539.7947\,, 0.0006)$$

$$\boldsymbol{Right_{Coordinates}} = (-5339.4447\,, 4339.1809\,, 18.0473)$$

$$\boldsymbol{Left_{Coordinates}} = (-5156.0710\,, 4555.5561\,, -18.0460)$$

$$\boldsymbol{Front_{Coordinates}} = (-5236.0901\,, 4461.1360\,, 141.8140)$$

$$\boldsymbol{Back_{Coordinates}} = (-5259.4256\,, 4433.6009\,, -141.8127)$$

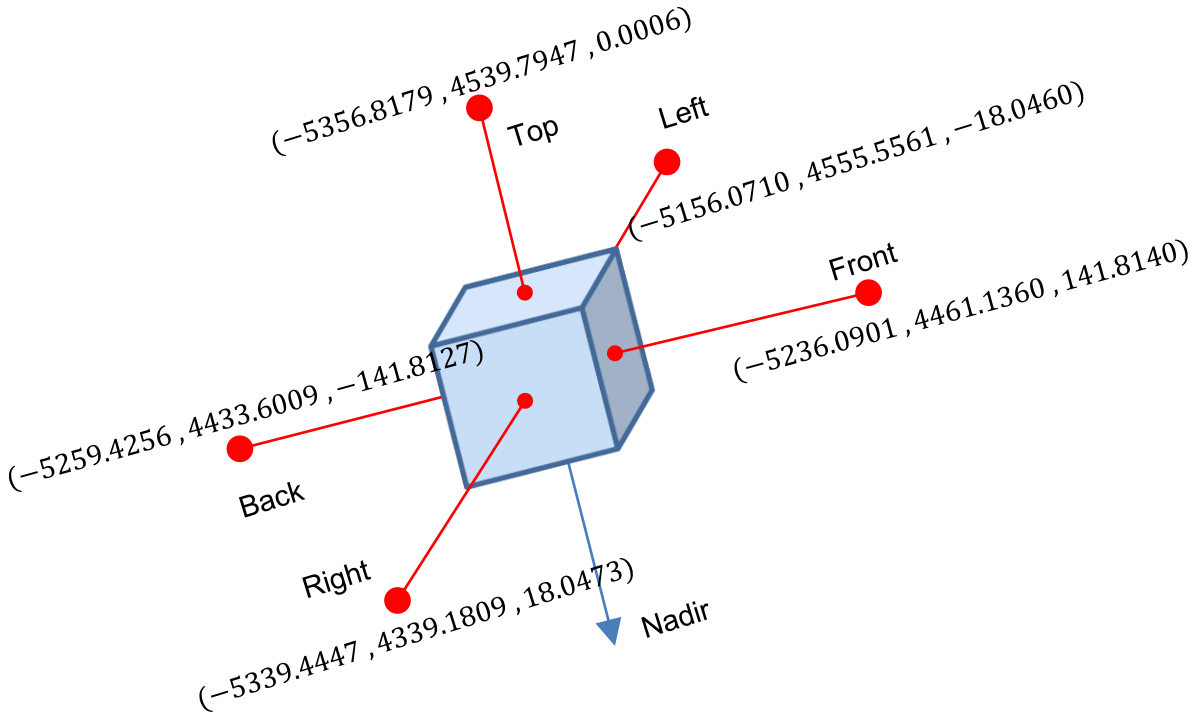

Figure 3.8: Face cone centre coordinates

3.1.4 Intersection determination

The intersection determination check needs to be performed for all antenna faces. The process stays the same – it is only the coordinates that change with the particular antenna face. The process is demonstrated below:

The node in question will have a particular position coordinate in the TEME reference frame, e.g., $\boldsymbol{NodeToCheck_{position}} \approx (-1322.4451 , -3403.4493 , -5992.7938)$

Referring back to figure 3.1, intersection is achieved if the position coordinate of another node in the swarm falls within one of the antenna cone-sections of the main node, generated at the position of the main node e.g.,

$\boldsymbol{MainNode_{current\ position}} \approx (-5247.7578 , 4447.3685 , 0.0006)$

The concept is illustrated in figure 3.9

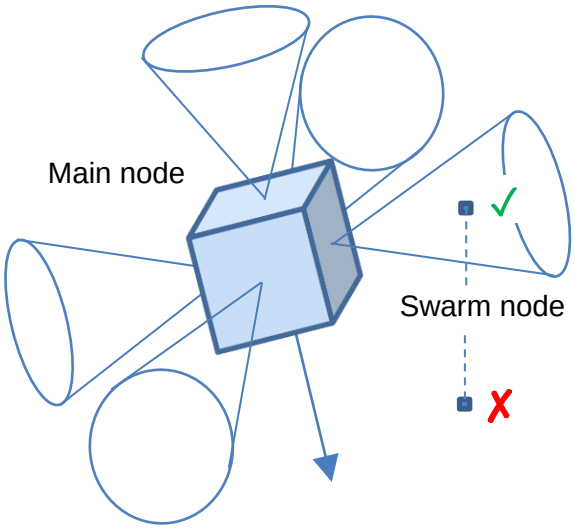

Figure 3.9: Intersection at front antenna

First the normalised face vectors were calculated:

$$\boldsymbol{Antenna_{Vector}} \approx \boldsymbol{MainNode_{current\ position}} - \boldsymbol{FaceVector_{Coordinates}}$$

$$\boldsymbol{Antenna_{VectorNormalised}} \approx \boldsymbol{Antenna_{Vector}} / Cone\ height$$

A cone can be thought of as an infinite number of circles around a straight line. The circle's radius is proportional to the node's projection on the straight-line over the distance from the main node position.

The straight-line distances were already calculated in section 3.1.3, giving the unique coordinate lines for each face on the main node at a particular epoch. The projection of the node in question on the straight line was found using the dot product between the normalised face vector and the vector between MainNode and NodeToCheck.

$$\boldsymbol{Projection_{OnStraightline}} = (\boldsymbol{NodeToCheck_{position}} - \boldsymbol{MainNode_{current\ position}}) \times \boldsymbol{Antenna_{VectorNormalised}}$$

$$\boldsymbol{Projection_{Length}} = Cone\ height - \boldsymbol{Projection_{OnStraightline}}$$

At this point, the following condition must be met. If not, the check for this face antenna can stop and the values can be excluded from the calculations as it is already out of reach:

$$\boldsymbol{Projection_{Length}} \leq Cone\ height$$

If the perpendicular distance of the cone straight line to the node in question (figure 3.10) fell within the proportional radius of the antenna beam, then intersection is achieved and possible link connection can be established.

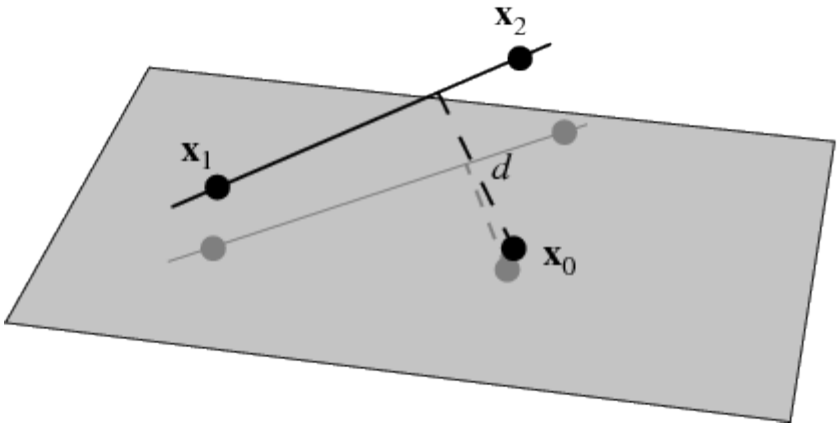

Figure 3.10: Node distance from cone straight line (Wolfram MathWorld, 2020)

$$\boldsymbol{Beam_{radius}} = \left({}^{Max\ beam\ radius}/_{Cone\ height}\right) \times \boldsymbol{Projection_{Length}}$$

$$\boldsymbol{ProjectionCoordinate_{OnStraightline}} = -\boldsymbol{Antenna_{VectorNorm}} \times \boldsymbol{Projection_{Length}} + \boldsymbol{MainNode_{current\ position}}$$

$$\boldsymbol{Node_{radius}} = \sqrt{\sum \left(\boldsymbol{NodeToCheck_{position}} - \boldsymbol{ProjectionCoordinate_{OnStraightline}}\right)^2}$$

And finally, if the following condition is true, then the nodes' antenna beams are intersecting:

$$\boldsymbol{Node_{radius}} \leq \boldsymbol{Beam_{radius}}$$

At this point, the intersection time is saved in the memory, together with the appropriate antenna direction at which the intersection occurs. The correct face antenna will then activate at the time of intersection. Using this analytical method, the onboard power resources should be conserved when compared to a scan algorithm that constantly searches for a node in the network.

3.1.5 Operational principal

Since the topological design is a simulation, there needs to be a speculative establishment of rules that govern how these cubesats would receive the TLE data. The TLE data is essentially what makes the cubesat “smart”, i.e., it is able to determine its own position and the positions of other nodes with this knowledge.

Rules

1. Every time a node passes over a ground station, the newest TLE data will be updated.
2. When nodes interact with each other, they will check who has the newest database and update their own TLE data to that of the newer revision.
3. When a new cubesat is launched, it will not contain an updated TLE data set and will not know where its peers are. It must first make contact with a base station. Upon contact, the newest TLE data will be sent.

Important notes

NORAD might not immediately be able to generate TLE data for the specific node upon launch, so it might take a few days for any new nodes to connect to the network. The node will establish contact via rules 1 and 2.

TLE data might be updated more frequently on Earth than it takes to spread throughout the swarm. This is acceptable, since the purpose of updating the TLE data is to increase the accuracy of on-board calculations when determining intersection.

3.2 DATA PREPARATION

As of 14-10-2020, 179 cubesats' TLE data could be obtained. The cubesats' TLE data, which were obtained from *celestrak.com,* were stored as text files. The orbital data for ZACube-2 and ZACube-1 were searched for and moved to the top of the list so that they will always be included in the simulations. The calculations that follow uses the first node, ZACube-2, as the main node on which the simulations are run. An excerpt from the text file is shown in figure 3.11.

```
ZACUBE-2
1 43907U 18111AH  20242.17299443  .00000496  00000-0  22826-4 0  9997
2 43907  97.2573 139.7194 0019833 245.0879 114.8298 15.24652637 93096
ZACUBE-1 (TSHEPISOSAT)
1 39417U 13066B   20241.98147533  .00000199  00000-0  31143-4 0  9994
2 39417  97.5685 235.9805 0059911  41.2521 319.3197 14.81308338365778
CUTE-1 (CO-55)
1 27844U 03031E   20241.89379352  .00000041  00000-0  38343-4 0  9997
2 27844  98.6828 248.5363 0009376 199.4377 160.6444 14.22252967890398
CUBESAT XI-IV (CO-57)
1 27848U 03031J   20242.01189617  .00000034  00000-0  35220-4 0  9992
2 27848  98.6894 249.2153 0009043 212.2525 147.8101 14.21838103890286
CUBESAT XI-V
1 28895U 05043F   20241.87245014  .00000084  00000-0  25021-4 0  9990
2 28895  98.0195  16.2388 0017858  55.5479 304.7408 14.63793593791203
CUTE-1.7+APD II (CO-65)
1 32785U 08021C   20241.73170021  .00000158  00000-0  22579-4 0  9999
2 32785  97.5782 226.5885 0011473 251.9024 108.0945 14.88505249668621
AAUSAT-II
1 32788U 08021F   20242.00140514  .00000296  00000-0  31925-4 0  9995
2 32788  97.4930 243.2825 0012013 164.6537 195.5051 14.95126054670250
DELFI-C3 (DO-64)
1 32789U 08021G   20241.86975266  .00001311  00000-0  89308-4 0  9996
2 32789  97.4133 282.1241 0013564  71.0693 289.2005 15.07879567672728
SEEDS II (CO-66)
1 32791U 08021J   20241.94298601  .00000271  00000-0  32675-4 0  9998
2 32791  97.5449 232.9077 0012219 215.5933 144.4472 14.91097140669266
```

Figure 3.11: Cubesat TLE data extract

For simulations of swarms that consisted of more than 179 nodes, cubesat data from 14-10-2020 were combined with TLE data from 05-11-2020. Leaving a timeframe of 22 days between TLE data will ensure sufficient drift to guarantee that they are not in the same position anymore and can thus be taken as separate nodes added to the swarm. Specifically, the original data from 14-10-2020 were always kept (with the two ZACube satellites moved to the top). ZACube-2's data were removed from the 05-11-2020 set. TLE data from 05-11-2020 were taken from the bottom upwards until a sufficient amount was reached to complete the swarm size.

3.3 DATA ACCURACY

The SGP4 algorithm uses a future Julian date array as input, as explained in section 3.1.1. The number of calculations that the nanosatellite will run is directly proportional to the time interval between future dates chosen. In order to ensure that a nanosatellite interaction is not missed, a suitable time interval needed to be chosen. The time interval must not be too small, otherwise, the calculation time will increase significantly and place unnecessary strain on the otherwise limited resources of the satellite. The time interval was chosen by comparing the information from a 200-strong nanosatellite swarm. The time intervals started at 8-seconds and were halved each time until no information was lost and no more new information could be obtained, thus reaching an equilibrium between calculation time and output. The below figures illustrate the selection choice of time parameters to run during the simulations.

<u>Simulation parameters for testing time intervals:</u>
Running for: ZACube-2
Time increments: 8, 4, 2, 1, 0.5 seconds
Julian time fraction: 9.259259259259259e-05 (in case of 8s)
Number of dates to plot: Time increments/24h
Number of Satellites: 200
Satellite reach: 148 km
Straight-line reach: 142.957km

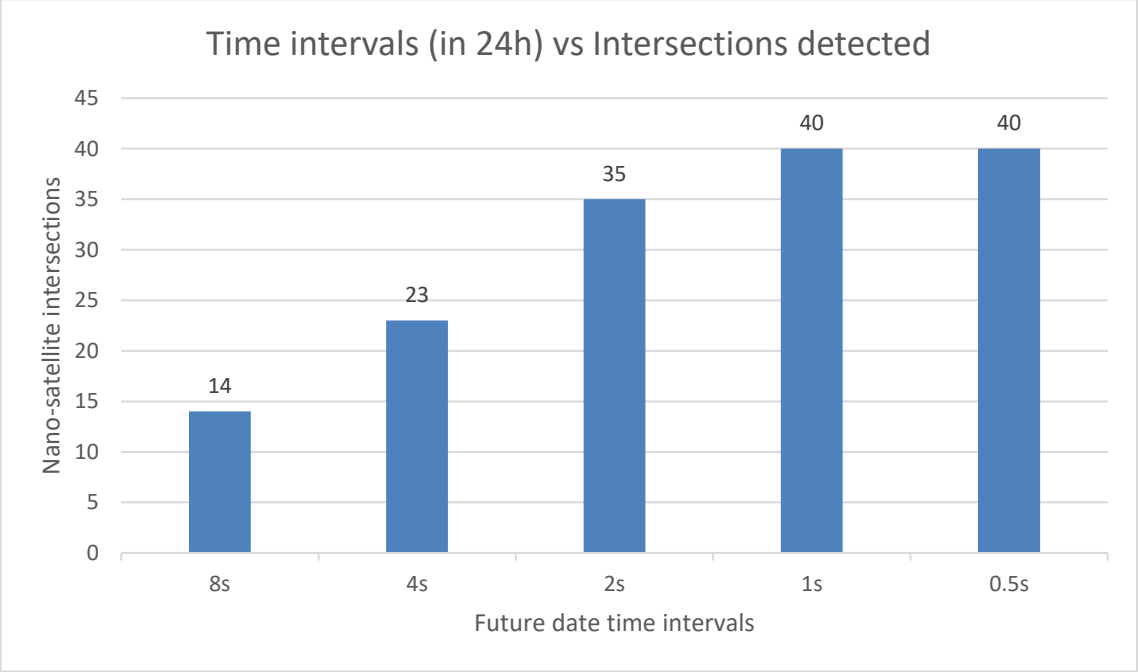

Figure 3.12: Time intervals vs Intersections detected

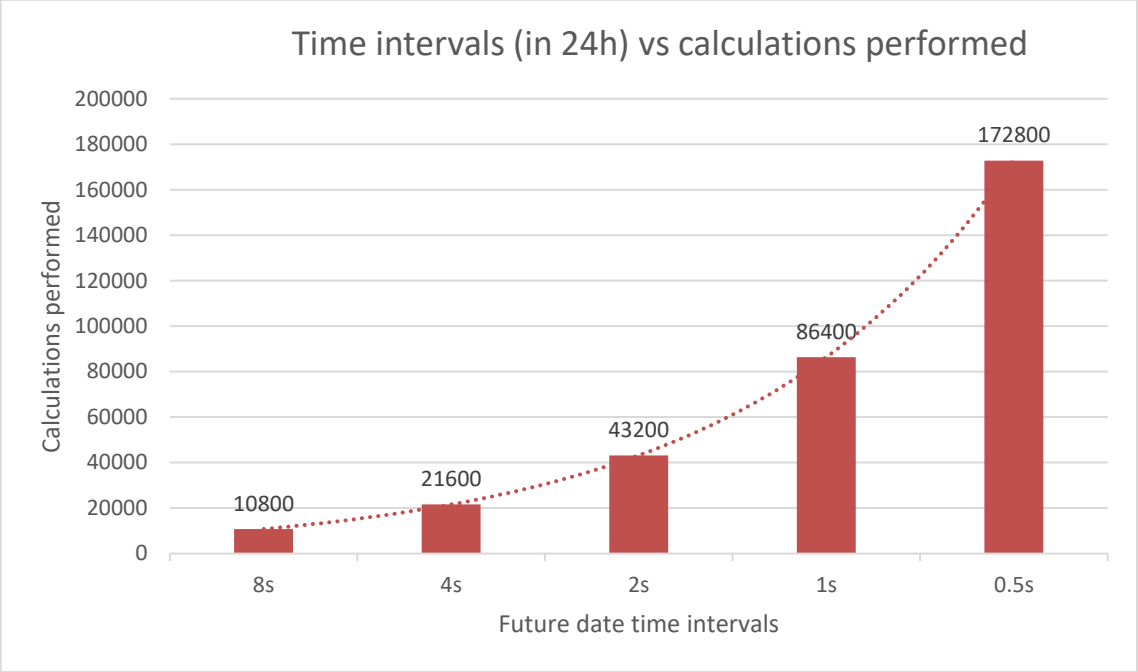

Figure 3.13: Time intervals vs calculations

Figure 3.12 show that intersection information is lost using time intervals greater than 1 second. Below 1 second, information is no longer lost. The number of dates to calculate increases exponentially with the halving of time intervals to fill a 24-hour period, as indicated by figure 3.13. Therefore, it makes sense to choose to run the simulation at:

Time interval = 1 second intervals, corresponding to a Julian date fraction of 1.1574074074074073e-05, which is 84600 calculations for a 24-hours forecast period.

Using this format will yield the fastest simulation time, without loss of information.

CHAPTER 4: RESULTS

4.1 OVERVIEW

Assumptions: The CubeSats' TLE data functions as nodes in the swarm.
Each node is equipped with P2P capabilities and an antenna setup as described in 2.5.2.
Any configuration below that does not fall within the P2P link budget in table 2.2 is deemed hypothetical and serves as an indicator for what technologies of such a reach can achieve.
The signals of the extended hypothetical distances are assumed to have sufficient energy levels to sustain communication.

Four different swarm sizes were analysed, each for a simulated 24-hour period, to see the following characteristics:

- **The unique number of nanosatellite nodes intersecting the main node.**
  This is the number of unique nanosatellites that intersect. If a unique nanosatellite intersects twice per day, it will only count as 1.
- **The number of node intersections.**
  This is the frequency of intersections. If a unique nanosatellite intersects twice per day, it will count as 2.
- **The average time between intersecting nodes.**
  Also stated as the "True mean time between intersections". This is a measure of how concentrated or dispersed the interactions are compared to the "Theoretical mean time between intersections" (24h/intersections). It starts at the first node of intersection and sums time till the last node of intersection, divided by the number of intersections minus 1, specific to the starting epoch of the main node for the duration of the simulation window (86400s).
  For example, 3 intersections are made in a 24h period by only 1 node. If a perfect constellation were designed to create the same effect, these interactions would take place at 28800-second intervals. However, the true mean time between intersections is 2866 seconds (much shorter), indicating that the intersections are concentrated. Note that the true mean time is dependent on the specific 24h window and will change if simulations are performed during another window. **To be able to compare the results, the same time window is always used during the simulations.**

Tables 4.1, 4.2 and 4.3 contain an overview of the parameters in the swarm, which were analysed using the methods discussed in sections 3.1.3 and 3.1.4.

Table 4.1: Simulation swarm sizes

Swarm sizes	50	100	150	200

Table 4.2: Simulation antenna angles

Antenna angle (offset)	15°	30°	45°	60°

Table 4.3: Simulation max reach distance

Max reach distance (from offset)	50km	100km	200km	300km	400km

Time increments: 1 second (discussed in 3.3)

Time period: 24-hours

Time period in Julian Date: 2459090.67299443 → 2459091.67299443

Epoch: 2020-08-29 04:09:06.718752+00:00

Main node: ZACube-2

TLE Line 1: 1 40380U 15003E 20241.70006236 .00001254 00000-0 58312-4 0 9992

TLE Line 2: 2 40380 99.1031 303.7242 0138535 114.4490 247.1260 15.14510546307485

An example of the simulation output is given in the appendix of swarm size 200, 30 degrees beam angle with 200km reach. During the output, the position of the intersecting antenna can also be seen.

4.2 SWARM SIZE: 50

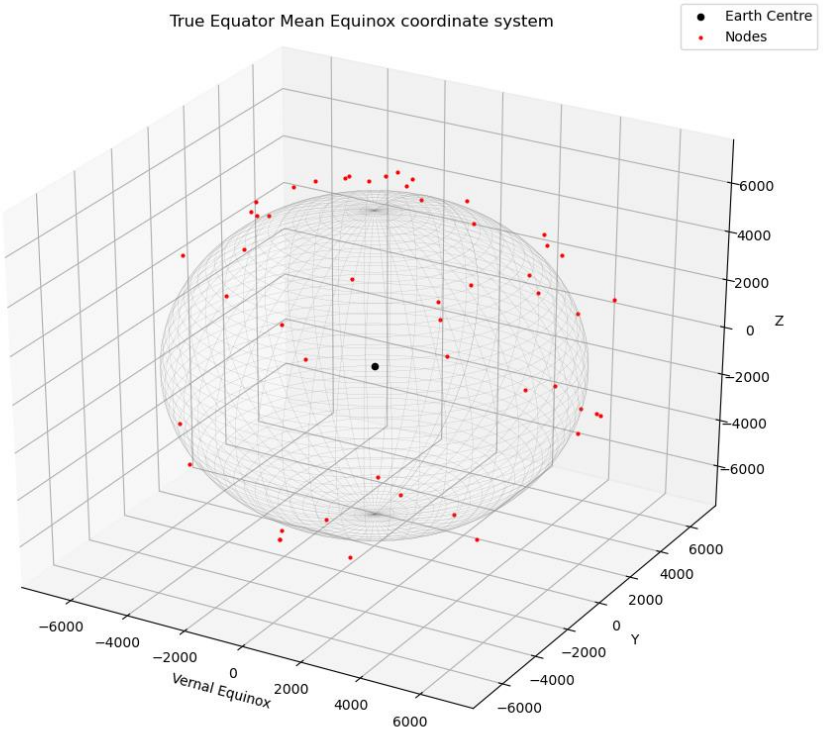

Figure 4.1: 50-Swarm nodes

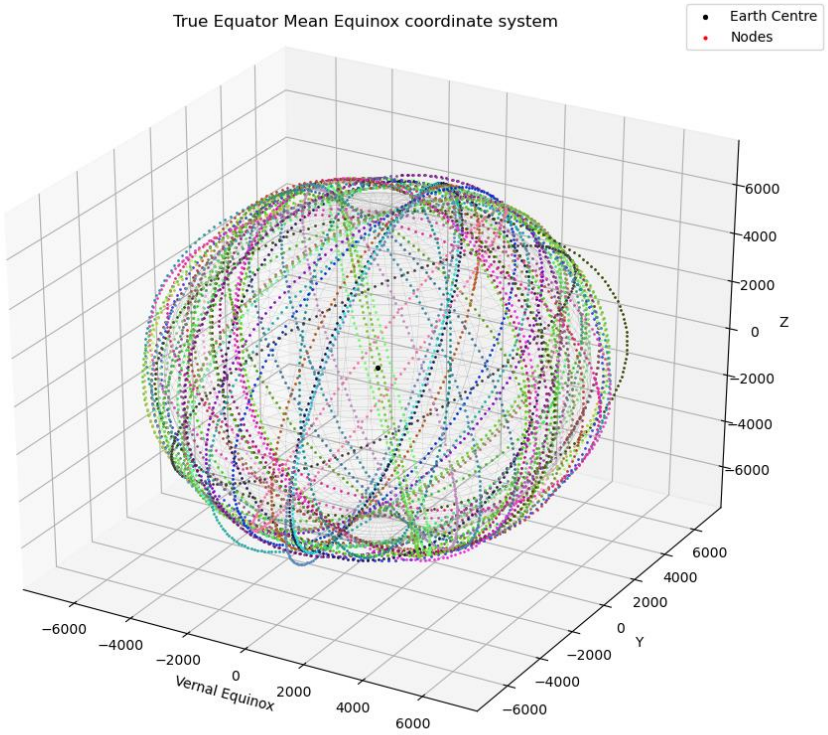

Figure 4.2: 50-Swarm nodes orbits

A visualisation of the simulated nodes is captured in figure 4.1 and orbits in figure 4.2.

4.2.1 Angle: 15°

Table 4.4: Antenna reach parameters 50 Swarm, 15°

Max Antenna Reach (km)	Parallel Straight-line reach (km)
50	49.572
100	99.144
200	198.289
300	297.433
400	396.578

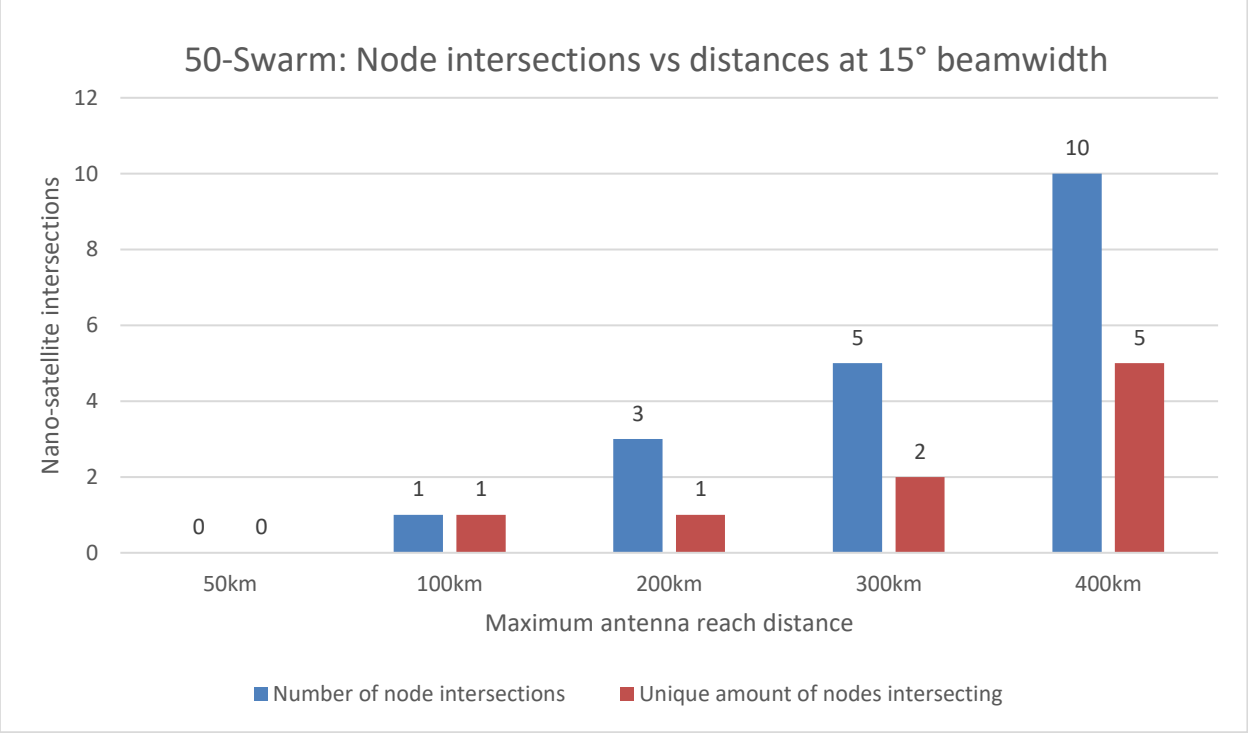

Figure 4.3: 50-Swarm: Node intersections vs distances at 15° beamwidth

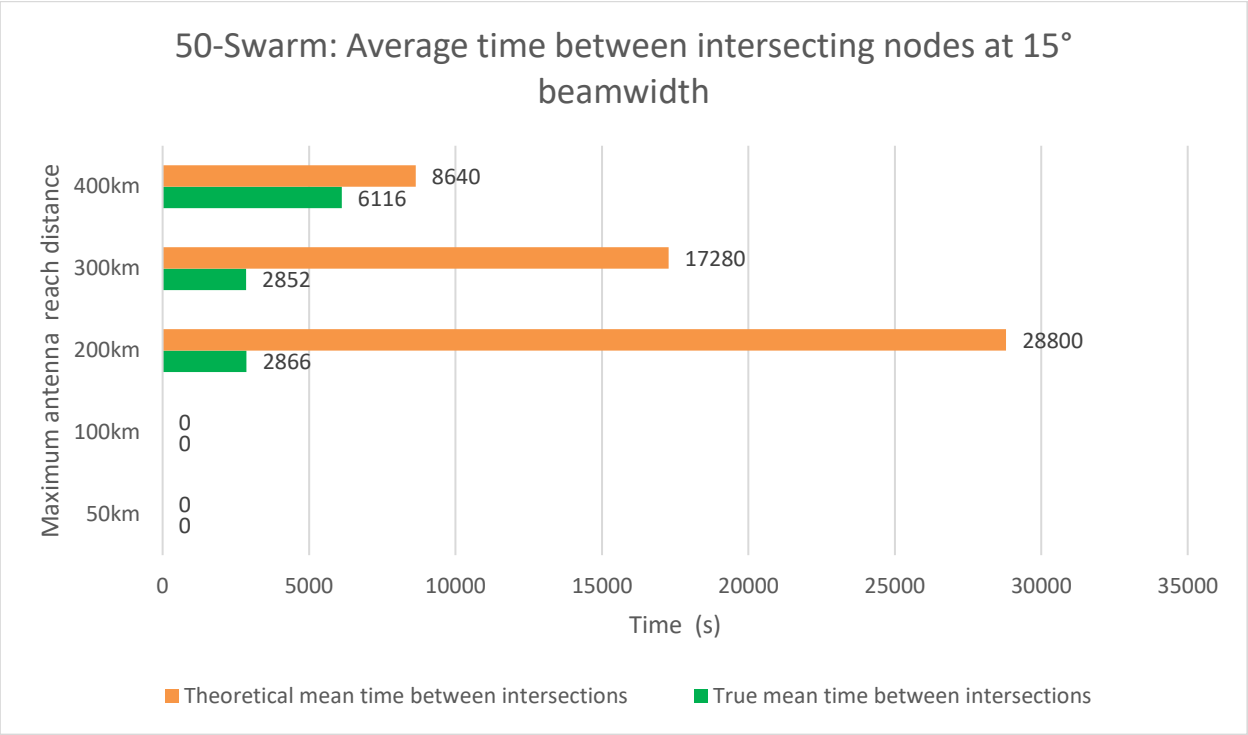

Figure 4.4: 50-Swarm: Average time between intersecting nodes at 15° beamwidth in the 24h-period

4.2.2 Discussion: 50-Swarm with 15° angle

The frequency of intersections is captured in figure 4.3 and the average time of intersections are captured in figure 4.4.

At 50km, no intersections took place, thus 0% connection with the swarm was achieved.

At 100km, 1 intersection was achieved, resulting in 2% connection with the swarm.

At 200km, 3 intersections were achieved but all from the same node, thus still only 2% swarm connection. The time difference is -25934s, indicating that the intersections are 90.05% more concentrated than spread out. This is because one node is orbiting close to the main node, connecting on 3 passes and then not again for the rest of the simulation period.

At 300km, 5 intersections were achieved, which is 166.67% the intersections from the previous range. The time difference is -14428s, making them 83.50% more concentrated. 2 unique nodes intersected, which is 200% the unique nodes from the previous range, connecting with 4% of the swarm.

At 400km, 10 intersections were achieved, which is 200% the intersections from the previous range. The time difference is -2524s, making them 29.21% more concentrated. 5 unique nodes intersected, which is 250% the unique nodes from the previous range, connecting with 10% of the swarm.

4.2.3 Angle: 30°

Table 4.5: Antenna reach parameters 50 Swarm, 30°

Max Antenna Reach (km)	Parallel Straight-line reach (km)
50	48.296
100	96.592
200	193.185
300	289.778
400	386.370

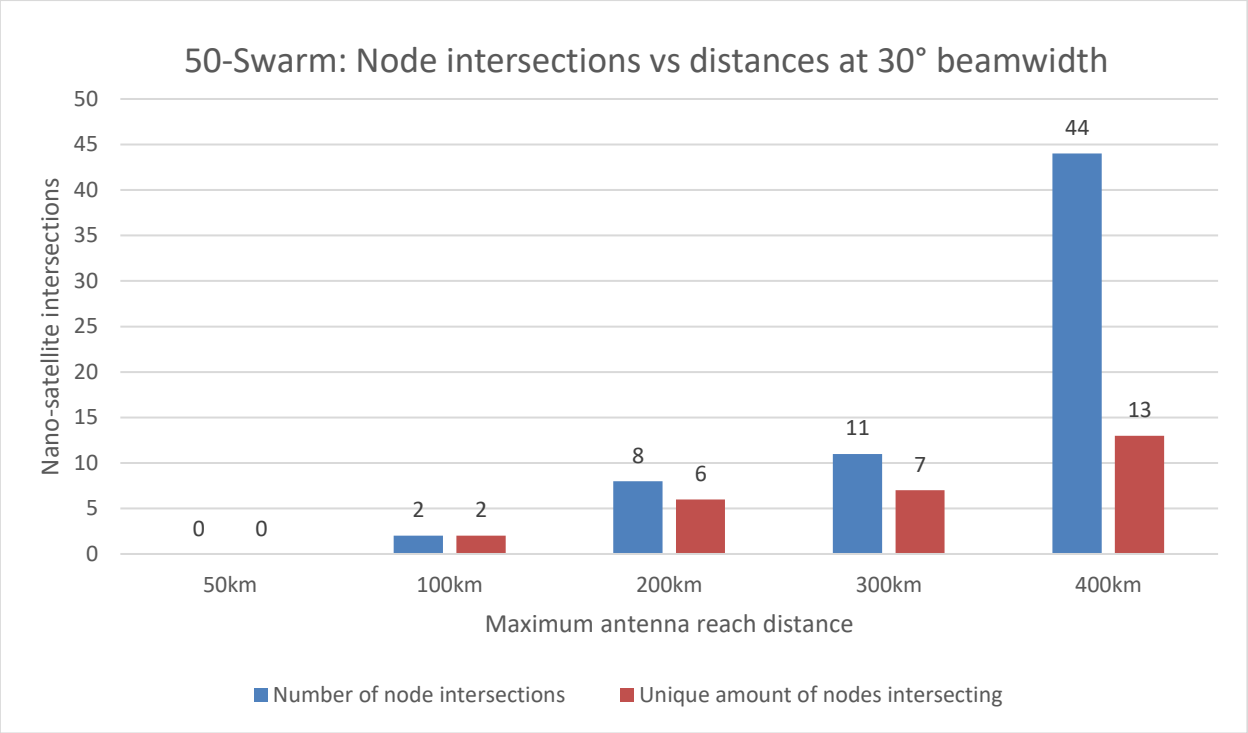

Figure 4.5: 50-Swarm: Node intersections vs distances at 30° beamwidth

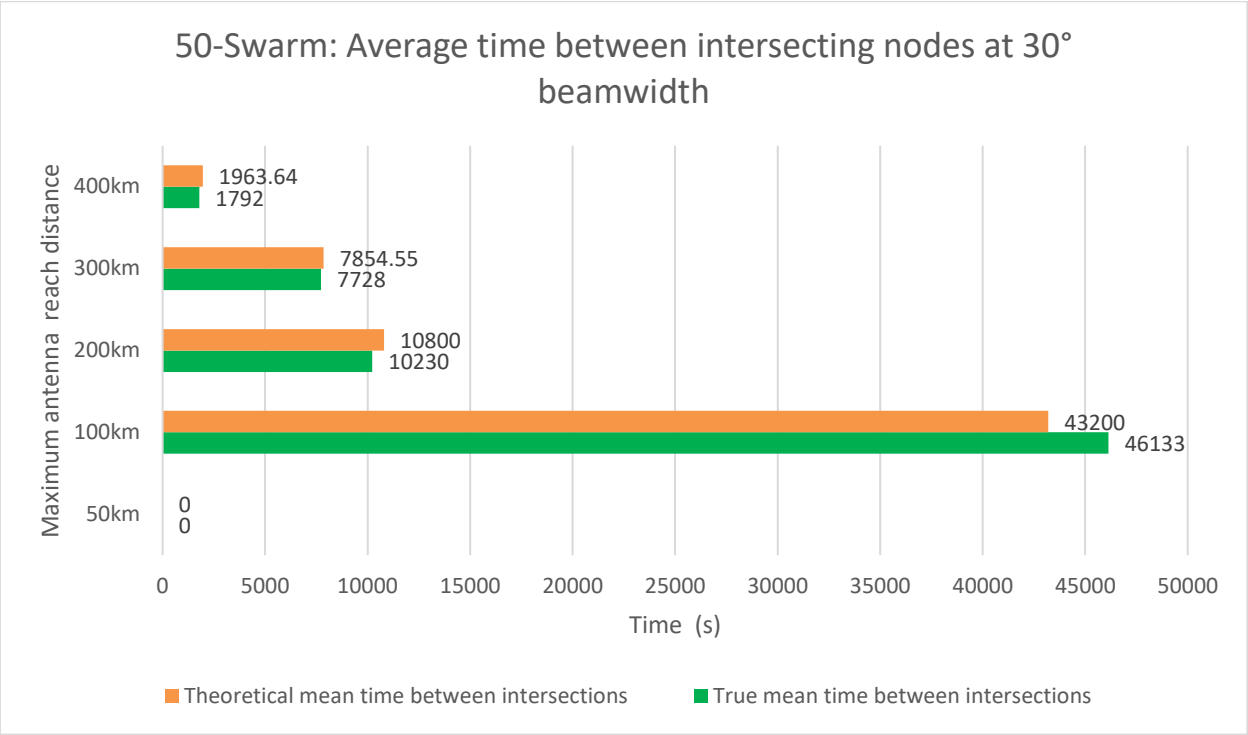

Figure 4.6: 50-Swarm: Average time between intersecting nodes at 30° beamwidth

4.2.4 Discussion: 50-Swarm with 30° angle

The frequency of intersections is captured in figure 4.5 and the average time of intersections are captured in figure 4.6.

At 50km, no intersections took place, thus 0% connection with the swarm was achieved.

At 100km, 2 intersections were achieved. The time difference is +2933s, making them 6.79% less concentrated. 2 unique nodes intersected, connecting with 4% of the swarm.

At 200km, 8 intersections were achieved, which is 400% the intersections from the previous range. The time difference is -570s, making them 5.28% more concentrated. 6 unique nodes intersected, which is 300% the unique nodes from the previous range, connecting with 12% of the swarm.

At 300km, 11 intersections were achieved, which is 137.5% the intersections from the previous range. The time difference is -126.55s, making them 1.61% more concentrated. 7 unique nodes intersected, which is 116.67% the unique nodes from the previous range, connecting with 14% of the swarm.

At 400km, 44 intersections were achieved, which is 400% the intersections from the previous range. The time difference is -171.64s, making them 8.74% more concentrated. 13 unique nodes intersected, which is 185.71% the unique nodes from the previous range, connecting with 26% of the swarm.

4.2.5 Angle: 45°

Table 4.6: Antenna reach parameters 50 Swarm, 45°

Max Antenna Reach (km)	Parallel Straight-line reach (km)
50	46.194
100	92.388
200	184.776
300	277.164
400	369.551

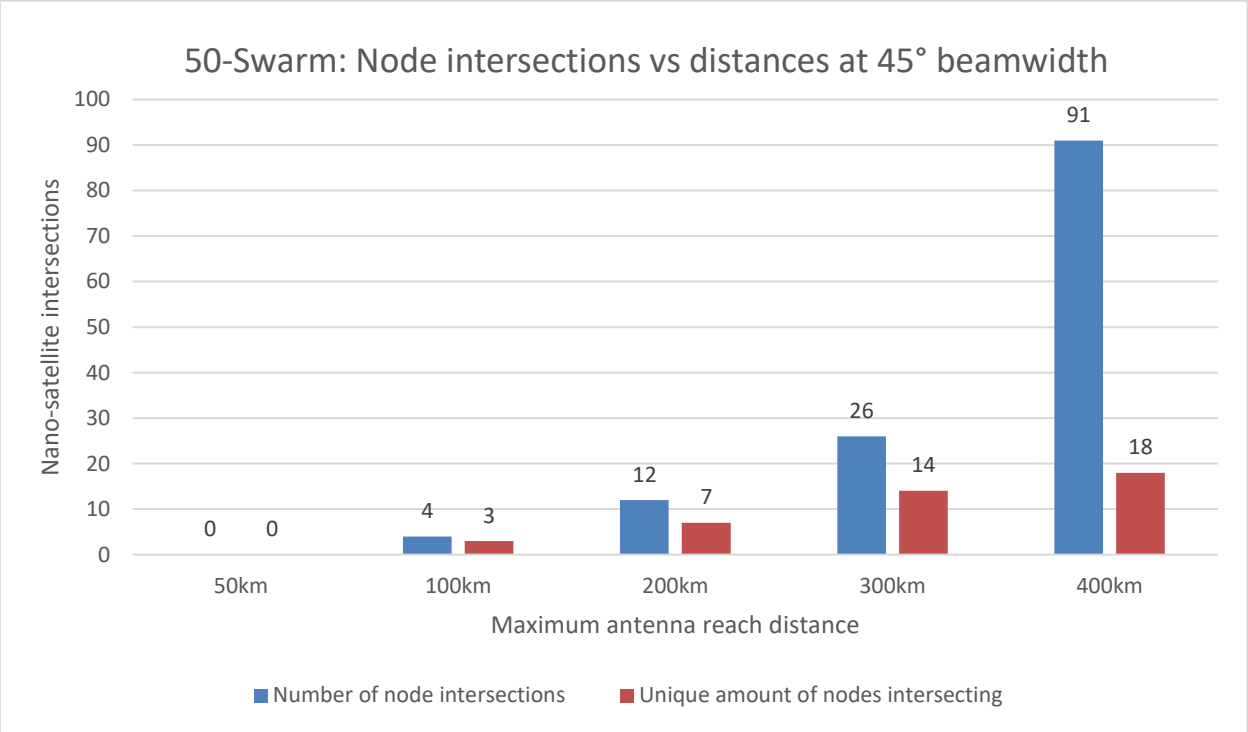

Figure 4.7: 50-Swarm: Node intersections vs distances at 45° beamwidth

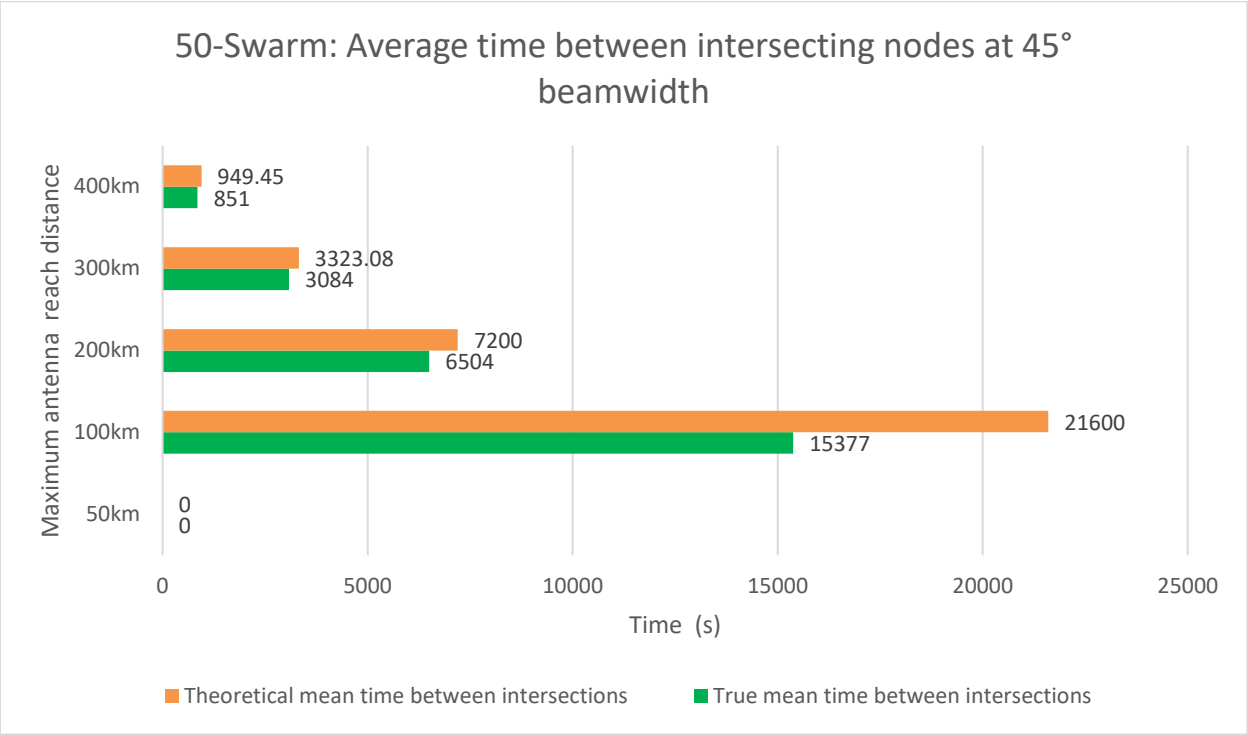

Figure 4.8: 50-Swarm: Average time between intersecting nodes at 45° beamwidth

4.2.6 Discussion: 50-Swarm with 45° angle

The frequency of intersections is captured in figure 4.7 and the average time of intersections are captured in figure 4.8.

At 50km, no intersections took place, thus 0% connection with the swarm was achieved.

At 100km, 4 intersections were achieved. The time difference is -6223s, making them 28.81% more concentrated. 3 unique nodes intersected, connecting with 6% of the swarm.

At 200km, 12 intersections were achieved, which is 300% the intersections from the previous range. The time difference is -696s, making them 9.67% more concentrated. 7 unique nodes intersected, which is 233.33% the unique nodes from the previous range, connecting with 14% of the swarm.

At 300km, 26 intersections were achieved, which is 216.67% the intersections from the previous range. The time difference is -239.08s, making them 7.19% more concentrated. 14 unique nodes intersected, which is 200% the unique nodes from the previous range, connecting with 28% of the swarm.

At 400km, 91 intersections were achieved, which is 350% the intersections from the previous range. The time difference is -98.45s, making them 10.37% more concentrated. 18 unique nodes intersected, which is 128.57% the unique nodes from the previous range, connecting with 36% of the swarm.

4.2.7 Angle: 60°

Table 4.7: Antenna reach parameters 50 Swarm, 60°

Max Antenna Reach (km)	Parallel Straight-line reach (km)
50	43.301
100	86.603
200	173.205
300	259.808
400	346.411

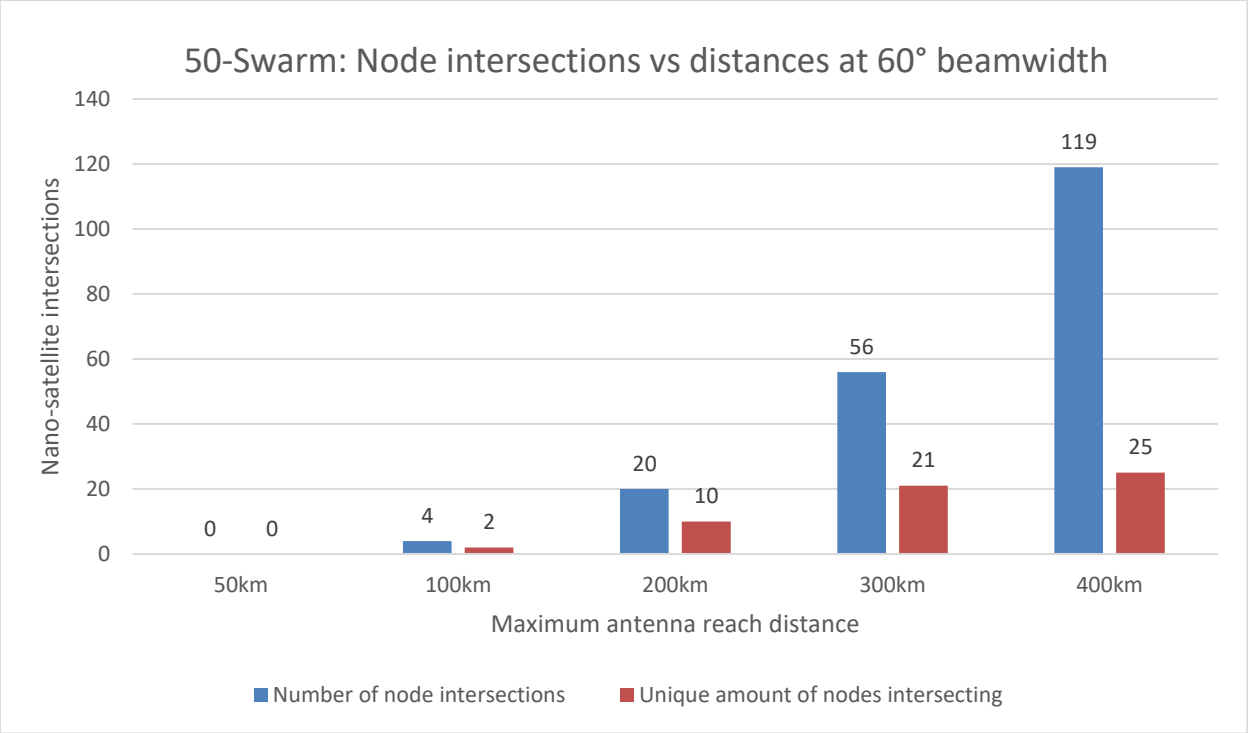

Figure 4.9: 50-Swarm: Node intersections vs distances at 60° beamwidth

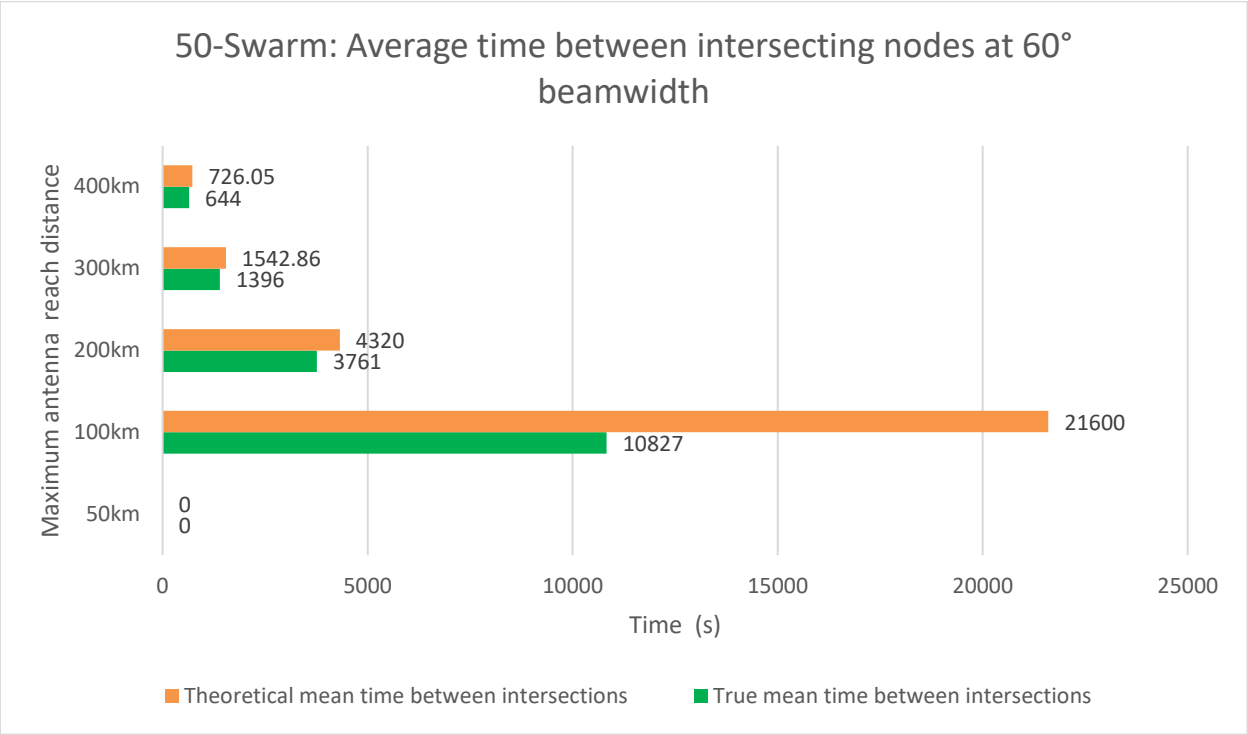

Figure 4.10: 50-Swarm: Average time between intersecting nodes at 60° beamwidth

4.2.8 Discussion: 50-Swarm with 60° angle

The frequency of intersections is captured in figure 4.9 and the average time of intersections are captured in figure 4.10.

At 50km, no intersections took place, thus 0% connection with the swarm was achieved.

At 100km, 4 intersections were achieved. The time difference is -10773s, making them 49.88% more concentrated. 2 unique nodes intersected, connecting with 4% of the swarm.

At 200km, 20 intersections were achieved, which is 500% the intersections from the previous range. The time difference is -559s, making them 12.94% more concentrated. 10 unique nodes intersected, which is 500% the unique nodes from the previous range, connecting with 20% of the swarm.

At 300km, 56 intersections were achieved, which is 280% the intersections from the previous range. The time difference is -146.86s, making them 9.52% more concentrated. 21 unique nodes intersected, which is 210% the unique nodes from the previous range, connecting with 42% of the swarm.

At 400km, 119 intersections were achieved, which is 212.5% the intersections from the previous range. The time difference is -82.05s, making them 11.30% more concentrated. 25 unique nodes intersected, which is 119.05% the unique nodes from the previous range, connecting with 50% of the swarm.

4.3 SWARM SIZE: 100

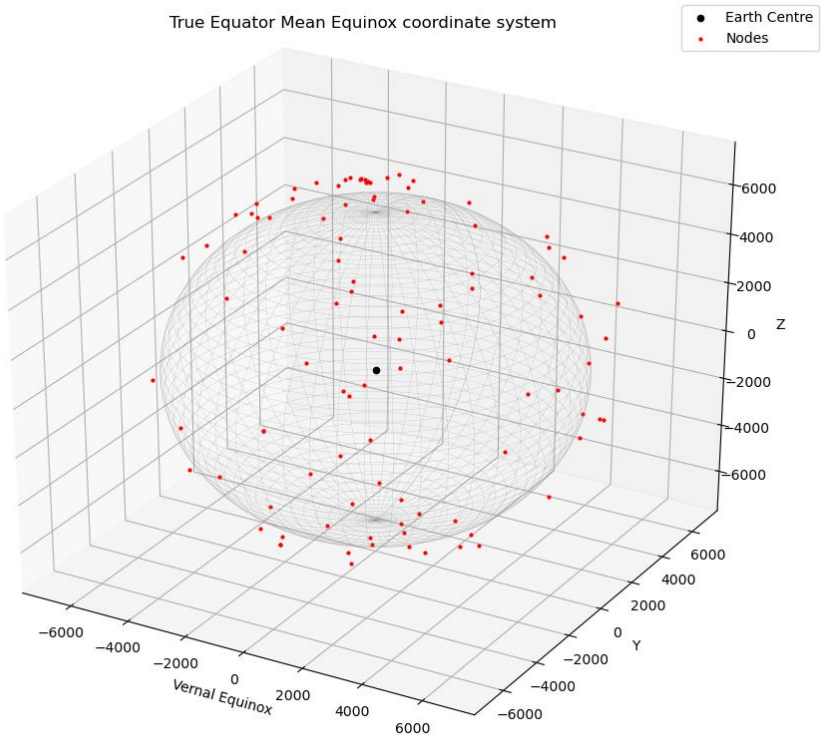

Figure 4.11: 100-Swarm nodes

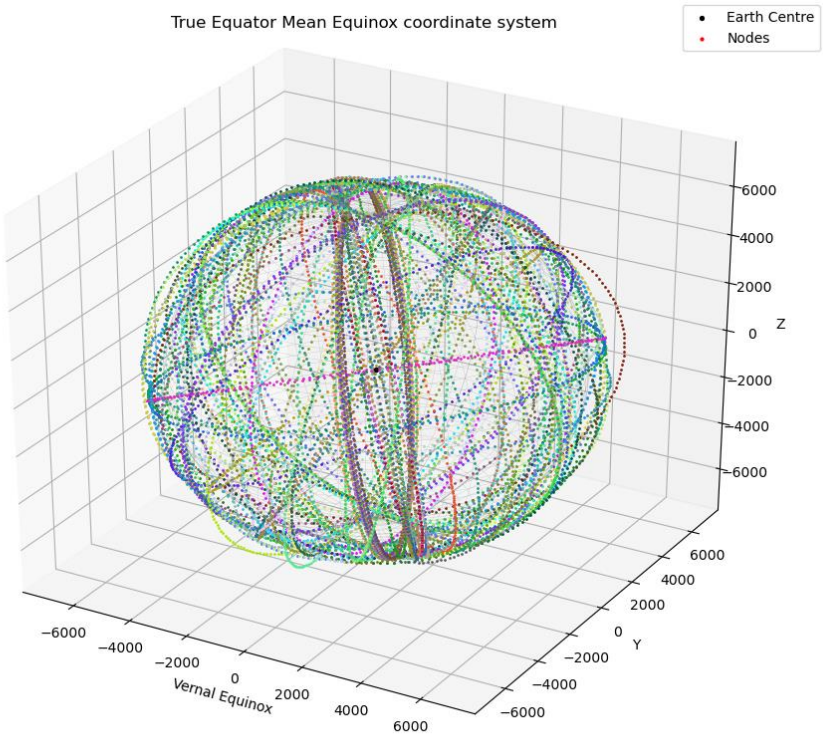

Figure 4.12: 100-Swarm nodes orbits

A visualisation of the simulated nodes is captured in figure 4.11 and orbits in figure 4.12.

4.3.1 Angle: 15°

Table 4.8: Antenna reach parameters 100 Swarm, 15°

Max Antenna Reach (km)	Parallel Straight-line reach (km)
50	49.572
100	99.144
200	198.289
300	297.433
400	396.578

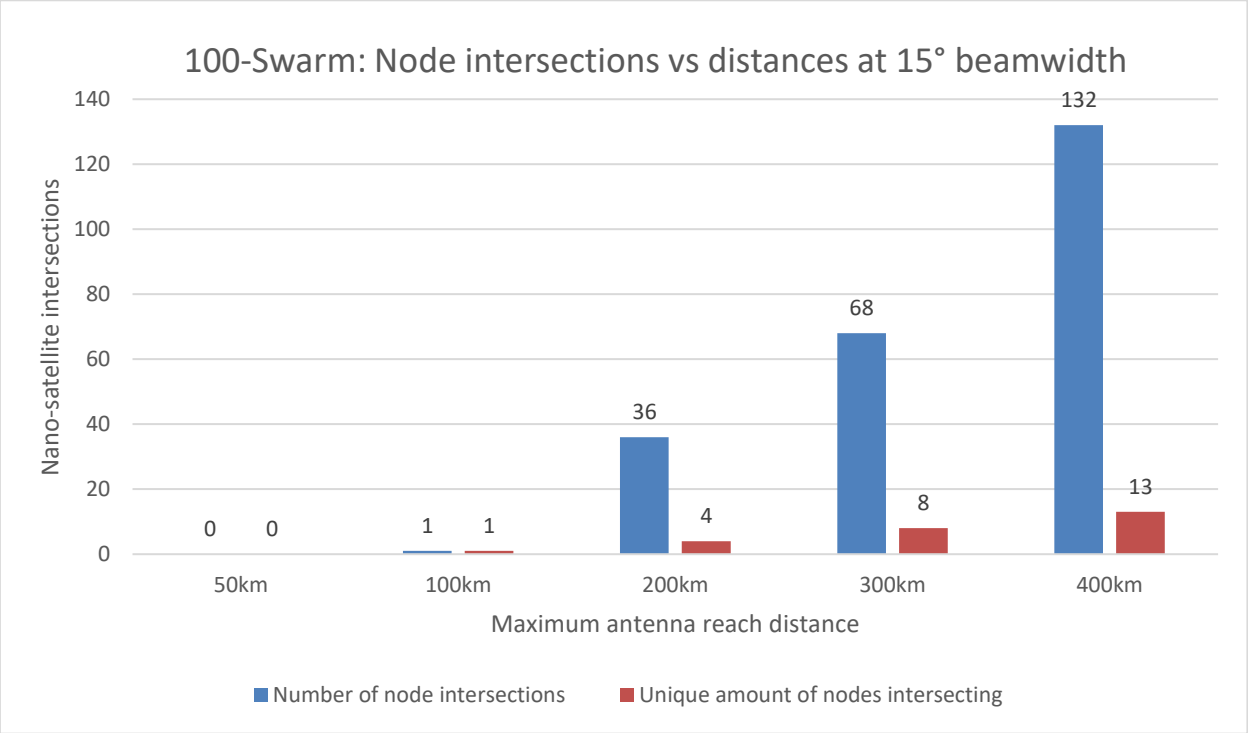

Figure 4.13: 100-Swarm: Node intersections vs distances at 15° beamwidth

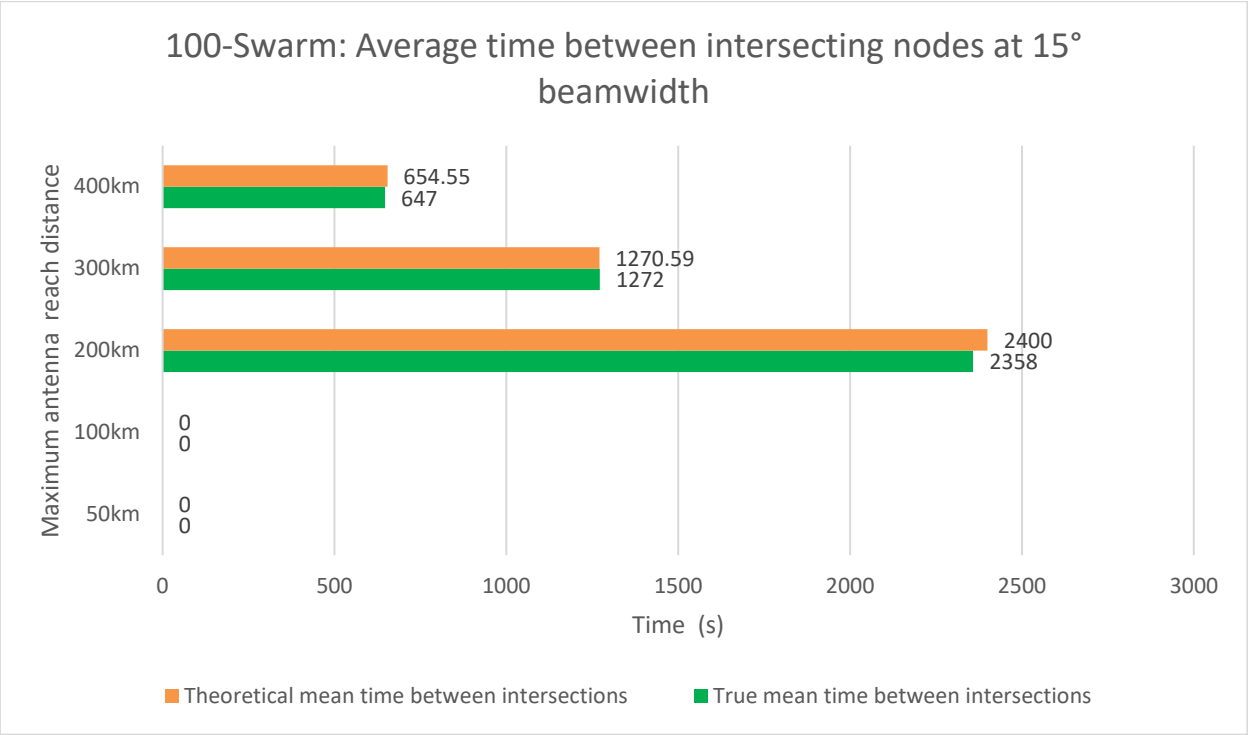

Figure 4.14: 100-Swarm: Average time between intersecting nodes at 15° beamwidth

4.3.2 Discussion: 100-Swarm with 15° angle

The frequency of intersections is captured in figure 4.13 and the average time of intersections are captured in figure 4.14.

At 50km, no intersections took place, thus 0% connection with the swarm was achieved.

At 100km, 1 intersection was achieved, resulting in 1% connection with the swarm.

At 200km, 36 intersections were achieved, which is 3600% the intersections from the previous range. The time difference is -42s, making them 1.75% more concentrated. 4 unique nodes intersected, which is 400% the unique nodes from the previous range, connecting with 4% of the swarm.

At 300km, 68 intersections were achieved, which is 188.89% the intersections from the previous range. The time difference is +1.41, making them 0.11% less concentrated. 8 unique nodes intersected, which is 200% the unique nodes from the previous range, connecting with 8% of the swarm.

At 400km, 132 intersections were achieved, which is 194.12% the intersections from the previous range. The time difference is -7.55s, making them 1.15% more concentrated. 13 unique nodes intersected, which is 162.5% the unique nodes from the previous range, connecting with 13% of the swarm.

4.3.3 Angle: 30°

Table 4.9: Antenna reach parameters 100 Swarm, 30°

Max Antenna Reach (km)	Parallel Straight-line reach (km)
50	48.296
100	96.592
200	193.185
300	289.778
400	386.370

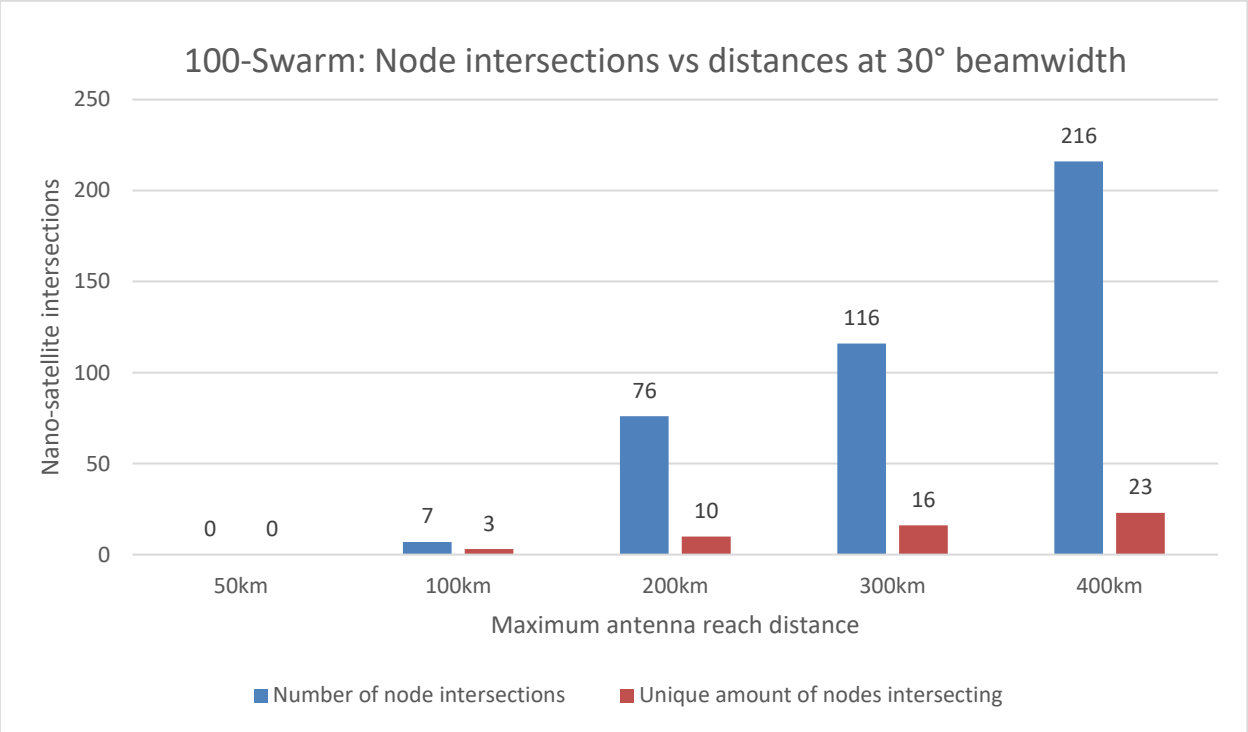

Figure 4.15: 100-Swarm: Node intersections vs distances at 30° beamwidth

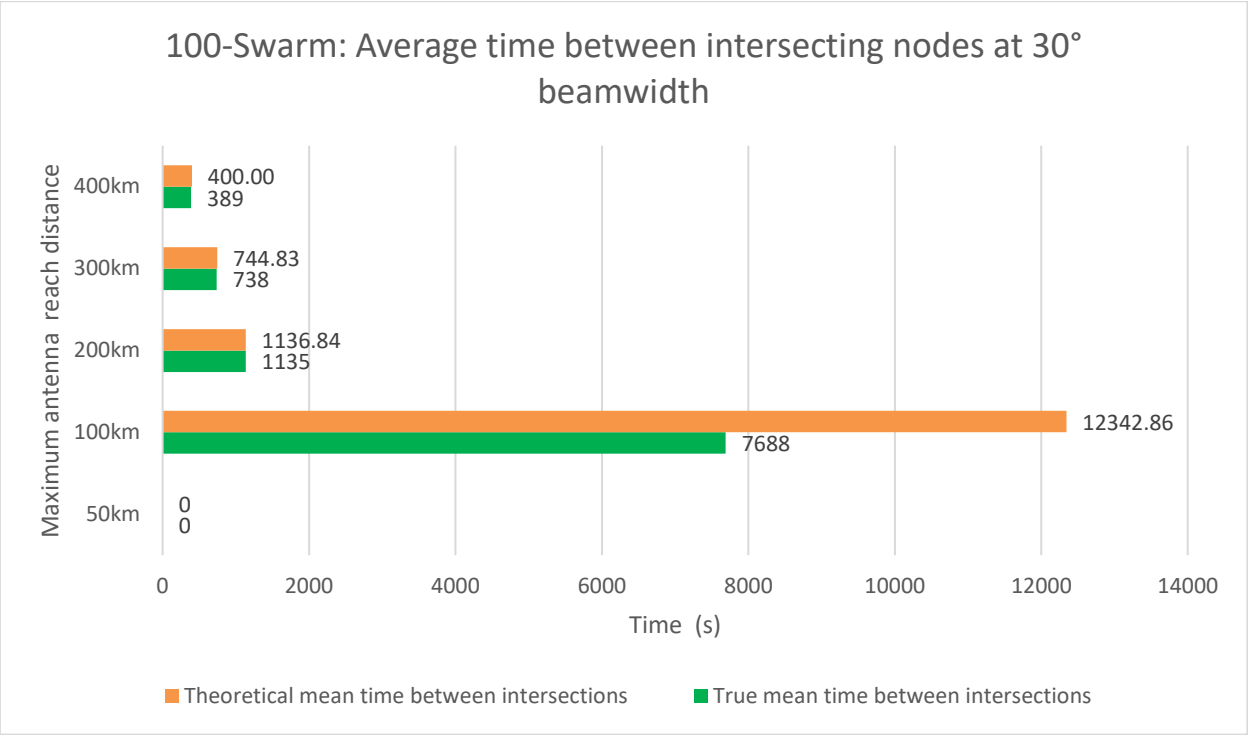

Figure 4.16: 100-Swarm: Average time between intersecting nodes at 30° beamwidth

4.3.4 Discussion: 100-Swarm with 30° angle

The frequency of intersections is captured in figure 4.15 and the average time of intersections are captured in figure 4.16.

At 50km, no intersections took place, thus 0% connection with the swarm was achieved.

At 100km, 7 intersections were achieved. The time difference is -4654.86s, making them 37.71% more concentrated. 3 unique nodes intersected, connecting with 3% of the swarm.

At 200km, 76 intersections were achieved, which is 1085.71% the intersections from the previous range. The time difference is -1.84s, making them 0.16% more concentrated. 10 unique nodes intersected, which is 333.33% the unique nodes from the previous range, connecting with 10% of the swarm.

At 300km, 116 intersections were achieved, which is 152.63% the intersections from the previous range. The time difference is -6.83s, making them 0.92% more concentrated. 16 unique nodes intersected, which is 160% the unique nodes from the previous range, connecting with 16% of the swarm.

At 400km, 216 intersections were achieved, which is 186.21% the intersections from the previous range. The time difference is -11s, making them 2.75% more concentrated. 23 unique nodes intersected, which is 143.75% the unique nodes from the previous range, connecting with 23% of the swarm.

4.3.5 Angle: 45°

Table 4.10: Antenna reach parameters 100 Swarm, 45°

Max Antenna Reach (km)	Parallel Straight-line reach (km)
50	46.194
100	92.388
200	184.776
300	277.164
400	369.551

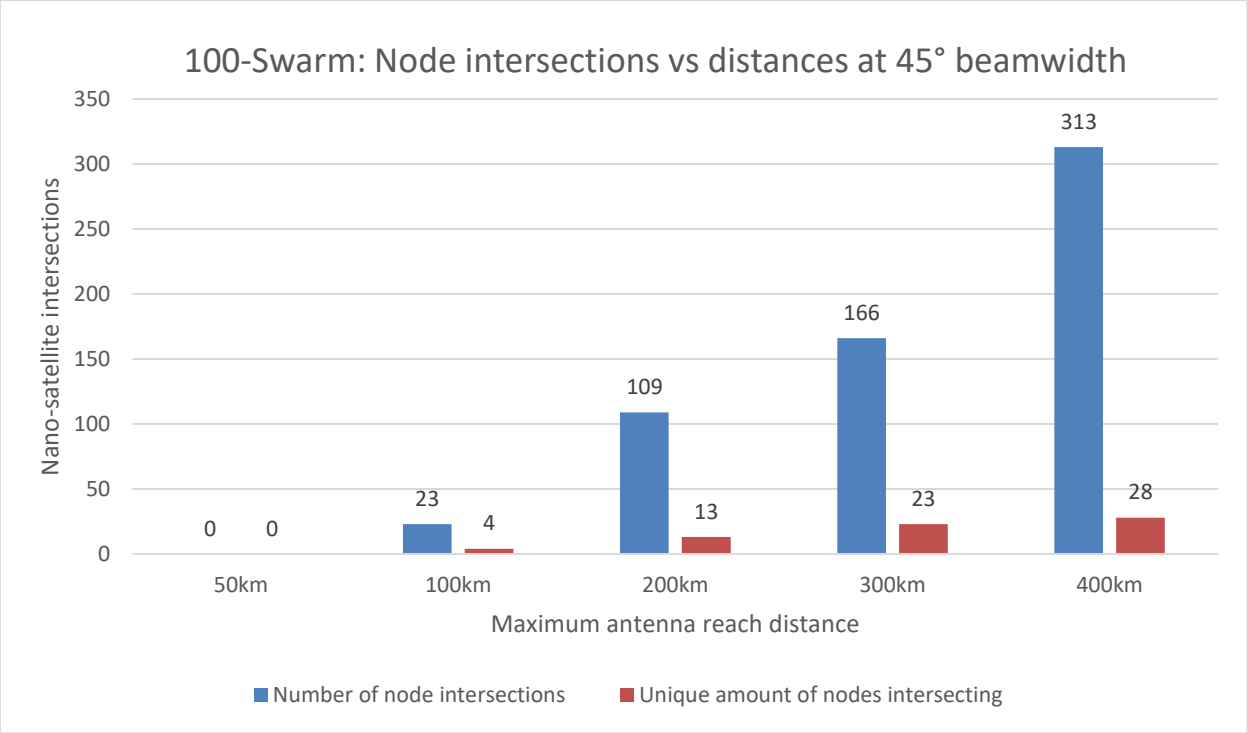

Figure 4.17: 100-Swarm: Node intersections vs distances at 45° beamwidth

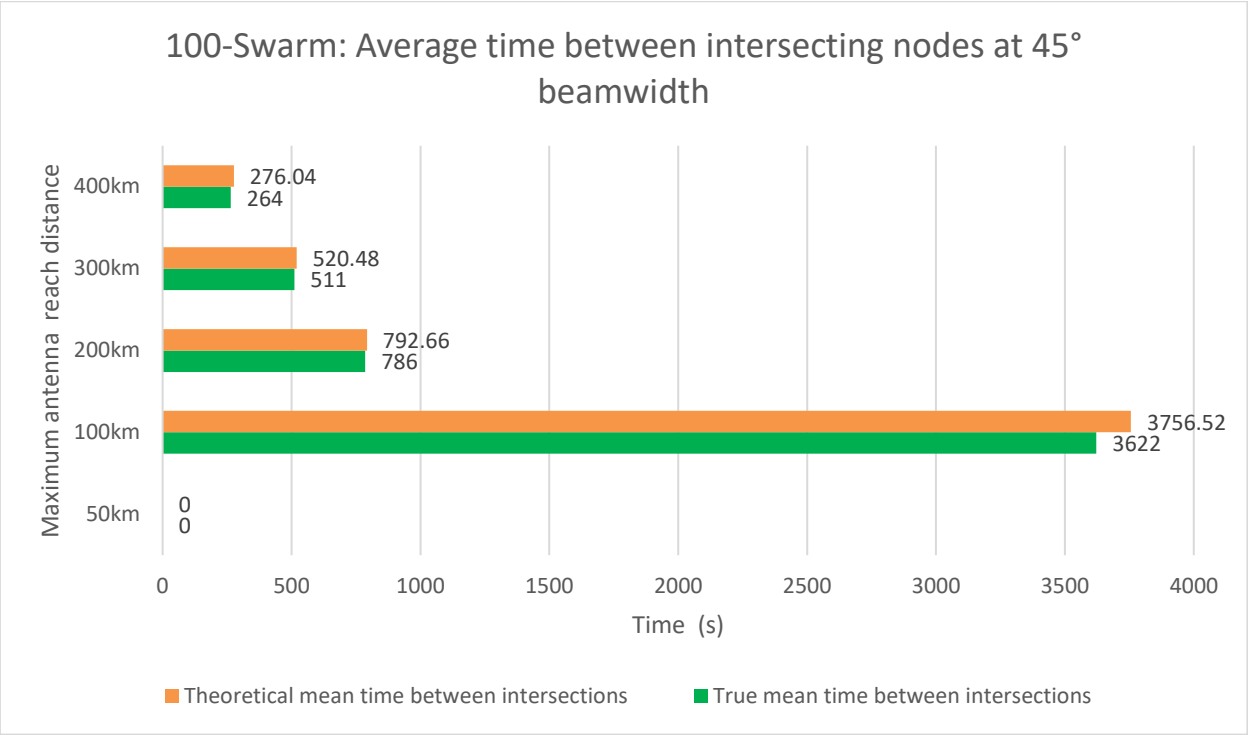

Figure 4.18: 100-Swarm: Average time between intersecting nodes at 45° beamwidth

4.3.6 Discussion: 100-Swarm with 45° angle

The frequency of intersections is captured in figure 4.17 and the average time of intersections are captured in figure 4.18.

At 50km, no intersections took place, thus 0% connection with the swarm was achieved.

At 100km, 23 intersections were achieved. The time difference is -134,52s, making them 3.58% more concentrated. 4 unique nodes intersected, connecting with 4% of the swarm.

At 200km, 109 intersections were achieved, which is 473.91% the intersections from the previous range. The time difference is -6.66s, making them 0.84% more concentrated. 13 unique nodes intersected, which is 325% the unique nodes from the previous range, connecting with 13% of the swarm.

At 300km, 166 intersections were achieved, which is 152.29% the intersections from the previous range. The time difference is -9.48s, making them 1.82% more concentrated. 23 unique nodes intersected, which is 176.92% the unique nodes from the previous range, connecting with 23% of the swarm.

At 400km, 313 intersections were achieved, which is 188.55% the intersections from the previous range. The time difference is -12.04s, making them 4.36% more concentrated. 28 unique nodes intersected, which is 121.74% the unique nodes from the previous range, connecting with 28% of the swarm.

4.3.7 Angle: 60°

Table 4.11: Antenna reach parameters 100 Swarm, 60°

Max Antenna Reach (km)	Parallel Straight-line reach (km)
50	43.301
100	86.603
200	173.205
300	259.808
400	346.411

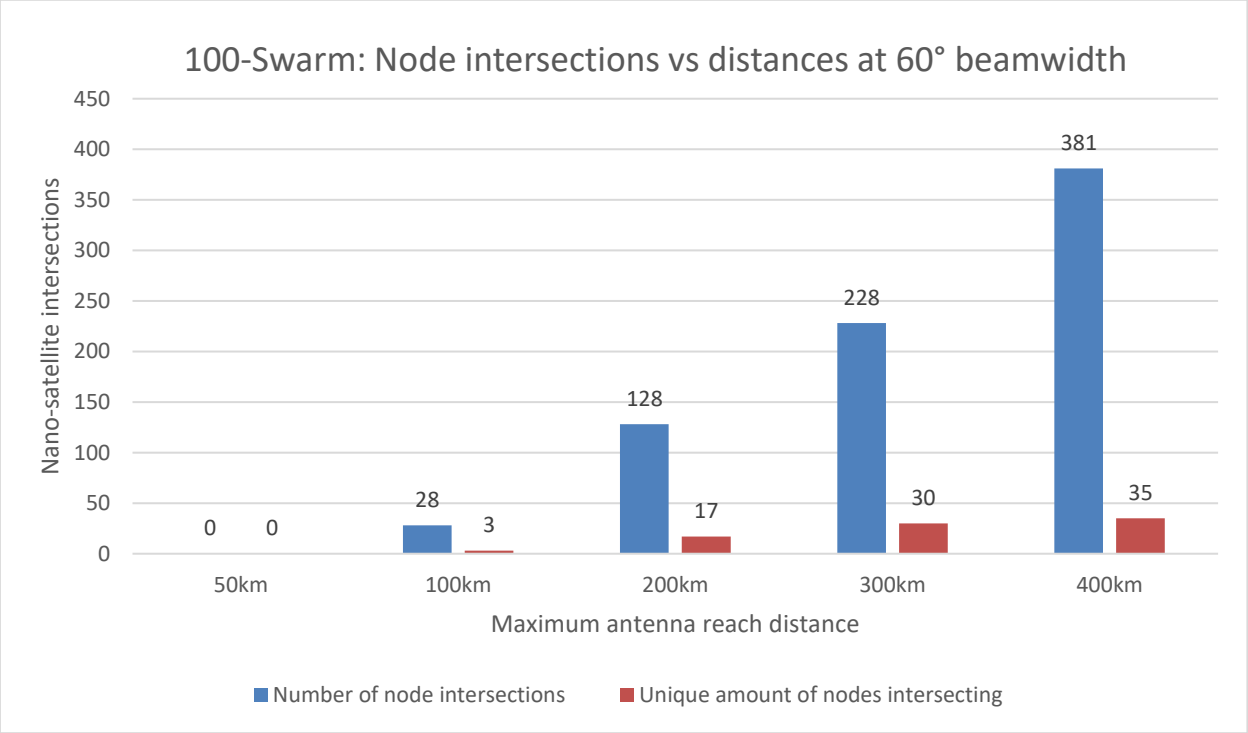

Figure 4.19: 100-Swarm: Node intersections vs distances at 60° beamwidth

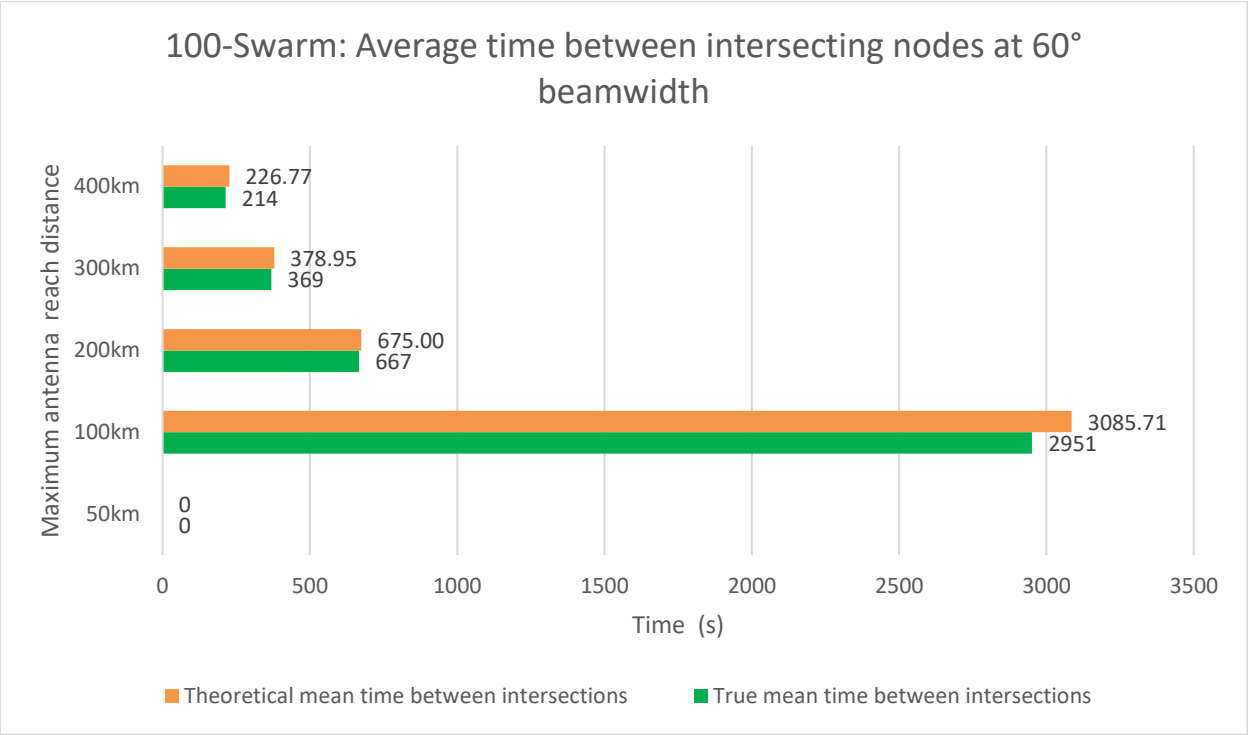

Figure 4.20: 100-Swarm: Average time between intersecting nodes at 60° beamwidth

4.3.8 Discussion: 100-Swarm with 60° angle

The frequency of intersections is captured in figure 4.19 and the average time of intersections are captured in figure 4.20.

At 50km, no intersections took place, thus 0% connection with the swarm was achieved.

At 100km, 28 intersections were achieved. The time difference is -134.71s, making them 4.37% more concentrated. 3 unique nodes intersected, connecting with 3% of the swarm.

At 200km, 128 intersections were achieved, which is 457.14% the intersections from the previous range. The time difference is -8s, making them 1.19% more concentrated. 17 unique nodes intersected, which is 566.67% the unique nodes from the previous range, connecting with 17% of the swarm.

At 300km, 228 intersections were achieved, which is 178.13% the intersections from the previous range. The time difference is -9.95s, making them 2.63% more concentrated. 30 unique nodes intersected, which is 176.47% the unique nodes from the previous range, connecting with 30% of the swarm.

At 400km, 381 intersections were achieved, which is 167.11% the intersections from the previous range. The time difference is -12.77s, making them 5.63% more concentrated. 35 unique nodes intersected, which is 116.67% the unique nodes from the previous range, connecting with 35% of the swarm.

4.4 SWARM SIZE: 150

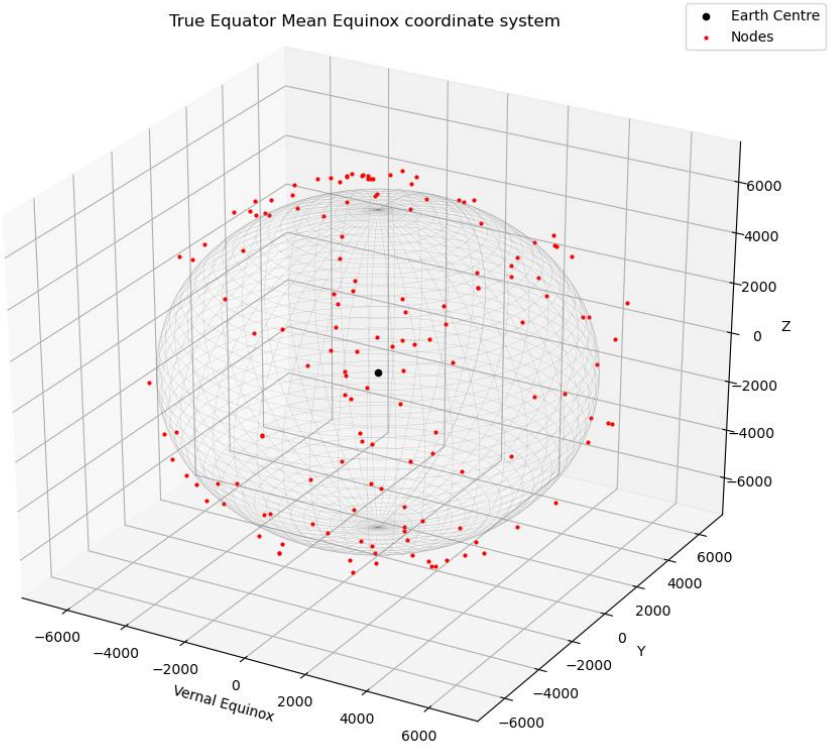

Figure 4.21: 150-Swarm nodes

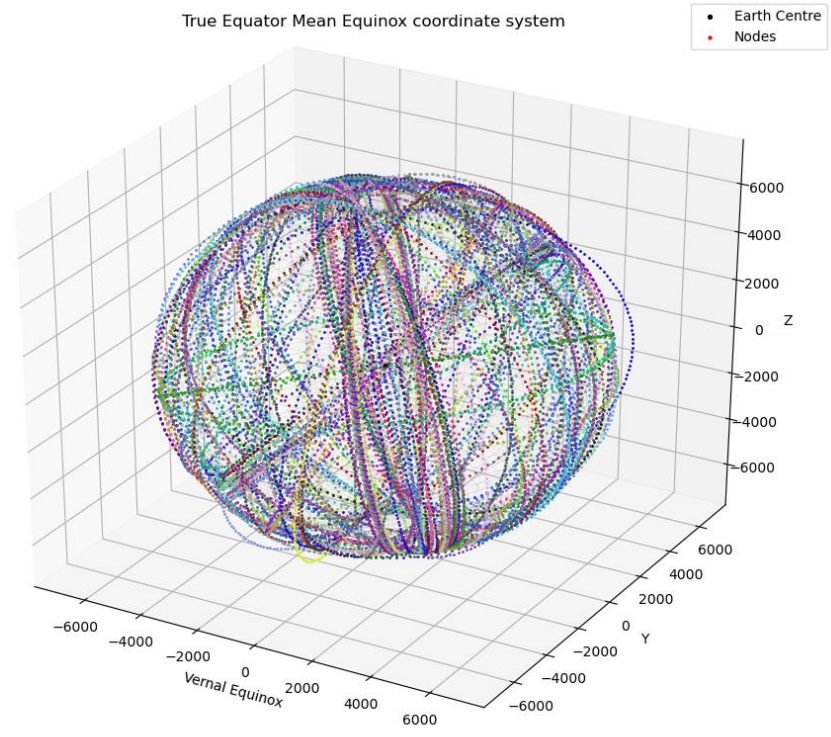

Figure 4.22: 150-Swarm nodes orbits

A visualisation of the simulated nodes is captured in figure 4.21 and orbits in figure 4.22.

4.4.1 Angle: 15°

Table 4.12: Antenna reach parameters 150 Swarm, 15°

Max Antenna Reach (km)	Parallel Straight-line reach (km)
50	49.572
100	99.144
200	198.289
300	297.433
400	396.578

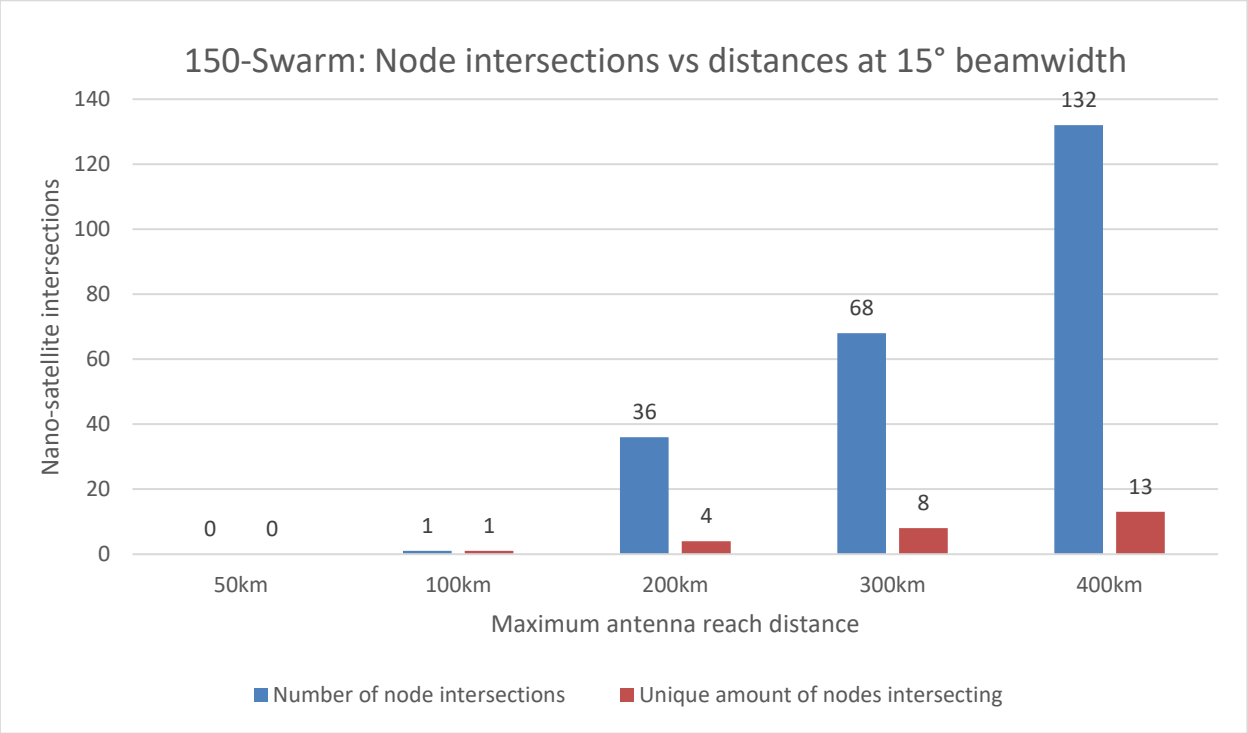

Figure 4.23: 150-Swarm: Node intersections vs distances at 15° beamwidth

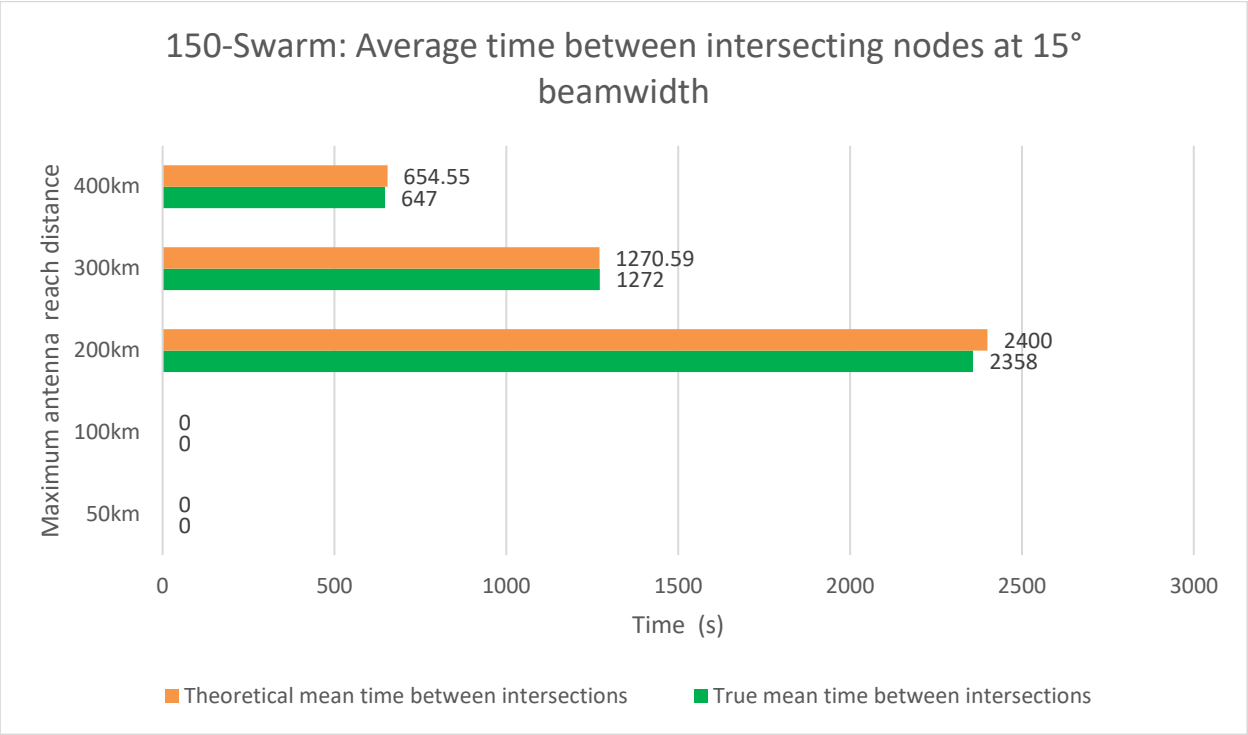

Figure 4.24: 150-Swarm: Average time between intersecting nodes at 15° beamwidth

4.4.2 Discussion: 150-Swarm with 15° angle

The frequency of intersections is captured in figure 4.23 and the average time of intersections are captured in figure 4.24.

At 50km, no intersections took place, thus 0% connection with the swarm was achieved.

At 100km, 1 intersection was achieved, resulting in 0.67% connection with the swarm.

At 200km, 36 intersections were achieved, which is 3600% the intersections from the previous range. The time difference is -42s, making them 1.75% more concentrated. 4 unique nodes intersected, which is 400% the unique nodes from the previous range, connecting with 2.67% of the swarm.

At 300km, 68 intersections were achieved, which is 188.89% the intersections from the previous range. The time difference is +1.41, making them 0.11% less concentrated. 8 unique nodes intersected, which is 200% the unique nodes from the previous range, connecting with 5.33% of the swarm.

At 400km, 132 intersections were achieved, which is 194.12% the intersections from the previous range. The time difference is -7.55s, making them 1.15% more concentrated. 13 unique nodes intersected, which is 162.5% the unique nodes from the previous range, connecting with 8.67% of the swarm.

4.4.3 Angle: 30°

Table 4.13: Antenna reach parameters 150 Swarm, 30°

Max Antenna Reach (km)	Parallel Straight-line reach (km)
50	48.296
100	96.592
200	193.185
300	289.778
400	386.370

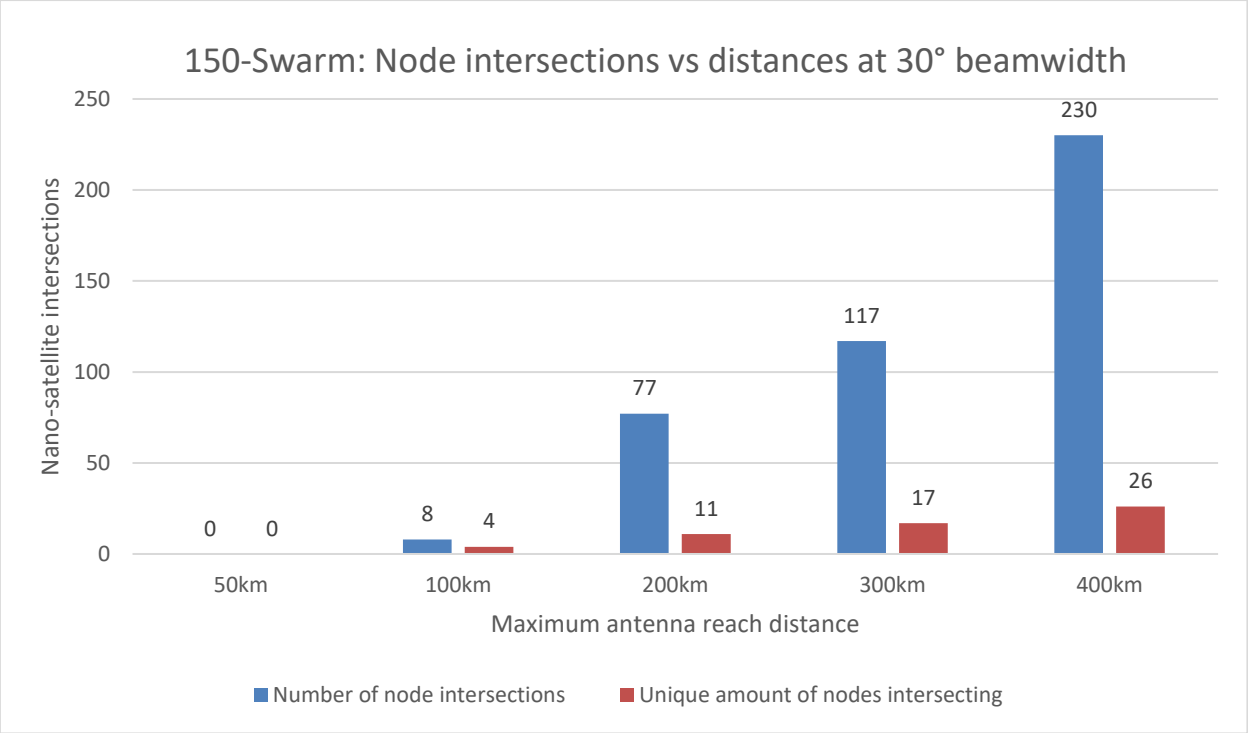

Figure 4.25: 150-Swarm: Node intersections vs distances at 30° beamwidth

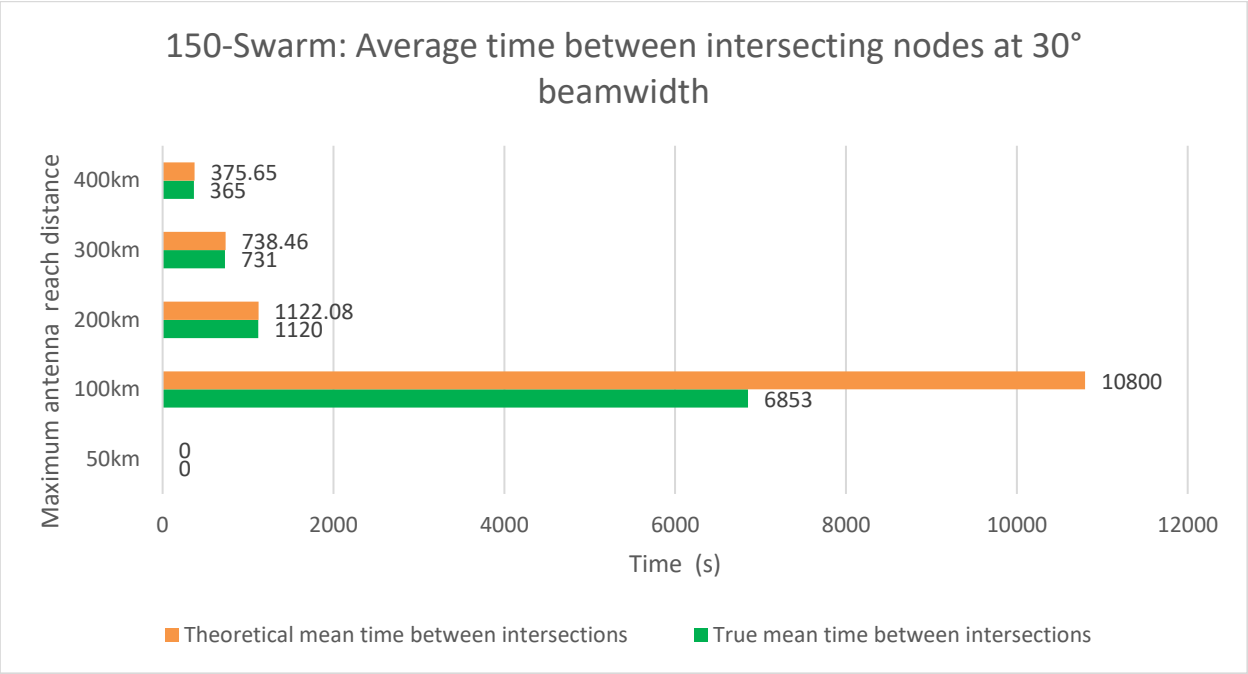

Figure 4.26: 150-Swarm: Average time between intersecting nodes at 30° beamwidth

4.4.4 Discussion: 150-Swarm with 30° angle

The frequency of intersections is captured in figure 4.25 and the average time of intersections are captured in figure 4.26.

At 50km, no intersections took place, thus 0% connection with the swarm was achieved.

At 100km, 8 intersections were achieved. The time difference is -3947s, making them 36.55% more concentrated. 4 unique nodes intersected, connecting with 2.67% of the swarm.

At 200km, 77 intersections were achieved, which is 962.5% the intersections from the previous range. The time difference is -2.08s, making them 0.19% more concentrated. 11 unique nodes intersected, which is 275% the unique nodes from the previous range, connecting with 11.33% of the swarm.

At 300km, 117 intersections were achieved, which is 151.95% the intersections from the previous range. The time difference is -7.46s, making them 1.01% more concentrated. 17 unique nodes intersected, which is 154.55% the unique nodes from the previous range, connecting with 11.33% of the swarm.

At 400km, 230 intersections were achieved, which is 196.58% the intersections from the previous range. The time difference is -10.65s, making them 2.84% more concentrated. 26 unique nodes intersected, which is 152.94% the unique nodes from the previous range, connecting with 17.33% of the swarm.

4.4.5 Angle: 45°

Table 4.14: Antenna reach parameters 150 Swarm, 45°

Max Antenna Reach (km)	Parallel Straight-line reach (km)
50	46.194
100	92.388
200	184.776
300	277.164
400	369.551

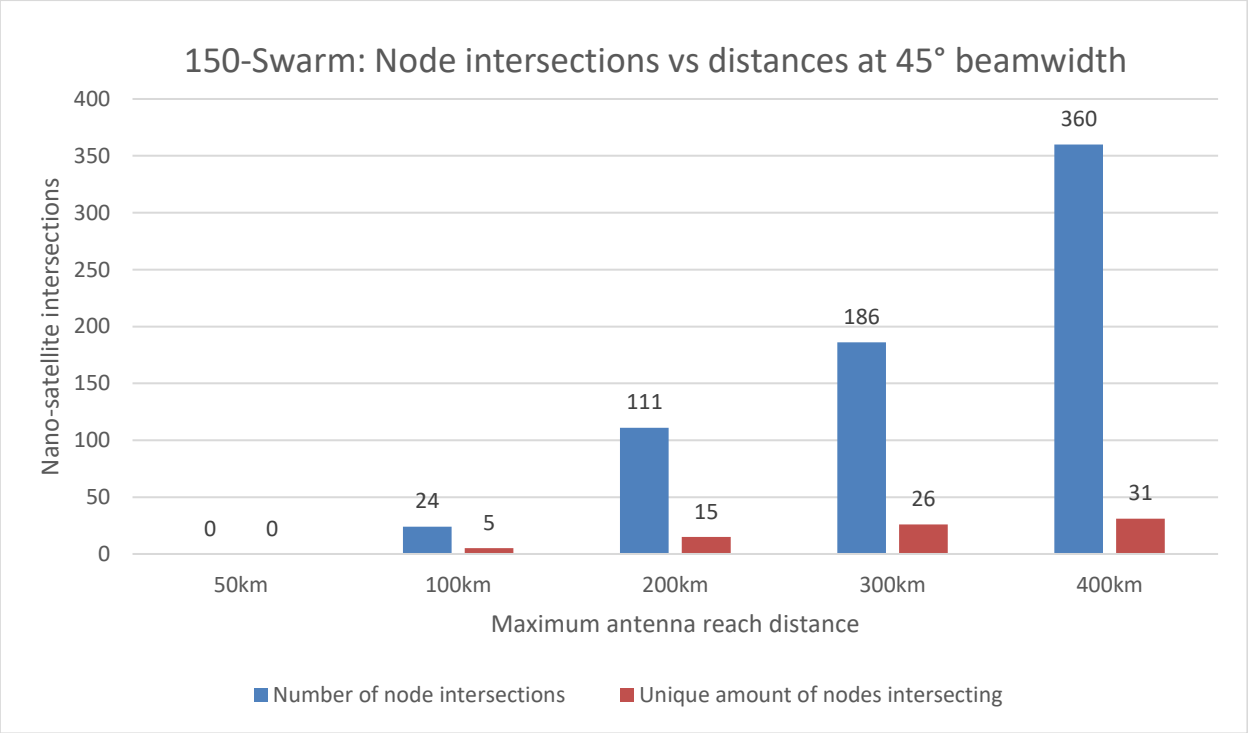

Figure 4.27: 150-Swarm: Node intersections vs distances at 45° beamwidth

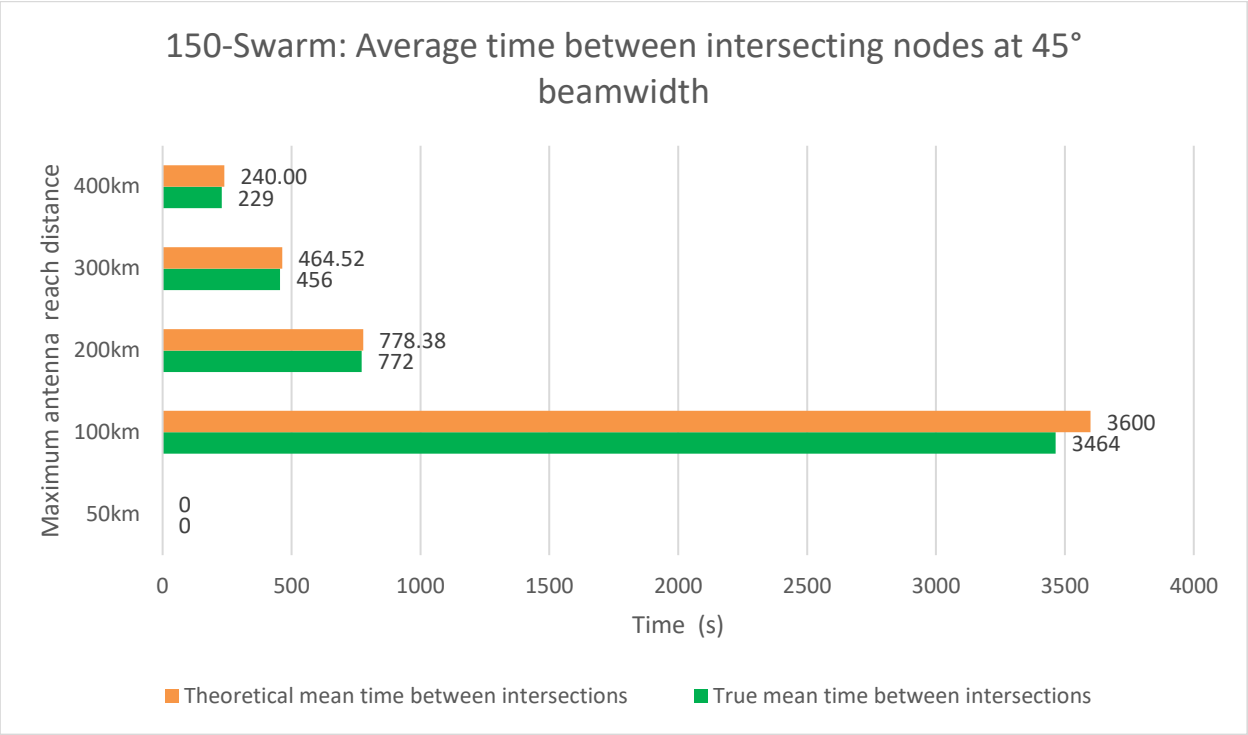

Figure 4.28: 150-Swarm: Average time between intersecting nodes at 45° beamwidth

4.4.6 Discussion: 150-Swarm with 45° angle

The frequency of intersections is captured in figure 4.27 and the average time of intersections are captured in figure 4.28.

At 50km, no intersections took place, thus 0% connection with the swarm was achieved.

At 100km, 24 intersections were achieved. The time difference is -136s, making them 3.78% more concentrated. 5 unique nodes intersected, connecting with 3.33% of the swarm.

At 200km, 111 intersections were achieved, which is 462.5% the intersections from the previous range. The time difference is -6.38s, making them 0.82% more concentrated. 15 unique nodes intersected, which is 300% the unique nodes from the previous range, connecting with 10% of the swarm.

At 300km, 186 intersections were achieved, which is 167.57% the intersections from the previous range. The time difference is -8.52s, making them 1.83% more concentrated. 26 unique nodes intersected, which is 173.33% the unique nodes from the previous range, connecting with 17.33% of the swarm.

At 400km, 360 intersections were achieved, which is 193.55% the intersections from the previous range. The time difference is -11s, making them 4.58% more concentrated. 31 unique nodes intersected, which is 119.23% the unique nodes from the previous range, connecting with 20.67% of the swarm.

4.4.7 Angle: 60°

Table 4.15: Antenna reach parameters 150 Swarm, 60°

Max Antenna Reach (km)	Parallel Straight-line reach (km)
50	43.301
100	86.603
200	173.205
300	259.808
400	346.411

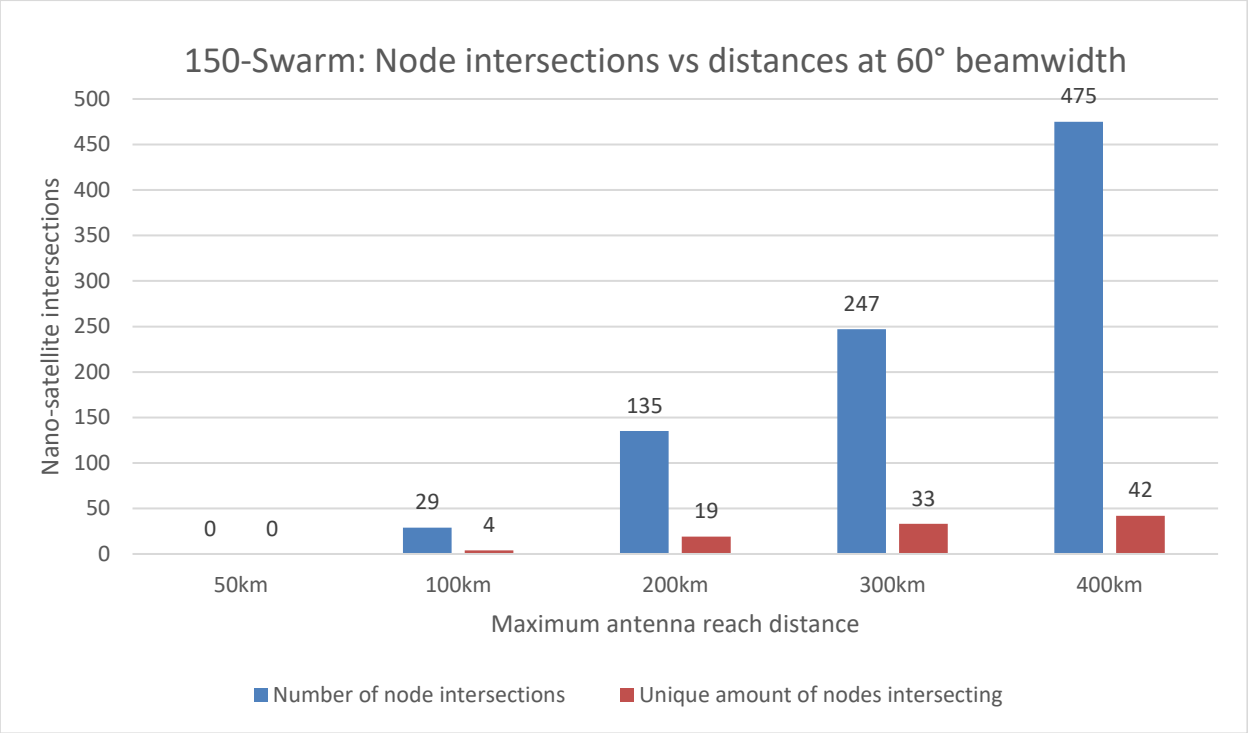

Figure 4.29: 150-Swarm: Node intersections vs distances at 60° beamwidth

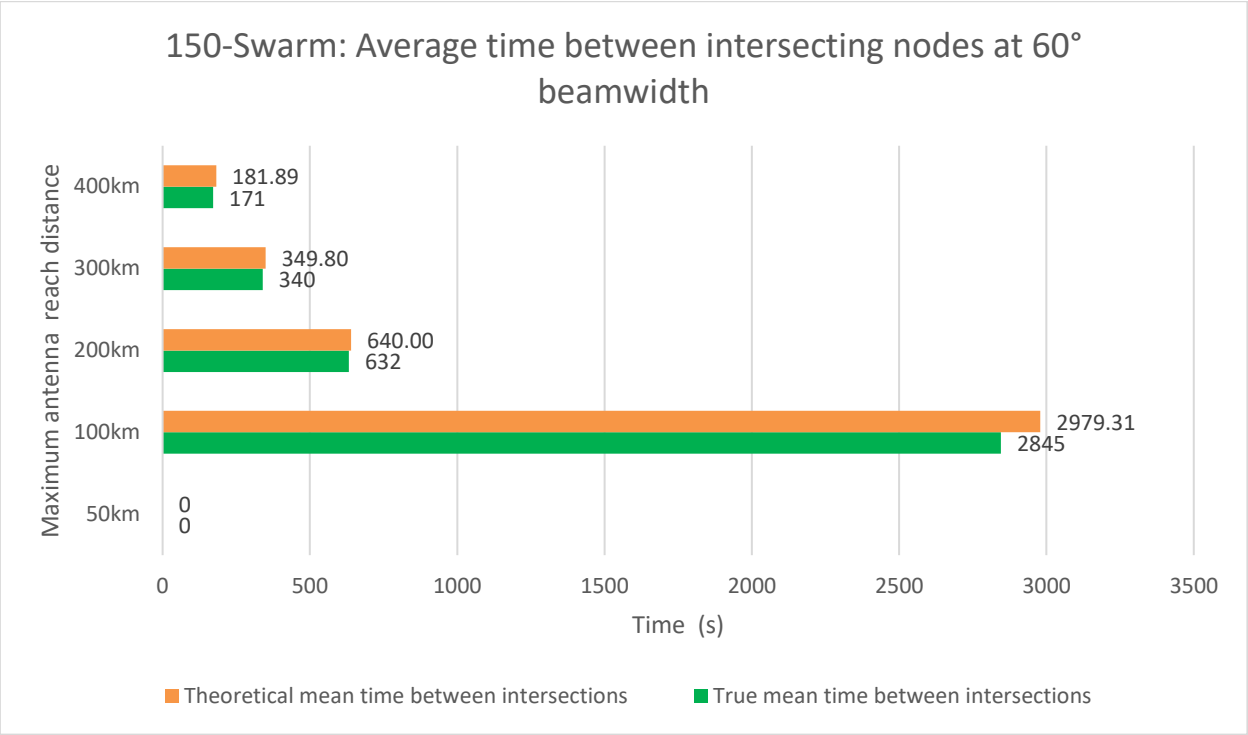

Figure 4.30: 150-Swarm: Average time between intersecting nodes at 60° beamwidth

4.4.8 Discussion: 150-Swarm with 60° angle

The frequency of intersections is captured in figure 4.29 and the average time of intersections are captured in figure 4.30.

At 50km, no intersections took place, thus 0% connection with the swarm was achieved.

At 100km, 29 intersections were achieved. The time difference is -134.31s, making them 4.51% more concentrated. 4 unique nodes intersected, connecting with 2.67% of the swarm.

At 200km, 135 intersections were achieved, which is 465.52% the intersections from the previous range. The time difference is -8s, making them 1.25% more concentrated. 19 unique nodes intersected, which is 475% the unique nodes from the previous range, connecting with 12.67% of the swarm.

At 300km, 247 intersections were achieved, which is 182.96% the intersections from the previous range. The time difference is -9.8s, making them 2.8% more concentrated. 33 unique nodes intersected, which is 173.68% the unique nodes from the previous range, connecting with 22% of the swarm.

At 400km, 475 intersections were achieved, which is 192.31% the intersections from the previous range. The time difference is -10.89s, making them 5.99% more concentrated. 42 unique nodes intersected, which is 127.27% the unique nodes from the previous range, connecting with 28% of the swarm.

4.5 SWARM SIZE: 200

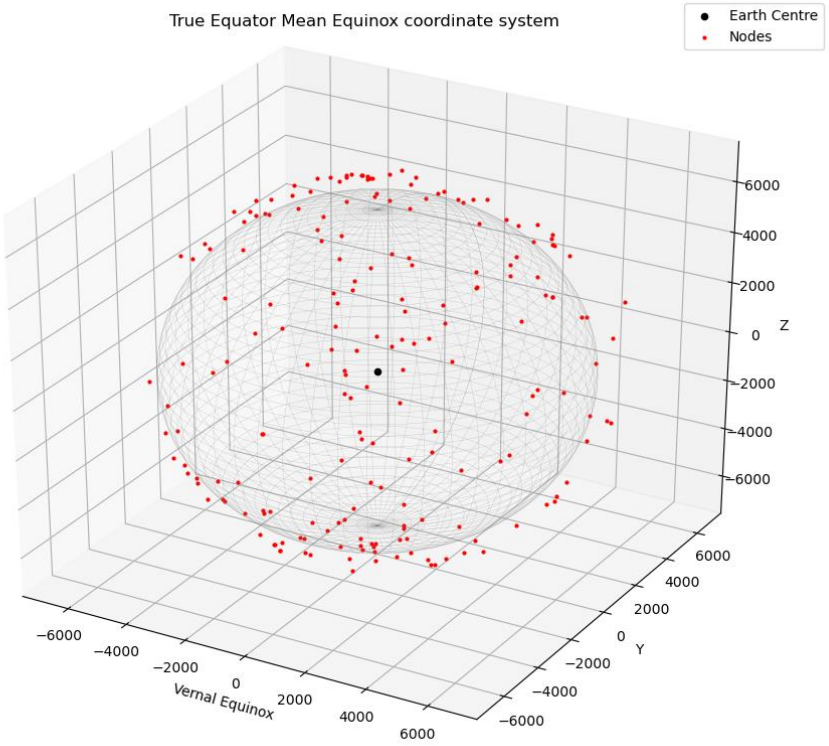

Figure 4.31: 200-Swarm nodes

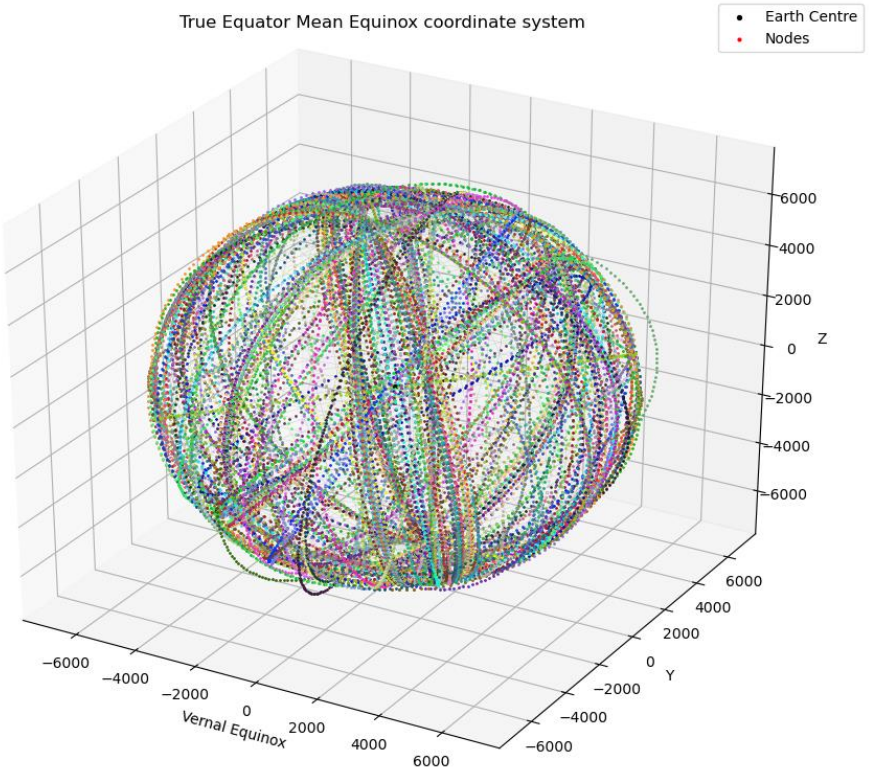

Figure 4.32: 200-Swarm nodes orbits

A visualisation of the simulated nodes is captured in figure 4.31 and orbits in figure 4.32.

4.5.1 Angle: 15°

Table 4.16: Antenna reach parameters 200 Swarm, 15°

Max Antenna Reach (km)	Parallel Straight-line reach (km)
50	49.572
100	99.144
200	198.289
300	297.433
400	396.578

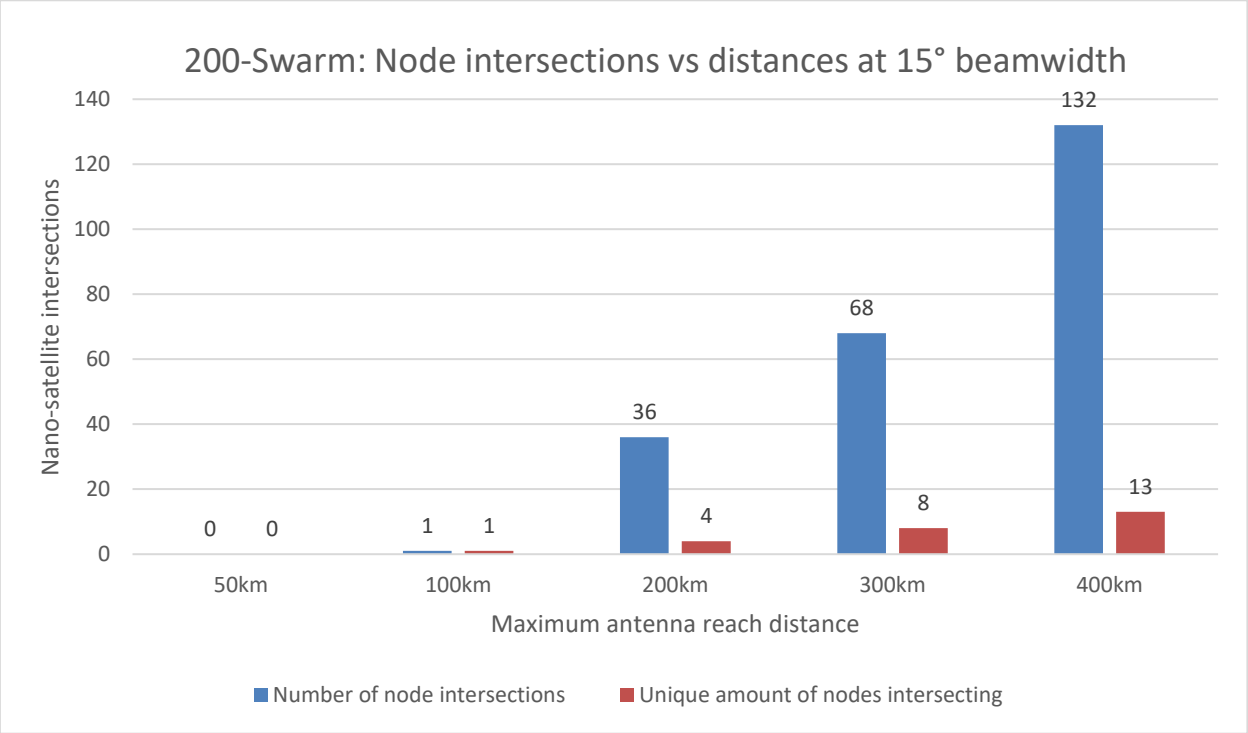

Figure 4.33: 200-Swarm: Node intersections vs distances at 15° beamwidth

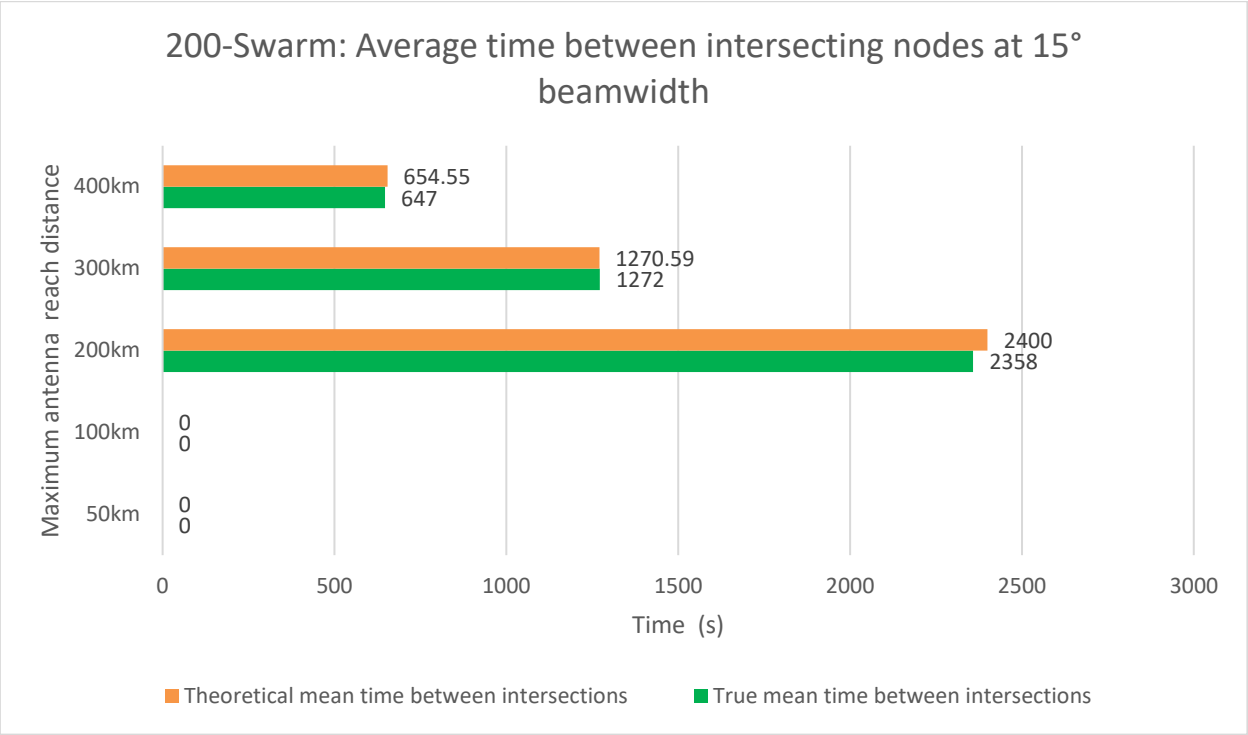

Figure 4.34: 200-Swarm: Average time between intersecting nodes at 15° beamwidth

4.5.2 Discussion: 200-Swarm with 15° angle

The frequency of intersections is captured in figure 4.33 and the average time of intersections are captured in figure 4.34.

At 50km, no intersections took place, thus 0% connection with the swarm was achieved.

At 100km, 1 intersection was achieved, resulting in 0.5% connection with the swarm.

At 200km, 36 intersections were achieved, which is 3600% the intersections from the previous range. The time difference is -42s, making them 1.75% more concentrated. 4 unique nodes intersected, which is 400% the unique nodes from the previous range, connecting with 2% of the swarm.

At 300km, 68 intersections were achieved, which is 188.89% the intersections from the previous range. The time difference is +1.41, making them 0.11% less concentrated. 8 unique nodes intersected, which is 200% the unique nodes from the previous range, connecting with 4% of the swarm.

At 400km, 132 intersections were achieved, which is 194.12% the intersections from the previous range. The time difference is -7.55s, making them 1.15% more concentrated. 13 unique nodes intersected, which is 162.5% the unique nodes from the previous range, connecting with 6.5% of the swarm.

4.5.3 Angle: 30°

Table 4.17: Antenna reach parameters 200 Swarm, 30°

Max Antenna Reach (km)	Parallel Straight-line reach (km)
50	48.296
100	96.592
200	193.185
300	289.778
400	386.370

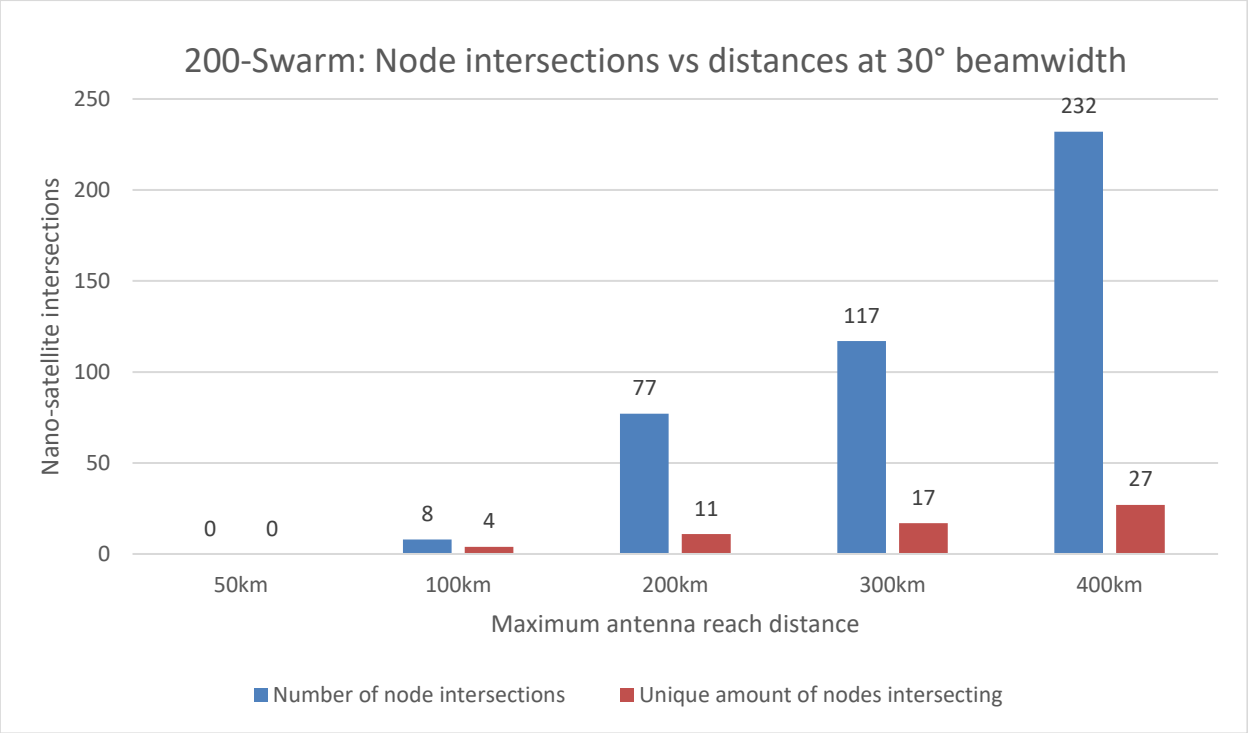

Figure 4.35: 200-Swarm: Node intersections vs distances at 30° beamwidth

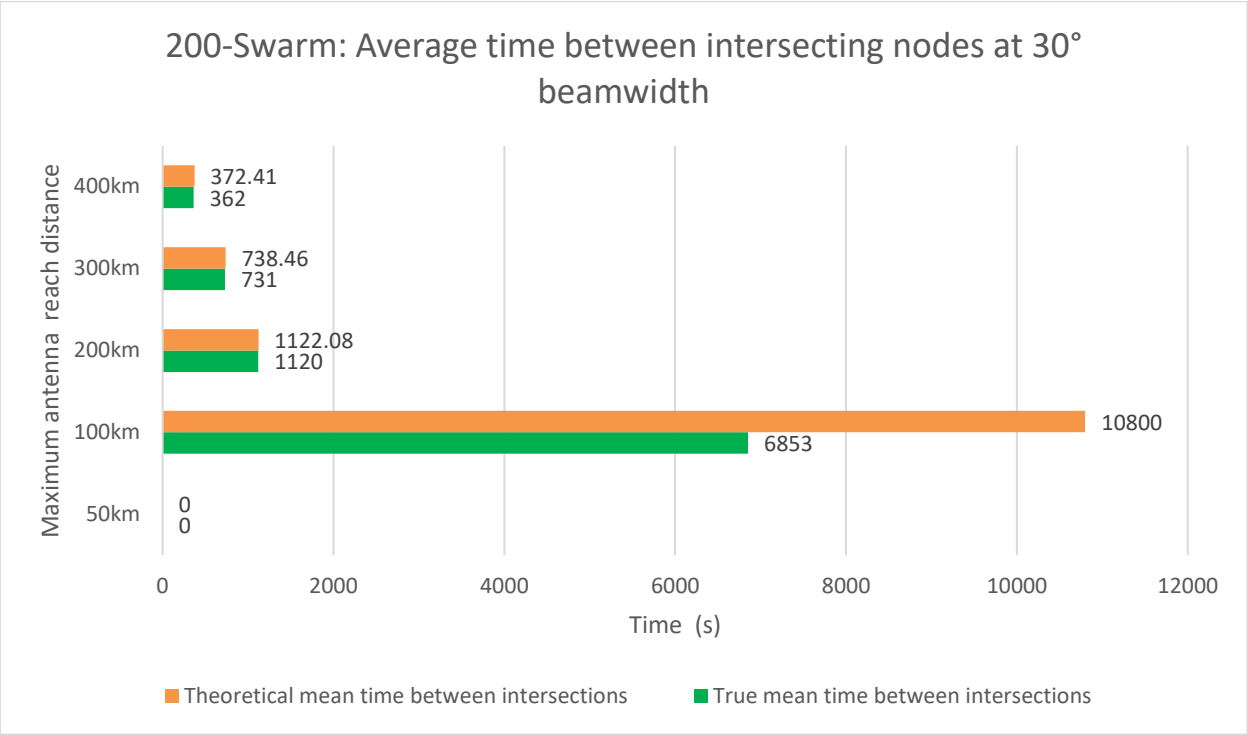

Figure 4.36: 200-Swarm: Average time between intersecting nodes at 30° beamwidth

4.5.4 Discussion: 200-Swarm with 30° angle

The frequency of intersections is captured in figure 4.35 and the average time of intersections are captured in figure 4.36.

At 50km, no intersections took place, thus 0% connection with the swarm was achieved.

At 100km, 8 intersections were achieved. The time difference is -3947s, making them 36.55% more concentrated. 4 unique nodes intersected, connecting with 2% of the swarm.

At 200km, 77 intersections were achieved, which is 962.5% the intersections from the previous range. The time difference is -2.08s, making them 0.19% more concentrated. 11 unique nodes intersected, which is 275% the unique nodes from the previous range, connecting with 5.5% of the swarm.

At 300km, 117 intersections were achieved, which is 151.95% the intersections from the previous range. The time difference is -7.46s, making them 1.01% more concentrated. 17 unique nodes intersected, which is 154.55% the unique nodes from the previous range, connecting with 8.5% of the swarm.

At 400km, 232 intersections were achieved, which is 198.29% the intersections from the previous range. The time difference is -10.41s, making them 2.80% more concentrated. 27 unique nodes intersected, which is 158.82% the unique nodes from the previous range, connecting with 13.5% of the swarm.

4.5.5 Angle: 45°

Table 4.18: Antenna reach parameters 200 Swarm, 45°

Max Antenna Reach (km)	Parallel Straight-line reach (km)
50	46.194
100	92.388
200	184.776
300	277.164
400	369.551

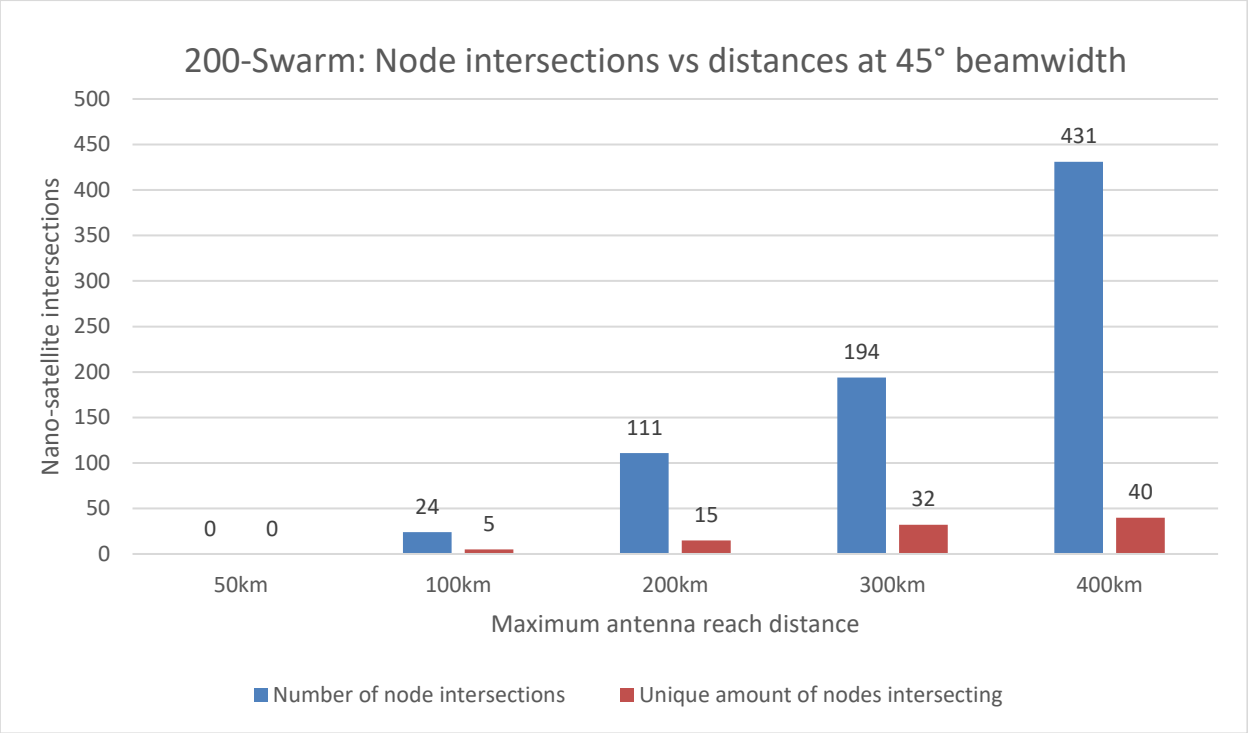

Figure 4.37: 200-Swarm: Node intersections vs distances at 45° beamwidth

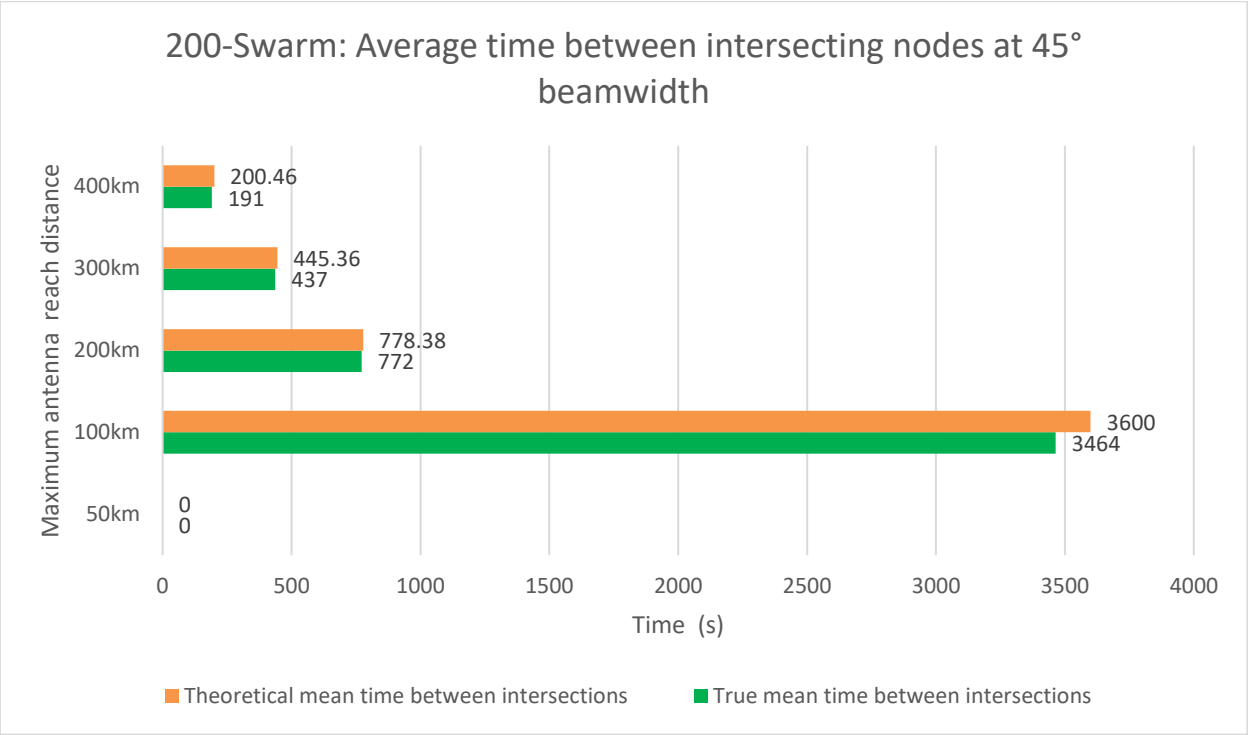

Figure 4.38: 200-Swarm: Average time between intersecting nodes at 45° beamwidth

4.5.6 Discussion: 200-Swarm with 45° angle

The frequency of intersections is captured in figure 4.37 and the average time of intersections are captured in figure 4.38.

At 50km, no intersections took place, thus 0% connection with the swarm was achieved.

At 100km, 24 intersections were achieved. The time difference is -136s, making them 3.78% more concentrated. 5 unique nodes intersected, connecting with 2.5% of the swarm.

At 200km, 111 intersections were achieved, which is 462.5% the intersections from the previous range. The time difference is -6.38s, making them 0.82% more concentrated. 15 unique nodes intersected, which is 300% the unique nodes from the previous range, connecting with 7.5% of the swarm.

At 300km, 194 intersections were achieved, which is 174.77% the intersections from the previous range. The time difference is -8.36s, making them 1.88% more concentrated. 32 unique nodes intersected, which is 213.33% the unique nodes from the previous range, connecting with 16% of the swarm.

At 400km, 421 intersections were achieved, which is 222.16% the intersections from the previous range. The time difference is 9.46s, making them 4.72% more concentrated. 40 unique nodes intersected, which is 125% the unique nodes from the previous range, connecting with 20% of the swarm.

4.5.7 Angle: 60°

Table 4.19: Antenna reach parameters 200 Swarm, 60°

Max Antenna Reach (km)	Parallel Straight-line reach (km)
50	43.301
100	86.603
200	173.205
300	259.808
400	346.411

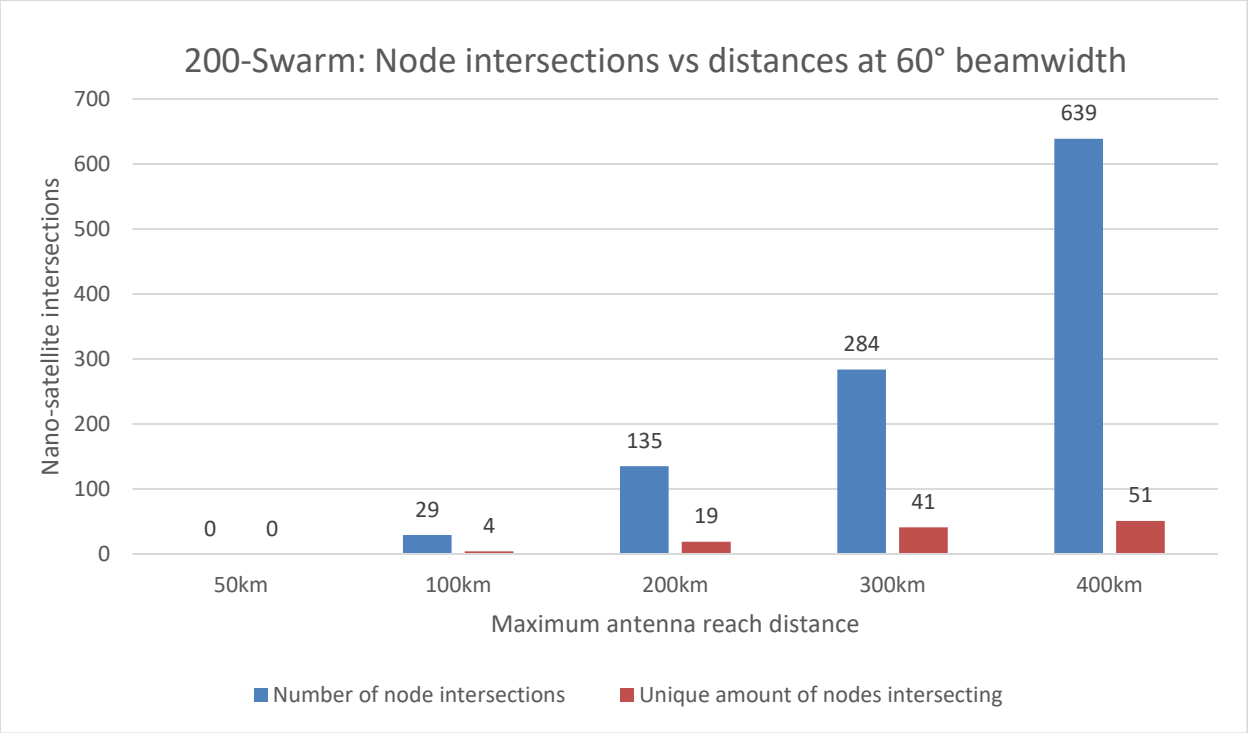

Figure 4.39: 200-Swarm: Node intersections vs distances at 60° beamwidth

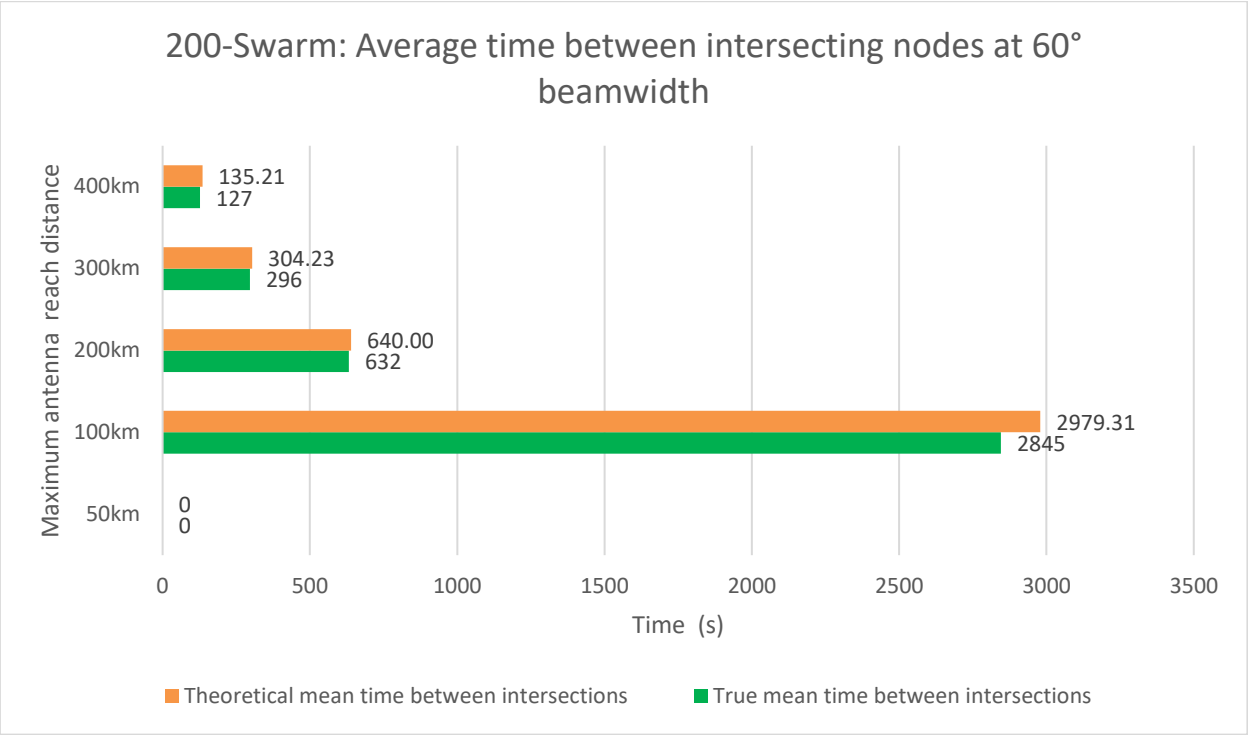

Figure 4.40: 200-Swarm: Average time between intersecting nodes at 60° beamwidth

4.5.8 Discussion: 200-Swarm with 60° angle

The frequency of intersections is captured in figure 4.39 and the average time of intersections are captured in figure 4.40.

At 50km, no intersections took place, thus 0% connection with the swarm was achieved.

At 100km, 29 intersections were achieved. The time difference is -134.31s, making them 4.51% more concentrated. 4 unique nodes intersected, connecting with 2% of the swarm.

At 200km, 135 intersections were achieved, which is 465.52% the intersections from the previous range. The time difference is -8s, making them 1.25% more concentrated. 19 unique nodes intersected, which is 475% the unique nodes from the previous range, connecting with 9.5% of the swarm.

At 300km, 284 intersections were achieved, which is 210.37% the intersections from the previous range. The time difference is -8.23s, making them 2.7% more concentrated. 41 unique nodes intersected, which is 215.79% the unique nodes from the previous range, connecting with 20.5% of the swarm.

At 400km, 639 intersections were achieved, which is 225% the intersections from the previous range. The time difference is -8.21s, making them 6.07% more concentrated. 51 unique nodes intersected, which is 124.39% the unique nodes from the previous range, connecting with 25.5% of the swarm.

4.6 SWARM INTERSECTION COMPARISON

A summary of the number of intersections compared to each swarm is given in tables 4.20, 4.21, 4.22 and 4.23 at beam angles of 15°, 30°, 45° and 60°, respectively.

Table 4.20: Swarm intersection comparison at 15° beamwidth

Angle: 15°	50-Swarm	100-Swarm	150-Swarm	200-Swarm
50km	0	0	0	0
100km	1	1	1	1
200km	3	36	36	36
300km	5	68	68	68
400km	10	132	132	132

Table 4.21: Swarm intersection comparison at 30° beamwidth

Angle: 30°	50-Swarm	100-Swarm	150-Swarm	200-Swarm
50km	0	0	0	0
100km	2	7	8	8
200km	8	76	77	77
300km	11	116	117	117
400km	44	216	230	232

Table 4.22: Swarm intersection comparison at 45° beamwidth

Angle: 45°	50-Swarm	100-Swarm	150-Swarm	200-Swarm
50km	0	0	0	0
100km	4	23	24	24
200km	12	109	111	111
300km	26	166	186	194
400km	91	313	360	431

Table 4.23: Swarm intersection comparison at 60° beamwidth

Angle: 60°	50-Swarm	100-Swarm	150-Swarm	200-Swarm
50km	0	0	0	0
100km	4	28	29	29
200km	20	128	135	135
300km	56	228	247	284
400km	119	381	475	639

Link budgets with reaches of ≤ 50km yield no results. Swarm size 50 produced, as expected, the least number of intersections when compared to the other swarm sizes. For swarm sizes 100, 150 and 200: they all have the same number of intersections at 15° beamwidth. Likewise, at 30° beamwidth, small differences in the number of intersections are observed (7% at most). At 45° beamwidth, the results are relatively equal at reaches ≤ 200km (within 2%). At 60° beamwidth and reaches ≤ 200km, the number of intersections was relatively equal as well (within 5%). At both 45° beamwidth and 60° beamwidth, substantial differences in the number of intersections, compared with their swarm sizes, are observed (within 167%). Comparing table 4.20 with table 4.21 and table 4.21 with table 4.23, the beamwidth has a greatest impact above 200km range. In some cases, doubling the beamwidth produced more than double the number of intersections for the same swarm size at the same range.

4.7 SWARM UTILISATION COMPARISON

Table 4.24: Swarm utilisation comparison at 15° beamwidth

Angle: 15°	50-Swarm	100-Swarm	150-Swarm	200-Swarm
50km	0.0 %	0.0 %	0.0 %	0.0 %
100km	2.0 %	1.0 %	0.7 %	0.5 %
200km	2.0 %	4.0 %	2.7 %	2.0 %
300km	4.0 %	8.0 %	5.3 %	4.0 %
400km	10.0 %	13.0 %	8.7 %	6.5 %

Table 4.25: Swarm utilisation comparison at 30° beamwidth

Angle: 30°	50-Swarm	100-Swarm	150-Swarm	200-Swarm
50km	0.0 %	0.0 %	0.0 %	0.0 %
100km	4.0 %	3.0 %	2.7 %	2.0 %
200km	12.0 %	10.0 %	7.3 %	5.5 %
300km	14.0 %	16.0 %	11.3 %	8.5 %
400km	26.0 %	23.0 %	17.3 %	13.5 %

Table 4.26: Swarm utilisation comparison at 45° beamwidth

Angle: 45°	50-Swarm	100-Swarm	150-Swarm	200-Swarm
50km	0.0 %	0.0 %	0.0 %	0.0 %
100km	6.0 %	4.0 %	3.3 %	2.5 %
200km	14.0 %	13.0 %	10.0 %	7.5 %
300km	28.0 %	23.0 %	17.3 %	16.0 %
400km	36.0 %	28.0 %	20.7 %	20.0 %

Table 4.27: Swarm utilisation comparison at 60° beamwidth

Angle: 60°	50-Swarm	100-Swarm	150-Swarm	200-Swarm
50km	0.0 %	0.0 %	0.0 %	0.0 %
100km	4.0 %	3.0 %	2.7 %	2.0 %
200km	20.0 %	17.0 %	12.7 %	9.5 %
300km	42.0 %	30.0 %	22.0 %	20.5 %
400km	50.0 %	35.0 %	28.0 %	25.5 %

Tables 4.24, 4.25, 4.26 and 4.27 indicate the swarm utilisation at beam angles of 15°, 30°, 45° and 60°, respectively. The utilisation is calculated as follow:

$$\text{Utilisation } \% = \frac{Amount\ of\ unique\ nodes\ intersecting\ main\ node}{Swarm\ sze} \times 100$$

Swarm size 50 achieved 50% swarm utilisation at 60° beamwidth and 400km reach - the greatest out of all swarms. Link budgets with reaches of ≤ 50km yield no results. In all swarm scenarios, swarm utilisation increases with increasing beamwidths and increasing antenna reach. However, swarm utilisation decreases with swarm size increase, which indicates that smaller portions of the added nodes in the bigger swarms intersect with the main node during the simulation window. The only exception is swarm size 100, which yield better utilisation results than swarm size 50 at beam angles ≤ 30°. This is most likely because the beam angle is too small to pick up the surrounding nodes at swarm size 50, as the exception breaks down and the statement above again holds true for all swarm scenarios at beamwidths ≥ 45°.

CHAPTER 5: FUTURE WORK AND CONCLUSION

5.1 FUTURE WORK

The design in this thesis is limited in scope, therefore there exist many areas to be explored, such as:

Exploring the impact of power consumption. The S-NET mission makes use of a scan algorithm to find nearby nodes. The results in this thesis show that there might be long waiting times between node intersections. This makes orbit determination on a conceptual level more ideal to pinpoint intersection dates. In practice, however, the OBC would be under more strain. How would the usage of computational power fare against the use of a scan algorithm? Which one would use less power to obtain the same intersection results?

The implementation of this code on a cubesat. As an example, the results of all simulations were captured in arrays so that they could be studied. This method of running the code is impractical for cubesats, because of the vast amount of memory space needed to store everything. It would make more sense to run the code in increments, storing only useful information like dates of intersection, antennae position et cetera and discarding all other information. This will shorten execution time and help with memory optimisation.

The code implementation topic alone will have many subdivisions such as code optimisation affecting speed, efficiency, language usage (using C or C++), memory usage and storage space. Compatibility of hardware for peer-to-peer capabilities need also be explored since swarm intersection opportunities increase almost exponentially with extended range on nanosatellites antennae. Part of the link budget parameters would also be calculating the shortest timeframe needed by the hardware to send something meaningful and exclude any connections where the intersection time will be less than this calculated time. Consideration of error due to orbital drift from the specified orbital data epoch needs to be investigated in more detail and also taken into account.

Protocol of operation for the network and making it fault-tolerant. The effects of time-delays relaying TLE data from the ground station up to the swarm need to be analysed. The propagation of information between nodes can be analysed to see how much time it will take to reach all nodes via P2P intersections. Lastly, the TLE data used in the simulations were obtained from real-world objects. For future mission designs, one would need to create their own sets of orbital data for testing in order to make the simulations mission-specific.

5.2 CONCLUSION

The different topologies for nanosatellite configurations have been explored in the literature review. A swarm of nanosatellites with P2P capabilities forming a partially connected mesh topology was investigated in more detail. A numerical solution to find node locations were obtained. Orbital data was used in conjunction with the SGP4 algorithm in order to predict the positions of nanosatellites relative to one another in order to determine future dates of intersection and the position of the communicating antenna. Analysis was performed on the frequency of intersections based on various link budget specifications for a 24-hour period.

The time between intersections reduces with an increase in swarm size. The difference between intersection time vs equally spaced time intervals (theoretical mean time) is less than 5% with the exception of 36.55% deviation for 30° angle at 100km, however, this anomaly is likely to reduce with different simulation time windows. The simulations show that link budgets with reaches of ≤ 50km yield no results. In all swarm scenarios, swarm utilisation increases with increasing beamwidths and increasing antenna reach. However, swarm utilisation generally decreases with swarm size increase, which indicates that smaller portions of the added nodes in the bigger swarms intersect with the main node during the simulation window.

In all reach angle scenarios, an increase in reach distance from 100km to 200km, yields the most increase in intersections (more than 4.6 times) and is thus the dominant variable. Subsequent reach range increases produce intersection increases just below double the previous number of intersections. The results show that after increasing the range to 200km, it is more beneficial to increase the reach angle, as a doubling in beamwidth can produce over double the number of intersections for the same reach range. Beamwidth thus becomes the dominant variable at this point onwards. The results serve as an indicator for the feasibility of using swarms of nanosatellites and can be used in consideration of future nanosatellite swarm networks.

BIBLIOGRAPHY

18 SPCS, 2018. *Space Surveillance Network*. [online] Twitter. Available at: https://twitter.com/18SPCS/status/963629809921351680 [Accessed 4 Nov 2020].

Africanews, 2017. *Armyworm Invasion: Ghana Declares Agric 'State Of Emergency'*. [online] Available at: https://www.africanews.com/2017/05/08/armyworm-invasion-ghana-declares-agric-state-of-emergency// [Accessed 20 August 2020].

Aragon, B., Houborg, R., Tu, K., Fisher, J.B. and McCabe, M., 2018. CubeSats enable high spatiotemporal retrievals of crop-water use for precision agriculture. *Remote Sensing*, *10*(12), p.1867.

Chapter IV: Resolutions of the General Assembly, 1999. *Transactions of the International Astronomical Union, 23*(2), 25-51. doi:10.1017/S0251107X00011913

Cput.ac.za., n.d. *Operation Phakisa | French South African Institute of Technology*. [online] Available at: http://www.cput.ac.za/blogs/fsati/operation-phakisa/ [Accessed 6 Apr. 2017].

CSSI. 2020. *Welcome To Center For Space Standards & Innovation (CSSI)*. [online] Available at: http://www.centerforspace.com/downloads/ [Accessed 4 November 2020].

de Villiers, D., van Zyl, R., 2015. *ZACube-2: The successor to Africa's first nanosatellite*. [ebook] Cape Town: French South African Institute of Technology (F'SATI), Cape Peninsula University of Technology (CPUT), p.5. Available at: http://www.amsatsa.org.za/ZACube-2%20%20The%20successor%20to%20Africa%E2%80%99s%20first%20nanosatellite.pdf [Accessed 5 May 2017].

Dershowitz, N., Reingold, E.M., 2008. *Calendrical calculations*. Cambridge University Press. p.16.

Dijkstra, E.W., 1959. A note on two problems in connexion with graphs. *Numerische mathematik*, *1*(1), pp.269-271.

Dong, F., Huang, Q., Li, H., Kong, B. and Zhang, W., 2015. A novel M2M backbone network architecture. *International journal of distributed sensor networks*, *11*(11), p.512321.

Herschel, J.F.W., 1870. *Outlines of astronomy*. Blanchard & Lea. pp. 531-535

Hoots, F.R., Roehrich, R.L., 1980. Spacetrack report no. 3, Models for Propagation of NORAD Element Sets. http://www. itc. nl/-bakker/orbit. html.

ITU. Radio Regulations, Vol. 1; Technical Report; International Telecommunication Union: Geneva, Switzerland, 2016.

Jooinn.com. 2021. *Earth from space*. [online] Available at: https://jooinn.com/img/startdownload?url=earth-from-space-40.png [Accessed 14 October 2020].

Kelso, T.S., 2019a. *Celestrak: "Orbital Coordinate Systems, Part I"*. [online] Celestrak.com. Available at: https://celestrak.com/columns/v02n01/ [Accessed 23 October 2020].

Kelso, T.S., 2019b. *Celestrak: "More Frequently Asked Questions"*. [online] Celestrak.com. Available at: https://celestrak.com/columns/v04n05/ [Accessed 23 October 2020].

Kelso, T.S., 2019c. *Celestrak: "Faqs: Two-Line Element Set Format"*. [online] Celestrak.com. Available at: https://www.celestrak.com/columns/v04n03/ [Accessed 4 November 2020].

Kelso, T.S., 2019d. *Celestrak: Two-Line Element Set Checksum Controversy*. [online] Celestrak.com. Available at: http://celestrak.com/NORAD/documentation/checksum.php [Accessed 4 November 2020].

Khabbazan, S., Vermunt, P., Steele-Dunne, S., Ratering Arntz, L., Marinetti, C., van der Valk, D., Iannini, L., Molijn, R., Westerdijk, K. and van der Sande, C., 2019. Crop monitoring using Sentinel-1 data: a case study from The Netherlands. *Remote Sensing*, *11*(16), p.1887.

Lane, M.H., Hoots, F.R., 1979. *General perturbations theories derived from the 1965 lane drag theory*. AEROSPACE DEFENSE COMMAND PETERSON AFB CO OFFICE OF ASTRODYNAMICS.

Mathworld.wolfram.com, 2020. *Point-Line Distance--3-Dimensional -- From Wolfram Mathworld*. [online] Available at: https://mathworld.wolfram.com/Point-LineDistance3-Dimensional.html [Accessed 20 October 2020].

McCarthy, D.D., 1998. The julian and modified julian dates. *Journal for the History of Astronomy*, *29*(4), pp.327-330.

Muthusamy, V., 2003. *An Introduction to Peer-to-Peer Networks*.

Operation Phakisa, 2015. *Operation Phakisa: Unlocking the Economic Potential of South Africa's Oceans*. Marine Protection Services and Governance Lab Report. [online] p.4. Available at: http://www.operationphakisa.gov.za/operations/oel/pmpg/Marine%20Protection%20and%20

Govenance%20Documents/Marine%20Protection%20and%20Govenance/OPOceans%20MPSG%20Executive%20Summary.pdf [Accessed 24 Apr. 2017].

Operationphakisa.gov.za., n.d. *Introduction*. [online] Available at: http://www.operationphakisa.gov.za/Pages/Home.aspx [Accessed 11 Apr. 2017].

Pranajaya, F.M., Zee, R.E., Cain, J. and Kolacz, R., 2010. *NANOSATELLITE TRACKING SHIPS: COST-EFFECTIVE RESPONSIVE SPACE*. University of Toronto Institute for Aerospace Studies Space Flight Laboratory, p.2. Available at: https://utias-sfl.net/wp-content/uploads/IAC2010-S16-1-Nanosatellite-tracking-F-Pranajaya.pdf [Accessed 13 Feb. 2020].

Rhodes, B., 2020a. *Sgp4*. [online] PyPI. Available at: https://pypi.org/project/sgp4/ [Accessed 24 October 2020].

Rhodes, B., 2020b. *Brandon-Rhodes/Python-Sgp4*. [online] GitHub. Available at: https://github.com/brandon-rhodes/python-sgp4 [Accessed 24 October 2020].

South African Government, 2013. *National Development Plan 2030 | South African Government*. [online] Available at: http://www.gov.za/issues/national-development-plan-2030 [Accessed 10 Apr. 2017].

Space-track.org., n.d. *Introduction To The API*. [online] Available at: <https://www.space-track.org/documentation#api> [Accessed 4 November 2020].

Vallado, D.A., Crawford, P., Hujsak, R. and Kelso T. S., 2006. “Revisiting Spacetrack Report #3”, AIAA 2006-6753

Weeden, B., 2019. *US Policy And Capabilities On SSA*. [ebook] Seoul, South Korea: Secure World Foundation, p.7. Available at: https://swfound.org/media/.../weeden-us-policy-and-capabilities-for-ssa.pdf [Accessed 4 November 2020].

Yaglioglu, B., 2011. *A fractionated spacecraft architecture for earth observation missions* (Masters Thesis, University of Tokyo).

Yoon, Z., Frese, W. and Briess, K., 2019. Design and implementation of a narrow-band intersatellite network with limited onboard resources for IoT. *Sensors*, *19*(19), pp. 19-20.

Zuma, J., 2014. *Operation Phakisa: Unlocking the Economic Potential of the Ocean Economy*.

APPENDIX

SIMULATION SWARM SIZE 200, 30 DEGREES, 200KM REACH

```
INFORMATION
-------------------------------------------------------------------------------
Epoch: 2020-08-29 04:09:06.718752+00:00 Julian Date: 2459090.5 Fr: 0.17299443
-------------------------------------------------------------------------------
TLE Line 1: 1 45727U 20037E 20322.59617450 .00000863 00000-0 92096-4 0 9990


TLE Line 2: 2 45727 97.7022 139.1622 0013849 147.4761 212.7301 14.91260358 20842

*******************************************************************************

INPUT
-------------------------------------------------------------------------------
Running for: ZACube-2
Time increments: 1.0 seconds
Period: 24 hours
Julian time fraction: 1.1574074074074073e-05
Number of dates to plot: 86400
Number of Satellites: 200
Satellite reach: 200 km
Beamwidth: 30 degrees
Straight-line reach: 193.18516525781365 km

Running... Intersection Calculations...
Plot Satellites...

OUTPUT
-------------------------------------------------------------------------------
Intersection will happen at the following dates:

Running... Intersection dates array...
Node 1 & Node 76 JD: 2459090.5 Fraction: 0.17971896703703272 Left antenna. Distance 131.0181 km
Node 1 & Node 76 JD: 2459090.5 Fraction: 0.17973054111110678 Left antenna. Distance 131.5366 km
Node 1 & Node 76 JD: 2459090.5 Fraction: 0.17974211518518085 Left antenna. Distance 133.7507 km
Node 1 & Node 76 JD: 2459090.5 Fraction: 0.17975368925925492 Left antenna. Distance 137.5784 km
Node 1 & Node 89 JD: 2459090.5 Fraction: 0.18361942999999317 Left antenna. Distance 127.531 km
Node 1 & Node 89 JD: 2459090.5 Fraction: 0.18363100407406724 Left antenna. Distance 130.0779 km
Node 1 & Node 89 JD: 2459090.5 Fraction: 0.1836425781481413 Left antenna. Distance 134.2074 km
Node 1 & Node 89 JD: 2459090.5 Fraction: 0.18365415222221537 Left antenna. Distance 139.7793 km
Node 1 & Node 76 JD: 2459090.5 Fraction: 0.21255461518515975 Right antenna. Distance 126.0071 km
Node 1 & Node 76 JD: 2459090.5 Fraction: 0.21256618925923382 Right antenna. Distance 126.049 km
Node 1 & Node 76 JD: 2459090.5 Fraction: 0.21257776333330788 Right antenna. Distance 127.8683 km
Node 1 & Node 76 JD: 2459090.5 Fraction: 0.21258933740738195 Right antenna. Distance 131.3912 km
Node 1 & Node 76 JD: 2459090.5 Fraction: 0.21260091148145602 Right antenna. Distance 136.4859 km
Node 1 & Node 89 JD: 2459090.5 Fraction: 0.21644350407404614 Right antenna. Distance 119.8583 km
Node 1 & Node 89 JD: 2459090.5 Fraction: 0.2164550781481202 Right antenna. Distance 122.079 km
Node 1 & Node 89 JD: 2459090.5 Fraction: 0.21646665222219427 Right antenna. Distance 125.9953 km
Node 1 & Node 89 JD: 2459090.5 Fraction: 0.21647822629626834 Right antenna. Distance 131.4558 km
Node 1 & Node 76 JD: 2459090.5 Fraction: 0.24533239296291645 Left antenna. Distance 136.1105 km
Node 1 & Node 76 JD: 2459090.5 Fraction: 0.24534396703699052 Left antenna. Distance 137.4853 km
Node 1 & Node 16 JD: 2459090.5 Fraction: 0.24535554111106458 Front antenna. Distance 179.9183 km
Node 1 & Node 76 JD: 2459090.5 Fraction: 0.24535554111106458 Left antenna. Distance 140.462 km
Node 1 & Node 16 JD: 2459090.5 Fraction: 0.24536711518513865 Front antenna. Distance 165.6877 km
Node 1 & Node 76 JD: 2459090.5 Fraction: 0.24536711518513865 Left antenna. Distance 144.9419 km
Node 1 & Node 16 JD: 2459090.5 Fraction: 0.24537868925921272 Front antenna. Distance 151.592 km
Node 1 & Node 16 JD: 2459090.5 Fraction: 0.24539026333328678 Front antenna. Distance 137.6726 km
Node 1 & Node 16 JD: 2459090.5 Fraction: 0.24540183740736085 Front antenna. Distance 123.9891 km
Node 1 & Node 16 JD: 2459090.5 Fraction: 0.24549442999995338 Right antenna. Distance 52.765 km
Node 1 & Node 16 JD: 2459090.5 Fraction: 0.24550600407402745 Right antenna. Distance 56.7225 km
Node 1 & Node 89 JD: 2459090.5 Fraction: 0.2492675781480991 Left antenna. Distance 122.7753 km
Node 1 & Node 89 JD: 2459090.5 Fraction: 0.24927915222217317 Left antenna. Distance 125.6366 km
Node 1 & Node 89 JD: 2459090.5 Fraction: 0.24929072629624724 Left antenna. Distance 130.1176 km
Node 1 & Node 76 JD: 2459090.5 Fraction: 0.27816804111111104 Right antenna. Distance 130.83 km
Node 1 & Node 76 JD: 2459090.5 Fraction: 0.27817961518518514 Right antenna. Distance 131.789 km
Node 1 & Node 76 JD: 2459090.5 Fraction: 0.27819118925925923 Right antenna. Distance 134.4307 km
Node 1 & Node 76 JD: 2459090.5 Fraction: 0.2782027633333333 Right antenna. Distance 138.659 km
Node 1 & Node 89 JD: 2459090.5 Fraction: 0.28209165222222904 Right antenna. Distance 115.0284 km
Node 1 & Node 89 JD: 2459090.5 Fraction: 0.28210322629630313 Right antenna. Distance 117.5999 km
```

Node 1 & Node 89 JD: 2459090.5 Fraction: 0.28211480037037723 Right antenna. Distance 121.9106 km
Node 1 & Node 76 JD: 2459090.5 Fraction: 0.31093424481487225 Left antenna. Distance 141.069 km
Node 1 & Node 76 JD: 2459090.5 Fraction: 0.31094581888894635 Left antenna. Distance 141.653 km
Node 1 & Node 76 JD: 2459090.5 Fraction: 0.31095739296302044 Left antenna. Distance 143.812 km
Node 1 & Node 76 JD: 2459090.5 Fraction: 0.31096896703709453 Left antenna. Distance 147.4768 km
Node 1 & Node 76 JD: 2459090.5 Fraction: 0.31098054111116863 Left antenna. Distance 152.539 km
Node 1 & Node 16 JD: 2459090.5 Fraction: 0.3116865596296884 Left antenna. Distance 150.7944 km
Node 1 & Node 16 JD: 2459090.5 Fraction: 0.3116981337037625 Left antenna. Distance 144.9522 km
Node 1 & Node 16 JD: 2459090.5 Fraction: 0.3117097077778366 Left antenna. Distance 140.4625 km
Node 1 & Node 16 JD: 2459090.5 Fraction: 0.31172128185191067 Left antenna. Distance 137.458 km
Node 1 & Node 16 JD: 2459090.5 Fraction: 0.31173285592598476 Left antenna. Distance 136.0372 km
Node 1 & Node 89 JD: 2459090.5 Fraction: 0.3149157262963607 Left antenna. Distance 118.0789 km
Node 1 & Node 89 JD: 2459090.5 Fraction: 0.3149273003704348 Left antenna. Distance 121.2777 km
Node 1 & Node 89 JD: 2459090.5 Fraction: 0.3149388744445089 Left antenna. Distance 126.1317 km
Node 1 & Node 76 JD: 2459090.5 Fraction: 0.343769892963078 Right antenna. Distance 135.9889 km
Node 1 & Node 76 JD: 2459090.5 Fraction: 0.3437814670371521 Right antenna. Distance 136.1431 km
Node 1 & Node 76 JD: 2459090.5 Fraction: 0.3437930411112262 Right antenna. Distance 137.9432 km
Node 1 & Node 76 JD: 2459090.5 Fraction: 0.3438046151853003 Right antenna. Distance 141.3263 km
Node 1 & Node 76 JD: 2459090.5 Fraction: 0.3438161892593744 Right antenna. Distance 146.1825 km
Node 1 & Node 89 JD: 2459090.5 Fraction: 0.3477398003704924 Right antenna. Distance 110.2708 km
Node 1 & Node 89 JD: 2459090.5 Fraction: 0.3477513744445665 Right antenna. Distance 113.2209 km
Node 1 & Node 89 JD: 2459090.5 Fraction: 0.3477629485186406 Right antenna. Distance 117.9515 km
Node 1 & Node 76 JD: 2459090.5 Fraction: 0.37653609666683924 Left antenna. Distance 146.3723 km
Node 1 & Node 76 JD: 2459090.5 Fraction: 0.37654767074091333 Left antenna. Distance 146.2158 km
Node 1 & Node 76 JD: 2459090.5 Fraction: 0.3765592448149874 Left antenna. Distance 147.5957 km
Node 1 & Node 76 JD: 2459090.5 Fraction: 0.3765708188890615 Left antenna. Distance 150.4697 km
Node 1 & Node 76 JD: 2459090.5 Fraction: 0.3765823929631356 Left antenna. Distance 154.7546 km
Node 1 & Node 89 JD: 2459090.5 Fraction: 0.3805638744446241 Left antenna. Distance 113.4494 km
Node 1 & Node 89 JD: 2459090.5 Fraction: 0.3805754485186982 Left antenna. Distance 117.0107 km
Node 1 & Node 89 JD: 2459090.5 Fraction: 0.3805870225927723 Left antenna. Distance 122.26 km
Node 1 & Node 76 JD: 2459090.5 Fraction: 0.4093833188891191 Right antenna. Distance 140.8894 km
Node 1 & Node 76 JD: 2459090.5 Fraction: 0.4093948929631932 Right antenna. Distance 141.8925 km
Node 1 & Node 76 JD: 2459090.5 Fraction: 0.4094064670372673 Right antenna. Distance 144.4596 km
Node 1 & Node 76 JD: 2459090.5 Fraction: 0.4094180411113414 Right antenna. Distance 148.5095 km
Node 1 & Node 76 JD: 2459090.5 Fraction: 0.4094296151854155 Right antenna. Distance 153.9253 km
Node 1 & Node 89 JD: 2459090.5 Fraction: 0.41338794851875577 Right antenna. Distance 105.5954 km
Node 1 & Node 89 JD: 2459090.5 Fraction: 0.41339952259282986 Right antenna. Distance 108.9544 km
Node 1 & Node 70 JD: 2459090.5 Fraction: 0.4237930411113666 Top antenna. Distance 100.364 km
Node 1 & Node 70 JD: 2459090.5 Fraction: 0.4238046151854407 Top antenna. Distance 100.0555 km
Node 1 & Node 76 JD: 2459090.5 Fraction: 0.4421495225928803 Left antenna. Distance 151.137 km
Node 1 & Node 76 JD: 2459090.5 Fraction: 0.4421610966669544 Left antenna. Distance 151.7798 km
Node 1 & Node 76 JD: 2459090.5 Fraction: 0.4421726707410285 Left antenna. Distance 153.8929 km
Node 1 & Node 76 JD: 2459090.5 Fraction: 0.4421842448151026 Left antenna. Distance 157.4171 km
Node 1 & Node 76 JD: 2459090.5 Fraction: 0.4421958188891767 Left antenna. Distance 162.2606 km
Node 1 & Node 89 JD: 2459090.5 Fraction: 0.44621202259288745 Left antenna. Distance 108.8956 km
Node 1 & Node 89 JD: 2459090.5 Fraction: 0.44622359666696154 Left antenna. Distance 112.8462 km
Node 1 & Node 47 JD: 2459090.5 Fraction: 0.46042498555587535 Top antenna. Distance 134.5419 km
Node 1 & Node 76 JD: 2459090.5 Fraction: 0.4749851707410861 Right antenna. Distance 145.9887 km
Node 1 & Node 76 JD: 2459090.5 Fraction: 0.4749967448151602 Right antenna. Distance 146.2424 km
Node 1 & Node 76 JD: 2459090.5 Fraction: 0.4750083188892343 Right antenna. Distance 148.0283 km
Node 1 & Node 76 JD: 2459090.5 Fraction: 0.4750198929633084 Right antenna. Distance 151.2924 km
Node 1 & Node 76 JD: 2459090.5 Fraction: 0.47503146703738247 Right antenna. Distance 155.9416 km
Node 1 & Node 89 JD: 2459090.5 Fraction: 0.47903609666701913 Right antenna. Distance 101.0142 km
Node 1 & Node 89 JD: 2459090.5 Fraction: 0.4790476707410932 Right antenna. Distance 104.8144 km
Node 1 & Node 76 JD: 2459090.5 Fraction: 0.5077513744448101 Left antenna. Distance 156.3821 km
Node 1 & Node 76 JD: 2459090.5 Fraction: 0.5077629485188841 Left antenna. Distance 156.3314 km
Node 1 & Node 76 JD: 2459090.5 Fraction: 0.5077745225929582 Left antenna. Distance 157.7177 km
Node 1 & Node 76 JD: 2459090.5 Fraction: 0.5077860966670322 Left antenna. Distance 160.5037 km
Node 1 & Node 76 JD: 2459090.5 Fraction: 0.5077976707411063 Left antenna. Distance 164.6184 km
Node 1 & Node 89 JD: 2459090.5 Fraction: 0.5118485966670199 Left antenna. Distance 102.0241 km
Node 1 & Node 89 JD: 2459090.5 Fraction: 0.5118601707410939 Left antenna. Distance 104.4277 km
Node 1 & Node 89 JD: 2459090.5 Fraction: 0.511871744815168 Left antenna. Distance 108.7964 km
Node 1 & Node 76 JD: 2459090.5 Fraction: 0.5405870225928584 Right antenna. Distance 151.4043 km
Node 1 & Node 76 JD: 2459090.5 Fraction: 0.5405985966669324 Right antenna. Distance 150.9571 km
Node 1 & Node 76 JD: 2459090.5 Fraction: 0.5406101707410065 Right antenna. Distance 152.0009 km
Node 1 & Node 76 JD: 2459090.5 Fraction: 0.5406217448150805 Right antenna. Distance 154.5054 km
Node 1 & Node 76 JD: 2459090.5 Fraction: 0.5406333188891546 Right antenna. Distance 158.4014 km
Node 1 & Node 76 JD: 2459090.5 Fraction: 0.5406448929632286 Right antenna. Distance 163.5895 km
Node 1 & Node 89 JD: 2459090.5 Fraction: 0.5446842448150682 Right antenna. Distance 96.5408 km
Node 1 & Node 39 JD: 2459090.5 Fraction: 0.5497189670372751 Top antenna. Distance 134.8361 km
Node 1 & Node 39 JD: 2459090.5 Fraction: 0.5497305411113491 Top antenna. Distance 134.4534 km
Node 1 & Node 39 JD: 2459090.5 Fraction: 0.5497421151854232 Top antenna. Distance 134.1432 km
Node 1 & Node 39 JD: 2459090.5 Fraction: 0.5497536892594972 Top antenna. Distance 133.9059 km
Node 1 & Node 39 JD: 2459090.5 Fraction: 0.5497652633335712 Top antenna. Distance 133.742 km
Node 1 & Node 39 JD: 2459090.5 Fraction: 0.5497768374076453 Top antenna. Distance 133.6516 km

Node 1 & Node 39 JD: 2459090.5 Fraction: 0.5497884114817193 Top antenna. Distance 133.635 km
Node 1 & Node 39 JD: 2459090.5 Fraction: 0.5497999855557933 Top antenna. Distance 133.6922 km
Node 1 & Node 39 JD: 2459090.5 Fraction: 0.5498115596298674 Top antenna. Distance 133.8231 km
Node 1 & Node 39 JD: 2459090.5 Fraction: 0.5498231337039414 Top antenna. Distance 134.0275 km
Node 1 & Node 39 JD: 2459090.5 Fraction: 0.5498347077780155 Top antenna. Distance 134.305 km
Node 1 & Node 39 JD: 2459090.5 Fraction: 0.5498462818520895 Top antenna. Distance 134.6552 km
Node 1 & Node 76 JD: 2459090.5 Fraction: 0.5733648003705365 Left antenna. Distance 161.2185 km
Node 1 & Node 76 JD: 2459090.5 Fraction: 0.5733763744446105 Left antenna. Distance 161.9147 km
Node 1 & Node 76 JD: 2459090.5 Fraction: 0.5733879485186846 Left antenna. Distance 163.9894 km
Node 1 & Node 76 JD: 2459090.5 Fraction: 0.5733995225927586 Left antenna. Distance 167.3915 km
Node 1 & Node 76 JD: 2459090.5 Fraction: 0.5734110966668327 Left antenna. Distance 172.0422 km
Node 1 & Node 89 JD: 2459090.5 Fraction: 0.5774967448149684 Left antenna. Distance 97.2605 km
Node 1 & Node 89 JD: 2459090.5 Fraction: 0.5775083188890424 Left antenna. Distance 100.0576 km
Node 1 & Node 89 JD: 2459090.5 Fraction: 0.5775198929631165 Left antenna. Distance 104.8748 km
Node 1 & Node 76 JD: 2459090.5 Fraction: 0.6062004485185848 Right antenna. Distance 156.0027 km
Node 1 & Node 76 JD: 2459090.5 Fraction: 0.6062120225926588 Right antenna. Distance 156.3455 km
Node 1 & Node 76 JD: 2459090.5 Fraction: 0.6062235966667329 Right antenna. Distance 158.1215 km
Node 1 & Node 76 JD: 2459090.5 Fraction: 0.6062351707408069 Right antenna. Distance 161.2835 km
Node 1 & Node 76 JD: 2459090.5 Fraction: 0.606246744814881 Right antenna. Distance 165.7521 km
Node 1 & Node 89 JD: 2459090.5 Fraction: 0.6101819300000542 Front antenna. Distance 190.3679 km
Node 1 & Node 76 JD: 2459090.5 Fraction: 0.6389666522221888 Left antenna. Distance 166.4107 km
Node 1 & Node 76 JD: 2459090.5 Fraction: 0.6389782262962629 Left antenna. Distance 166.455 km
Node 1 & Node 76 JD: 2459090.5 Fraction: 0.6389898003703369 Left antenna. Distance 167.8488 km
Node 1 & Node 76 JD: 2459090.5 Fraction: 0.639001374444411 Left antenna. Distance 170.559 km
Node 1 & Node 76 JD: 2459090.5 Fraction: 0.639012948518485 Left antenna. Distance 174.5243 km
Node 1 & Node 76 JD: 2459090.5 Fraction: 0.639024522592559 Left antenna. Distance 179.6616 km
Node 1 & Node 89 JD: 2459090.5 Fraction: 0.6431448929629169 Left antenna. Distance 92.5724 km
Node 1 & Node 89 JD: 2459090.5 Fraction: 0.6431564670369909 Left antenna. Distance 95.799 km
Node 1 & Node 76 JD: 2459090.5 Fraction: 0.6718023003702371 Right antenna. Distance 161.3473 km
Node 1 & Node 76 JD: 2459090.5 Fraction: 0.6718138744443112 Right antenna. Distance 161.0312 km
Node 1 & Node 76 JD: 2459090.5 Fraction: 0.6718254485183852 Right antenna. Distance 162.1129 km
Node 1 & Node 76 JD: 2459090.5 Fraction: 0.6718370225924593 Right antenna. Distance 164.5648 km
Node 1 & Node 76 JD: 2459090.5 Fraction: 0.6718485966665333 Right antenna. Distance 168.3271 km
Node 1 & Node 76 JD: 2459090.5 Fraction: 0.6718601707406073 Right antenna. Distance 173.3144 km
Node 1 & Node 89 JD: 2459090.5 Fraction: 0.6758300781480027 Front antenna. Distance 186.2097 km
Node 1 & Node 14 JD: 2459090.5 Fraction: 0.685147207777604 Front antenna. Distance 195.198 km
Node 1 & Node 76 JD: 2459090.5 Fraction: 0.7045800781479152 Left antenna. Distance 171.3106 km
Node 1 & Node 76 JD: 2459090.5 Fraction: 0.7045916522219893 Left antenna. Distance 172.0558 km
Node 1 & Node 76 JD: 2459090.5 Fraction: 0.7046032262960633 Left antenna. Distance 174.0985 km
Node 1 & Node 76 JD: 2459090.5 Fraction: 0.7046148003701374 Left antenna. Distance 177.3939 km
Node 1 & Node 76 JD: 2459090.5 Fraction: 0.7046263744442114 Left antenna. Distance 181.8738 km
Node 1 & Node 89 JD: 2459090.5 Fraction: 0.7086425781479029 Front antenna. Distance 196.7638 km
Node 1 & Node 89 JD: 2459090.5 Fraction: 0.7086541522219769 Front antenna. Distance 183.6354 km
Node 1 & Node 89 JD: 2459090.5 Fraction: 0.7087930411108654 Left antenna. Distance 87.972 km
Node 1 & Node 89 JD: 2459090.5 Fraction: 0.7088046151849394 Left antenna. Distance 91.6676 km
Node 1 & Node 76 JD: 2459090.5 Fraction: 0.7374157262959635 Right antenna. Distance 166.0283 km
Node 1 & Node 76 JD: 2459090.5 Fraction: 0.7374273003700376 Right antenna. Distance 166.4516 km
Node 1 & Node 76 JD: 2459090.5 Fraction: 0.7374388744441116 Right antenna. Distance 168.2212 km
Node 1 & Node 76 JD: 2459090.5 Fraction: 0.7374504485181856 Right antenna. Distance 171.2951 km
Node 1 & Node 76 JD: 2459090.5 Fraction: 0.7374620225922597 Right antenna. Distance 175.6051 km
Node 1 & Node 76 JD: 2459090.5 Fraction: 0.7374735966663337 Right antenna. Distance 181.0627 km
Node 1 & Node 89 JD: 2459090.5 Fraction: 0.7414666522218771 Front antenna. Distance 195.4925 km
Node 1 & Node 89 JD: 2459090.5 Fraction: 0.7414782262959512 Front antenna. Distance 182.1222 km
Node 1 & Node 89 JD: 2459090.5 Fraction: 0.7414898003700252 Front antenna. Distance 168.9788 km
Node 1 & Node 76 JD: 2459090.5 Fraction: 0.7701819299995676 Left antenna. Distance 176.4547 km
Node 1 & Node 76 JD: 2459090.5 Fraction: 0.7701935040736416 Left antenna. Distance 176.5849 km
Node 1 & Node 76 JD: 2459090.5 Fraction: 0.7702050781477157 Left antenna. Distance 177.9871 km
Node 1 & Node 76 JD: 2459090.5 Fraction: 0.7702166522217897 Left antenna. Distance 180.6317 km
Node 1 & Node 76 JD: 2459090.5 Fraction: 0.7702282262958637 Left antenna. Distance 184.4651 km
Node 1 & Node 76 JD: 2459090.5 Fraction: 0.7702398003699378 Left antenna. Distance 189.4153 km
Node 1 & Node 89 JD: 2459090.5 Fraction: 0.7742907262958514 Front antenna. Distance 192.9073 km
Node 1 & Node 89 JD: 2459090.5 Fraction: 0.7743023003699254 Front antenna. Distance 179.6537 km
Node 1 & Node 89 JD: 2459090.5 Fraction: 0.7744411892588139 Left antenna. Distance 83.4743 km
Node 1 & Node 38 JD: 2459090.5 Fraction: 0.7794643374069468 Top antenna. Distance 90.4483 km
Node 1 & Node 38 JD: 2459090.5 Fraction: 0.7794759114810208 Top antenna. Distance 89.8379 km
Node 1 & Node 38 JD: 2459090.5 Fraction: 0.7794874855550948 Top antenna. Distance 89.3594 km
Node 1 & Node 38 JD: 2459090.5 Fraction: 0.7794990596291689 Top antenna. Distance 89.015 km
Node 1 & Node 38 JD: 2459090.5 Fraction: 0.7795106337032429 Top antenna. Distance 88.8061 km
Node 1 & Node 38 JD: 2459090.5 Fraction: 0.779522207777317 Top antenna. Distance 88.7338 km
Node 1 & Node 38 JD: 2459090.5 Fraction: 0.779533781851391 Top antenna. Distance 88.7983 km
Node 1 & Node 38 JD: 2459090.5 Fraction: 0.779545355925465 Top antenna. Distance 88.9994 km
Node 1 & Node 38 JD: 2459090.5 Fraction: 0.7795569299995391 Top antenna. Distance 89.3362 km
Node 1 & Node 38 JD: 2459090.5 Fraction: 0.7795685040736131 Top antenna. Distance 89.8071 km
Node 1 & Node 38 JD: 2459090.5 Fraction: 0.7795800781476871 Top antenna. Distance 90.41 km
Node 1 & Node 147 JD: 2459090.5 Fraction: 0.8009458188883629 Top antenna. Distance 94.2284 km

Node 1 & Node 147 JD: 2459090.5 Fraction: 0.800957392962437 Top antenna. Distance 94.8305 km
Node 1 & Node 76 JD: 2459090.5 Fraction: 0.8030175781476159 Right antenna. Distance 171.3086 km
Node 1 & Node 76 JD: 2459090.5 Fraction: 0.8030291522216899 Right antenna. Distance 171.1105 km
Node 1 & Node 76 JD: 2459090.5 Fraction: 0.803040726295764 Right antenna. Distance 172.2278 km
Node 1 & Node 76 JD: 2459090.5 Fraction: 0.803052300369838 Right antenna. Distance 174.6353 km
Node 1 & Node 76 JD: 2459090.5 Fraction: 0.8030638744443912 Right antenna. Distance 178.2808 km
Node 1 & Node 76 JD: 2459090.5 Fraction: 0.8030754485179861 Right antenna. Distance 183.0902 km
Node 1 & Node 89 JD: 2459090.5 Fraction: 0.8071148003698256 Front antenna. Distance 191.5977 km
Node 1 & Node 89 JD: 2459090.5 Fraction: 0.8071263744438997 Front antenna. Distance 178.1107 km
Node 1 & Node 89 JD: 2459090.5 Fraction: 0.8071379485179737 Front antenna. Distance 164.8371 km
Node 1 & Node 65 JD: 2459090.5 Fraction: 0.8223347077771868 Top antenna. Distance 161.1417 km
Node 1 & Node 65 JD: 2459090.5 Fraction: 0.8223462818512608 Top antenna. Distance 159.3218 km
Node 1 & Node 65 JD: 2459090.5 Fraction: 0.8223578559253348 Top antenna. Distance 158.8857 km
Node 1 & Node 65 JD: 2459090.5 Fraction: 0.8223694299994089 Top antenna. Distance 159.8447 km
Node 1 & Node 65 JD: 2459090.5 Fraction: 0.8223810040734829 Top antenna. Distance 162.174 km
Node 1 & Node 76 JD: 2459090.5 Fraction: 0.8357837818512199 Left antenna. Distance 181.8621 km
Node 1 & Node 76 JD: 2459090.5 Fraction: 0.835795355925294 Left antenna. Distance 181.4113 km
Node 1 & Node 76 JD: 2459090.5 Fraction: 0.835806929999368 Left antenna. Distance 182.2018 km
Node 1 & Node 76 JD: 2459090.5 Fraction: 0.835818504073442 Left antenna. Distance 184.2176 km
Node 1 & Node 76 JD: 2459090.5 Fraction: 0.8358300781475161 Left antenna. Distance 187.4192 km
Node 1 & Node 76 JD: 2459090.5 Fraction: 0.8358416522215901 Left antenna. Distance 191.7472 km
Node 1 & Node 76 JD: 2459090.5 Fraction: 0.8358532262956642 Left antenna. Distance 197.1274 km
Node 1 & Node 89 JD: 2459090.5 Fraction: 0.8399388744437999 Front antenna. Distance 189.1227 km
Node 1 & Node 89 JD: 2459090.5 Fraction: 0.8399504485178739 Front antenna. Distance 175.7444 km
Node 1 & Node 76 JD: 2459090.5 Fraction: 0.8686310040733423 Right antenna. Distance 176.0631 km
Node 1 & Node 76 JD: 2459090.5 Fraction: 0.8686425781474163 Right antenna. Distance 176.56 km
Node 1 & Node 76 JD: 2459090.5 Fraction: 0.8686541522214903 Right antenna. Distance 178.3259 km
Node 1 & Node 76 JD: 2459090.5 Fraction: 0.8686657262955644 Right antenna. Distance 181.3236 km
Node 1 & Node 76 JD: 2459090.5 Fraction: 0.8686773003696384 Right antenna. Distance 185.4936 km
Node 1 & Node 76 JD: 2459090.5 Fraction: 0.8686888744437125 Right antenna. Distance 190.7588 km
Node 1 & Node 89 JD: 2459090.5 Fraction: 0.8727629485177741 Front antenna. Distance 187.7827 km
Node 1 & Node 89 JD: 2459090.5 Fraction: 0.8727745225918482 Front antenna. Distance 174.1804 km
Node 1 & Node 89 JD: 2459090.5 Fraction: 0.8727860966659222 Front antenna. Distance 160.7775 km
Node 1 & Node 76 JD: 2459090.5 Fraction: 0.9013972077769463 Left antenna. Distance 186.5111 km
Node 1 & Node 76 JD: 2459090.5 Fraction: 0.9014087818510204 Left antenna. Distance 186.7197 km
Node 1 & Node 76 JD: 2459090.5 Fraction: 0.9014203559250944 Left antenna. Distance 188.1311 km
Node 1 & Node 76 JD: 2459090.5 Fraction: 0.9014319299991684 Left antenna. Distance 190.7186 km
Node 1 & Node 76 JD: 2459090.5 Fraction: 0.9014435040732425 Left antenna. Distance 194.4351 km
Node 1 & Node 89 JD: 2459090.5 Fraction: 0.9055870225917484 Front antenna. Distance 185.4145 km
Node 1 & Node 89 JD: 2459090.5 Fraction: 0.9055985966658224 Front antenna. Distance 171.9124 km
Node 1 & Node 89 JD: 2459090.5 Fraction: 0.9056101707398965 Front antenna. Distance 158.6329 km
Node 1 & Node 76 JD: 2459090.5 Fraction: 0.9342328559249946 Right antenna. Distance 181.2848 km
Node 1 & Node 76 JD: 2459090.5 Fraction: 0.9342444299990686 Right antenna. Distance 181.1937 km
Node 1 & Node 76 JD: 2459090.5 Fraction: 0.9342560040731427 Right antenna. Distance 182.3447 km
Node 1 & Node 76 JD: 2459090.5 Fraction: 0.9342675781472167 Right antenna. Distance 184.7148 km
Node 1 & Node 76 JD: 2459090.5 Fraction: 0.9342791522212908 Right antenna. Distance 188.2577 km
Node 1 & Node 76 JD: 2459090.5 Fraction: 0.9342907262953648 Right antenna. Distance 192.9089 km
Node 1 & Node 76 JD: 2459090.5 Fraction: 0.9343023003694388 Right antenna. Distance 198.5904 km
Node 1 & Node 89 JD: 2459090.5 Fraction: 0.9384110966657226 Front antenna. Distance 184.0525 km
Node 1 & Node 89 JD: 2459090.5 Fraction: 0.9384226707397967 Front antenna. Distance 170.3372 km
Node 1 & Node 89 JD: 2459090.5 Fraction: 0.9384342448138707 Front antenna. Distance 156.8067 km
Node 1 & Node 89 JD: 2459090.5 Fraction: 0.9384458188879448 Front antenna. Distance 143.5133 km
Node 1 & Node 76 JD: 2459090.5 Fraction: 0.9669990596285987 Left antenna. Distance 191.8618 km
Node 1 & Node 76 JD: 2459090.5 Fraction: 0.9670106337026727 Left antenna. Distance 191.5187 km
Node 1 & Node 76 JD: 2459090.5 Fraction: 0.9670222077767467 Left antenna. Distance 192.3514 km
Node 1 & Node 89 JD: 2459090.5 Fraction: 0.9712351707396969 Front antenna. Distance 181.7874 km
Node 1 & Node 89 JD: 2459090.5 Fraction: 0.9712467448137709 Front antenna. Distance 168.1633 km
Node 1 & Node 89 JD: 2459090.5 Fraction: 0.971258318887845 Front antenna. Distance 154.7459 km
Node 1 & Node 76 JD: 2459090.5 Fraction: 0.999834707776647 Right antenna. Distance 186.7521 km
Node 1 & Node 76 JD: 2459090.5 Fraction: 0.999846281850721 Right antenna. Distance 186.1055 km
Node 1 & Node 76 JD: 2459090.5 Fraction: 0.999857855924795 Right antenna. Distance 186.67 km
Node 1 & Node 76 JD: 2459090.5 Fraction: 0.9998694299988691 Right antenna. Distance 188.4346 km
Node 1 & Node 76 JD: 2459090.5 Fraction: 0.9998810040729431 Right antenna. Distance 191.3661 km
Node 1 & Node 89 JD: 2459090.5 Fraction: 1.004047670739597 Front antenna. Distance 194.3716 km
Node 1 & Node 89 JD: 2459090.5 Fraction: 1.0040592448136711 Front antenna. Distance 180.4128 km
Node 1 & Node 89 JD: 2459090.5 Fraction: 1.0040708188877452 Front antenna. Distance 166.5874 km
Node 1 & Node 89 JD: 2459090.5 Fraction: 1.0040823929618192 Front antenna. Distance 152.9317 km
Node 1 & Node 89 JD: 2459090.5 Fraction: 1.0040939670358933 Front antenna. Distance 139.4955 km
Node 1 & Node 76 JD: 2459090.5 Fraction: 1.032612485554325 Left antenna. Distance 196.5775 km
Node 1 & Node 89 JD: 2459090.5 Fraction: 1.0368717448135714 Front antenna. Distance 192.1398 km
Node 1 & Node 89 JD: 2459090.5 Fraction: 1.0368833188876454 Front antenna. Distance 178.2467 km
Node 1 & Node 89 JD: 2459090.5 Fraction: 1.0368948929617194 Front antenna. Distance 164.5029 km
Node 1 & Node 89 JD: 2459090.5 Fraction: 1.0369064670357935 Front antenna. Distance 150.9492 km
Node 1 & Node 89 JD: 2459090.5 Fraction: 1.0369180411098675 Front antenna. Distance 137.6419 km
Node 1 & Node 76 JD: 2459090.5 Fraction: 1.0654481337023733 Right antenna. Distance 191.2733 km

```
Node 1 & Node 76 JD: 2459090.5 Fraction: 1.0654597077764474 Right antenna. Distance 191.28 km
Node 1 & Node 76 JD: 2459090.5 Fraction: 1.0654712818505214 Right antenna. Distance 192.4632 km
Node 1 & Node 89 JD: 2459090.5 Fraction: 1.0696958188875456 Front antenna. Distance 190.9212 km
Node 1 & Node 89 JD: 2459090.5 Fraction: 1.0697073929616197 Front antenna. Distance 176.8692 km
Node 1 & Node 89 JD: 2459090.5 Fraction: 1.0697189670356937 Front antenna. Distance 162.9377 km
Node 1 & Node 89 JD: 2459090.5 Fraction: 1.0697305411097677 Front antenna. Distance 149.1602 km
Node 1 & Node 89 JD: 2459090.5 Fraction: 1.0697421151838418 Front antenna. Distance 135.5841 km
Node 1 & Node 89 JD: 2459090.5 Fraction: 1.0697536892579158 Front antenna. Distance 122.2763 km
Node 1 & Node 27 JD: 2459090.5 Fraction: 1.0745337818504939 Top antenna. Distance 167.099 km
Node 1 & Node 27 JD: 2459090.5 Fraction: 1.074545355924568 Top antenna. Distance 165.8761 km
Node 1 & Node 27 JD: 2459090.5 Fraction: 1.074556929998642 Top antenna. Distance 164.9803 km
Node 1 & Node 27 JD: 2459090.5 Fraction: 1.074568504072716 Top antenna. Distance 164.4166 km
Node 1 & Node 27 JD: 2459090.5 Fraction: 1.07458007814679 Top antenna. Distance 164.1888 km
Node 1 & Node 27 JD: 2459090.5 Fraction: 1.074591652220864 Top antenna. Distance 164.298 km
Node 1 & Node 27 JD: 2459090.5 Fraction: 1.074603226294938 Top antenna. Distance 164.7436 km
Node 1 & Node 27 JD: 2459090.5 Fraction: 1.0746148003690121 Top antenna. Distance 165.523 km
Node 1 & Node 27 JD: 2459090.5 Fraction: 1.0746263744430862 Top antenna. Distance 166.6314 km
Node 1 & Node 27 JD: 2459090.5 Fraction: 1.0746379485171602 Top antenna. Distance 168.0623 km
Node 1 & Node 89 JD: 2459090.5 Fraction: 1.1025198929615199 Front antenna. Distance 188.793 km
Node 1 & Node 89 JD: 2459090.5 Fraction: 1.102531467035594 Front antenna. Distance 174.7977 km
Node 1 & Node 89 JD: 2459090.5 Fraction: 1.102543041109668 Front antenna. Distance 160.9374 km
Node 1 & Node 89 JD: 2459090.5 Fraction: 1.102554615183742 Front antenna. Distance 147.25 km
Node 1 & Node 89 JD: 2459090.5 Fraction: 1.102566189257816 Front antenna. Distance 133.789 km
Node 1 & Node 76 JD: 2459090.5 Fraction: 1.1310499855540257 Right antenna. Distance 196.6762 km
Node 1 & Node 89 JD: 2459090.5 Fraction: 1.1353439670354941 Front antenna. Distance 187.5683 km
Node 1 & Node 89 JD: 2459090.5 Fraction: 1.1353555411095682 Front antenna. Distance 173.428 km
Node 1 & Node 89 JD: 2459090.5 Fraction: 1.1353671151836422 Front antenna. Distance 159.395 km
Node 1 & Node 89 JD: 2459090.5 Fraction: 1.1353786892577162 Front antenna. Distance 145.5006 km
Node 1 & Node 89 JD: 2459090.5 Fraction: 1.1353902633317903 Front antenna. Distance 131.7887 km
Node 1 & Node 89 JD: 2459090.5 Fraction: 1.1354018374058643 Front antenna. Distance 118.3228 km
Node 1 & Node 89 JD: 2459090.5 Fraction: 1.1681680411094684 Front antenna. Distance 185.5394 km
Node 1 & Node 89 JD: 2459090.5 Fraction: 1.1681796151835424 Front antenna. Distance 171.4462 km
Node 1 & Node 89 JD: 2459090.5 Fraction: 1.1681911892576164 Front antenna. Distance 157.4734 km
Node 1 & Node 89 JD: 2459090.5 Fraction: 1.1682027633316905 Front antenna. Distance 143.6561 km
Node 1 & Node 89 JD: 2459090.5 Fraction: 1.1682143374057645 Front antenna. Distance 130.0442 km
Node 1 & Node 89 JD: 2459090.5 Fraction: 1.1682259114798386 Front antenna. Distance 116.7094 km

Number of unique intersections: 77
Number of unique satellites: 11
Intersection satellite nodes: [ 14. 16. 27. 38. 39. 47. 65. 70. 76. 89. 147.]
Average time between intersections: 1120 seconds

That took 617.7257790565491 seconds
End of program
```